

Coupled Electron Proton Transfer Reactions in Biological Redox Active Substrates

Christine Fecenko Murphy

A dissertation submitted to the faculty of the University of North Carolina at Chapel Hill in partial fulfillment of the requirements for the degree of Doctor of Philosophy in the Department of Chemistry

Chapel Hill

2009

Approved By

Advisor: Professor H. Holden Thorp

Advisor: Professor Thomas J. Meyer

Reader: Professor Joseph Templeton

## ABSTRACT

Christine Fecenko Murphy: Coupled Electron Proton Transfer Reactions in Biological Redox Active Substrates

(Under the direction of H. Holden Thorp and Thomas J. Meyer)

The kinetics of oxidation of amino acids and nucleobases by the series of metal complex oxidants,  $M(\text{bpy})_3^{3+}$  ( $M = \text{Os}, \text{Fe}, \text{Ru}$ ) in aqueous solution at an ITO electrode, in the presence of added bases, was investigated utilizing catalytic cyclic voltammetry. A common mechanism involving initial formation of a hydrogen bond complex between the substrate and a base in solution was identified for all substrates. After association, oxidation can occur through two pathways - multiple site electron proton transfer (MS-EPT) or proton transfer followed by electron transfer (PT-ET). Kinetic isolation techniques were used to investigate each oxidation pathway individually, and have provided kinetic parameters and isotope effects for each step of the reaction mechanism for all substrates studied. Comparison between rate constants and isotope effects for each substrate provide insight into the role of proton transfer in biological system. The main emphasis of this study was to investigate the role of free energy change in MS-EPT reactions. We have found that the effects of free energy change on MS-EPT rate constant can be attributed to not only the base strength but also the oxidant reduction potential. Evaluation of rate constants and isotope effects for each system highlights the importance of the role of both the electron and the proton in redox active biological systems.

## Acknowledgements

Holden, first off, thank you for taking me on as a graduate student. When I first joined the group, I thought I wanted to be a biological chemist. In fact, I was shocked when I was handed the initial patent on tyrosine oxidation. You must have known what you were doing, because now I have found my passion for amino acid oxidation and how oxidoreductases function. You have always supported my ideas and interest both in the lab and out. I don't know any other advisor would have given a fourth year graduate student a high-five when she announced her pregnancy. It is for this and many other reasons, I'm so glad that I chose to work in your group and have learned so much from you.

Dr. Meyer, thank you for taking such an interest in me and my work. Our daily meetings to discuss science always left me with a great grasp on my work and my plate overflowing with work. You've kept me busy, productive, and on task. As someone that is as scatterbrained as me, it was definitely the fire under me that I needed. You've allowed me to do so many things in graduate school that many students only dream of and have supported even my craziest ideas. I doubt you ever thought you would venture into protein design and protein electrochemistry. I'm very grateful to you for selecting me to be part of your group. I've learned so much and have laid the ground work for my future interests.

Dr. Feldberg, you've taught me how to let the electrochemistry speak for itself. I looked forward to your visits to UNC every year, and have learned so much for your patient instruction.

To all the past and present members of the Thorp group, you've made working in lab a pleasure. Dom, thanks for being my electrochemistry mentor and sharing the ins and outs of digisim. Stephanie, your thesis has been more useful than you would have ever imagined when writing it. Julie, thanks for putting up with my 3 month hiatus into biochemistry. I learned so much, even though I wasted so many chemicals. Chris, I couldn't have found a better person to leave my project to, I know you'll do great things with it. To the Meyer group, thanks for all your ideas and thoughts on my project. Javier, sometimes I think you thought about my kinetics more than I did. Kyle, thanks for always being patient with me and saving me in my orals with a lesson on spin orbit coupling.

I would also like to thank my family and friends for their support in every aspect of my life. Mom and Dad, thanks for always pushing me to be my best, you always love and support me unconditionally. I'm grateful to you for everything! Jamie and Brian, you two are my

inspiration to always do my best. Karen, thanks for being my “best sister” and always answering you phone at 6am when I’m awake and want to chat. Alison and Chetna, you’re the best roommates I could ever ask for. Grant, thank you for putting up with my seemingly endless nights of work. You have let me bounce ideas off of you and listened to more practice talks than any husband should be expected to. Grant and Gavin, you’ve made me the luckiest mom and wife in the world.

## Table of Contents

<b>List of Figures</b> .....	ix
<b>List of Tables</b> .....	xii
<b>List of Abbreviations</b> .....	xiii
<b>Chapter 1: Introduction to EPT in Biological Redox Active Substrates</b> .....	1
1.1 Biological Oxidation.....	2
1.2 Proton Coupled Electron Transfer.....	4
1.3 Metal Mediated Electrocatalysis on ITO.....	7
1.4 Electrocatalysis of Amino Acids and Nucleobases.....	10
1.5 References.....	12
<b>Chapter 2: The Oxidation of Tyrosine through Parallel Rate Determining Proton Transfer and MS-EPT</b> .....	14
2.1 Abstract.....	15
2.2 Introduction.....	17
2.3 Methods and Materials.....	18
2.3.1: General.....	18
2.3.2: Buffer Preparation.....	18
2.3.3: Isotope Studies.....	18
2.3.4: Sample Preparation.....	19
2.3.5: Electrochemistry.....	19
2.3.6: Digital Simulation.....	20
2.3.7: <sup>31</sup> P NMR.....	21

2.3.8 Mixing Studies.....	22
2.4 Results and Discussion.....	23
2.4.1: Electrocatalytic Studies in Phosphate Buffer.....	23
2.4.2: Kinetic Studies on Tyrosine.....	25
2.5 Conclusions.....	29
2.6 References.....	31
<b>Chapter 3: Coupled Electron-Proton Transfer Pathways in Tyrosine Oxidation.....</b>	<b>33</b>
3.1 Abstract.....	34
3.2 Introduction.....	35
3.3 Methods and Materials.....	38
3.3.1: General.....	38
3.3.2: Isotope Studies.....	38
3.3.3: Electrochemistry.....	39
3.3.4: Rate Law.....	40
3.3.5: Digital Simulation.....	44
3.3.6: Electron Transfer Tyrosine and Anion.....	45
3.4 Results.....	47
3.4.1: Oxidation of Tyrosine and Anion.....	47
3.4.2: Determination of Rate Law.....	48
3.4.3: Pre-Association Between TyrOH + B.....	50
3.4.4: Dependence on [TyrOH] and [B].....	51
3.4.5: $K_A$ by $^{31}\text{P}$ NMR.....	52
3.4.6: Pre-Association between Complex and Metal.....	53
3.4.7: Rapid Pre-equilibrium Formation of TyrO <sup>-</sup> .....	54
3.4.8: Rate-Limiting Proton Transfer.....	55

3.4.9: Complete Rate Expression.....	57
3.4.10: H/D Isotope Effects.....	58
3.4.11: General Buffer Base Catalysis.....	61
3.5 Discussion.....	62
3.5.1: Pathways for Tyrosine Oxidation.....	63
3.5.2: Kinetic Parameters.....	66
3.5.3: Free Energy Dependence MS-EPT.....	73
3.5.4: Free Energy Dependence ET.....	75
3.6 Conclusions.....	78
3.7 References.....	80
<b>Chapter 4: pH Dependent or Base Assisted Tyrosine Oxidation.....</b>	<b>85</b>
4.1 Abstract.....	86
4.2 Introduction.....	85
4.3 Methods and Materials.....	87
4.3.1 General.....	87
4.3.2: Kinetics-Spectrophotometric Monitoring.....	89
4.3.3: Second Order Unequal Concentration Kinetics.....	89
4.3.4: Kinetics Cyclic Voltometric Studies.....	89
4.3.5: Digital Simulation.....	92
4.4 Results and Discussion.....	92
4.4.1: pH Dependence in the Oxidation of Tyrosine by Os(bpy) <sub>3</sub> <sup>3+</sup> .....	92
4.4.2: Hydroxide as an EPT Base.....	94
4.4.3: Additional EPT Bases.....	96
4.4.4: General Role of OH <sup>-</sup> .....	100
4.5 Conclusions.....	104

4.6 References.....	106
<b>Chapter 5: Coupled Electron Proton Transfer in Guanine Oxidation.....</b>	<b>108</b>
5.1 Abstract.....	109
5.2 Introduction.....	110
5.3 Methods and Materials.....	111
5.3.1: DNA.....	111
5.3.2: General.....	112
5.3.3: Isotope Studies.....	112
5.3.4: Electodes.....	113
5.3.5: Electrochemistry.....	113
5.3.6: Mixing Studies.....	115
5.4 Results and Discussion.....	117
5.4.1: Oxidation of dGMP.....	117
5.4.2: EPT Oxidation of dGMP and G with dCMP and C.....	127
5.4.3: Oxidation of ssDNA.....	130
5.4.4: Oxidation of ssDNA with Base Complement.....	132
5.4.5 Oxidation of dsDNA.....	133
5.5 Conclusions.....	135
5.6 References .....	143
<b>Bibliography.....</b>	<b>147</b>

## List of Figures

### Chapter 1: Introduction to EPT in Biological Redox Active Substrates

Figure 1: Electroactive amino acids.....	2
Figure 2: Electroactive nucleobases.....	3
Figure 3: Electron Transfer followed by Proton Transfer.....	5
Figure 4: Proton Transfer followed by Electron Transfer.....	6
Figure 5: Electron Proton Transfer.....	6
Figure 6: Electrocatalytic cyclic voltammogram.....	8
Figure 7: Digital simulation of electrocatalytic cyclic voltammogram.....	9

### Chapter 2: The Oxidation of Tyrosine through Parallel Rate-Determining Proton Transfer and Multi-Site Electron Proton Transfer

Figure 1: Driving force dependence of tyrosine and tryptophan.....	24
Figure 2: Electrocatalysis of tyrosine at constant pH.....	24
Figure 3: Cyclic Voltammogram at pH 8.0 showing loss of $\text{Os}(\text{bpy})_3^{3+}$ .....	28
Figure 4: Driving Force Dependence study at pH 7.5 and 6.0 phosphate.....	28

### Chapter 3: Coupled Electron Proton Transfer Pathways in Tyrosine Oxidation

Figure 1: Cyclic Voltammogram of $\text{Os}(\text{bpy})_3^{3+}$ with TyrOH A) no buffer, B) pH 6.0, and C) pH 8.5.....	46
Figure 2: Saturation kinetics exhibited from plots of $k_{\text{obs}}$ vs $[\text{HPO}_4^{2-}]$ .....	47
Figure 3: Kinetic plots from variation of A) Base and B) TyrOH.....	48
Figure 4: Association constant calculation from $^{31}\text{P}$ NMR.....	49
Figure 5: Saturation kinetics observed from plots of $k_{\text{obs}}$ vs $[\text{Os}(\text{bpy})_3^{3+}]$ .....	50
Figure 6: Linearization of Rate Law through plots of $k_{\text{obs}}$ vs $[\text{B}]/[\text{HB}^+]$ .....	51
Figure 7: Cyclic Voltammogram at pH 8.0 showing loss of $\text{Os}(\text{bpy})_3^{3+}$ .....	52
Figure 8: Variation of $k_{\text{obs}}$ with [Base] pH 8.0.....	53

Figure 9: Cyclic voltammogram and digital simulation at pH 7.5.....	54
Figure 10: Mole Fraction study under limiting conditions.....	55
Figure 11: $-\text{RTLn}k_1$ vs $\text{RTLn}K_{\text{HB}^+}$ .....	64
Figure 12: $\text{RTLn}k_1$ vs $\text{RTLn}K_a$ .....	65
Figure 13: Proton Transfer in the Inverted Region.....	66
Figure 14: $\text{RTLn}k_{\text{red}}$ vs $\text{RTLn}k_1$ .....	67
Figure 15: Variation of $k_{\text{obs}}$ by A) variation of oxidant or B) variation of base.....	69
Figure 16: Free Energy Dependence for MS-EPT.....	70
Figure 17: Driving force dependence study of anion.....	72

#### **Chapter 4: pH Dependent or Base Assisted Tyrosine Oxidation?**

Figure 1: pH dependent oxidation of Ru-Y adduct.....	88
Figure 2: Absorbance over time studies-First order kinetics.....	92
Figure 3: Plot of $k_{\text{obs}}/[\text{TyrOH}]$ vs pH.....	97
Figure 4: Plot of $k_{\text{obs}}/[\text{TyrOH}]$ vs $[\text{HPO}_4^{2-}]$ pH 7.0 and 9.0.....	98
Figure 5: Absorbance over time studies-Second order kinetic.....	99
Figure 6: Plot of $k_{\text{obs}}/[\text{TyrOH}]$ vs [Base].....	102
Figure 7: Plot of $k_{\text{obs}}/[\text{TyrOH}]$ vs $[\text{OH}^-]$ .....	103
Figure 8: Plot of $k_{\text{obs}}/[\text{TyrOH}]$ vs pH.....	104

#### **Chapter 5: Coupled Electron Proton Transfer in Guanine Oxidation**

Figure 1: Absorbance over time studies-first order kinetics.....	116
Figure 2: Saturation kinetics exhibited in plots of $k_{\text{obs}}$ vs $[\text{HPO}_4^{2-}]$ .....	120
Figure 3: Saturation kinetics exhibited in plots of $k_{\text{obs}}$ vs $[\text{Ru}(\text{bpy})_3^{3+}]$ .....	120
Figure 4: Cyclic voltammogram of dGMP in $\text{D}_2\text{O}$ and $\text{H}_2\text{O}$ .....	121
Figure 5: Variation of $k_{\text{obs}}$ by A) variation of oxidant and b) variation of base.....	123
Figure 6: Free Energy Dependence of MS-EPT.....	127

Figure 7: Cyclic voltammogram of dGMP with dCMP in phosphate buffer.....	128
Figure 8: Plot of $k_{\text{obs}}/[G]$ vs $[C]$ .....	129
Figure 9: Cyclic votammograms of ssDNA and dsDNA in phosphate buffer.....	131
Figure 10: Plot of $k_{\text{obs}}$ vs $[\text{HPO}_4^{2-}]$ obtained by stopped flow on ssDNA.....	132
Figure 11: Cyclic voltammogram and digital simulation of ssDNA with 7mer....	133
Figure 12: Plot of $k_{\text{obs}}$ vs $[\text{HPO}_4^{2-}]$ obtained by stopped flow on dsDNA.....	135

## List of Tables

### Chapter 1: Introduction to EPT in Biological Redox Active Substrates

### Chapter 2: The Oxidation of Tyrosine through Parallel Rate-Determining Proton Transfer and Multi-Site Electron Proton Transfer

Table 1: Rate and equilibrium constants for tyrosine in phosphate buffer.....26

Table 2: Isotope effects for tyrosine in phosphate buffer.....26

### Chapter 3: Coupled Electron Proton Transfer Pathways in Tyrosine Oxidation

Table 1: Rate constants for all bases.....58

Table 2: Isotope effects for all bases.....60

Table 3: Buffer bases with  $pK_a$ .....61

Table 4: Oxidant investigations with rate constants for  $k_2$  and  $k_{red}$ .....62

### Chapter 4: pH Dependent or Base Assisted Tyrosine Oxidation?

Table 1: Slope and Intercept from plot of  $k_{obs}/[TyrOH]$  vs  $[Base]$ .....102

### Chapter 5: Coupled Electron Proton Transfer in Guanine Oxidation

Table 1: Rate and Equilibrium constants for dGMP and TyrOH.....123

Table 2: Kinetic data on G-H complexes.....140

## List of Symbols and Abbreviations

$[\text{TyrOH}]_T$	total concentration of tyrosine
$\Delta E$	change in reduction potential
$\Delta G$	Free Energy
$\Delta G_{\text{EPT}}$	free energy change for electron proton transfer
$\Delta G_{\text{ET}}$	free energy change for electron transfer
$\Delta G_{\text{PT}}$	free energy change for proton transfer
$^{\circ}\text{C}$	degrees celsius
$^1\text{H NMR}$	Proton Nuclear Magnetic Resonance
$^{31}\text{P NMR}$	phosphorus nuclear magnetic resonance
A	Adenosine
A	Ampere
A	electrode area
Å	Angstrom
Abs	absorbance
Ag/AgCl	Silver/Silver Chloride Reference
B	base form of buffer
C	Cytosine
CV	cyclic voltammogram
CySH	Cysteine
d	distance
D+	deuteron
D <sub>2</sub> O	deuterium oxide
DCl	deuteriochloric acid
dCMP	deoxycytodine 5' monophosphate
DFT	density functional theory
dGMP	deoxyguanosine 5' monophosphate
dmb	dimethylbipyridine
DNA	Deoxyribonucleic Acid
dsDNA	double stranded DNA
E	electrode potential
$\epsilon$	molar absorbtivity
e-	electron
$E^{\circ'}$	Formal Potential
$E_{1/2}$	Midpoint Potential
EIE	equilibrium isotope effect
EPT	Electron Proton Transfer

ET-PT	Step-wise Electron Transfer followed by Proton Transfer
eV	electron volt
F	Faraday constant
Fe	Iron
FT-IR	fourier transfer infrared spectroscopy
G	Guanine
G-H <sup>+/-</sup> .	guanine radical cation
H <sup>+</sup>	proton
H <sub>190</sub>	Histidine 190 in Photosystem II
H <sub>2</sub> PO <sub>4</sub> <sup>-</sup>	monobasic hydrogen phosphate
H <sub>3</sub> O <sup>+</sup>	hydronium ion
HB+	acid form of buffer
HCl	Hydrochloric Acid
His	histidine
HPO <sub>4</sub> <sup>2-</sup>	dibasic hydrogen phosphate
i	electrode current
i <sub>o</sub>	exchange current density
ITO	Indium Tin Oxide
k <sub>D</sub>	rate constant for diffusion
k <sub>EPT</sub>	electron proton transfer rate constant
KIE	kinetic isotope effect
k <sub>obs</sub>	observed rate constant
k <sub>S</sub>	heterogeneous electron transfer rate constant
λ	reorganizational energy
λ <sub>max</sub>	maximum absorbance
M	Molar
M(bpy) <sub>3</sub> <sup>3+/2+</sup>	Metal tris(2,2'-bipyridine) complex
MeCN	acetonitrile
MLCT	metal-ligand charge transfer
mM	millimolar
MS-EPT	Multi-Site Electron Proton Transfer
N1	Proton in guanine
N <sub>A</sub>	Avogadros number
NaOD	Sodium Deuoxide
NaOH	Sodium Hydroxide
NHE	Normal Hydrogen Electrode
OAc-	acetate

OH <sup>-</sup>	hydroxide anion
Os	Osmium
P680	Pigment found in PSII acts as primary electron donar.
P <sub>680+</sub>	Oxidized form of P <sub>680</sub>
PCET	Proton Coupled Electron Transfer
pD	-Log[D <sup>+</sup> ]
pH	-Log[H <sup>+</sup> ]
phos	dibasic phosphate
pK <sub>a</sub>	-Log[K <sub>a</sub> ]
PSII	Photosystem II
PT-ET	Step-wise Proton Transfer followed by Electron Transfer
R	universal gas constant
RNR	Ribonucleotide Reductase
Ru	Ruthenium
ssDNA	single stranded DNA
Succ	succinate
T	Thiamine
T	Temperature
tris	tris base
TrpH	Tryptophan
TyrO <sup>-</sup>	tyrosyl anion
TyrO <sup>·</sup>	tyrosyl radical
TyrOH	Tyrosine
TyrOH <sup>+·</sup>	tyrosine radical cation
TyrOH--B	tyrosine adduct
UV	Ultraviolet
V	volts
Y <sub>z</sub>	Tyrosine 161 in Photosystem II
α	symmetry factor
δ	chemical shift
	difference between formal potential and electrode
η	potential
μM	micromolar
χ <sub>D</sub>	mole fraction deuterium
Ω	resistance

## **Chapter 1**

### **Introduction to Electron Proton Transfer in Biological Redox Active Substrates**

**1.1 Biological Oxidation:** Understanding oxidation and reduction reactions in biologically relevant systems is important to gain insight into how enzymes and DNA function. Amino acid oxidation acts as a redox mediator in vital life processes such as photosynthesis and respiration.<sup>1-5</sup> In photosystem II, tyrosine (Y<sub>z</sub>) aids in electron movement in the production of atmospheric oxygen in the thylakoid membrane of green plants.<sup>5</sup> Oxidation of the amino acids, tyrosine, tryptophan, and cysteine (Figure 1) is also of central importance to electron transfer reactions in oxidoreductases, a diverse family of redox active enzymes. Electroactive amino acids are involved in charge migration over long distances in the protein environment. Studies on ribonucleotide reductase (RNR), a DNA repair protein, have found that electron transfer occurs over a distance of ~35Å. EPR studies on RNR, isolate radical formation at tyrosines, tryptophans, and cysteines found within 10Å of one another in the protein framework.<sup>6</sup>

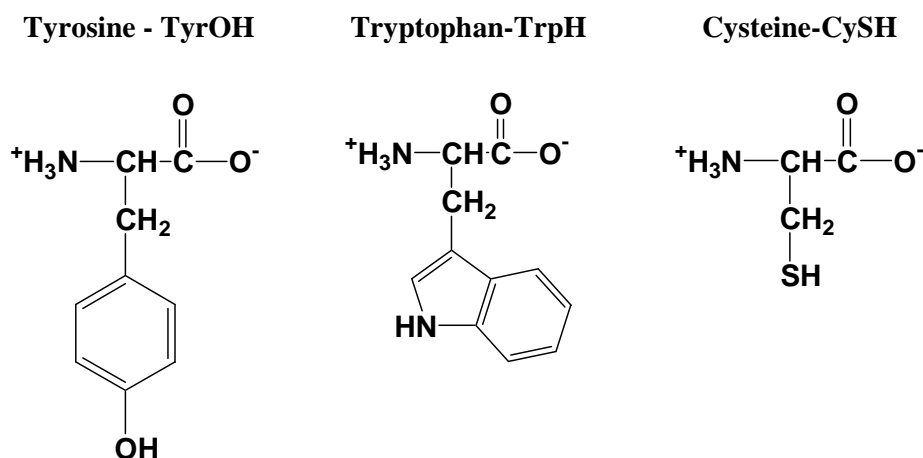


Figure 1: Structures of electroactive amino acids, tyrosine, tryptophan, and cysteine.

Oxidation of deoxyribonucleic acids (DNA) leads to DNA damage and degradation, and has been associated with neurodegenerative disorders such as Alzheimer's and Parkinson's disease.<sup>7-11</sup> DNA is composed of 4 nucleobases: adenosine, cytosine, guanine,

and thiamine (figure 2) that are found in hydrogen bond partners of A-T and G-C in the DNA phosphate backbone. Guanine acts as a radical trap due its low reduction potential of 1.1V vs NHE as compared to the other nucleobases and is often the site of oxidative damage.<sup>6,8</sup>

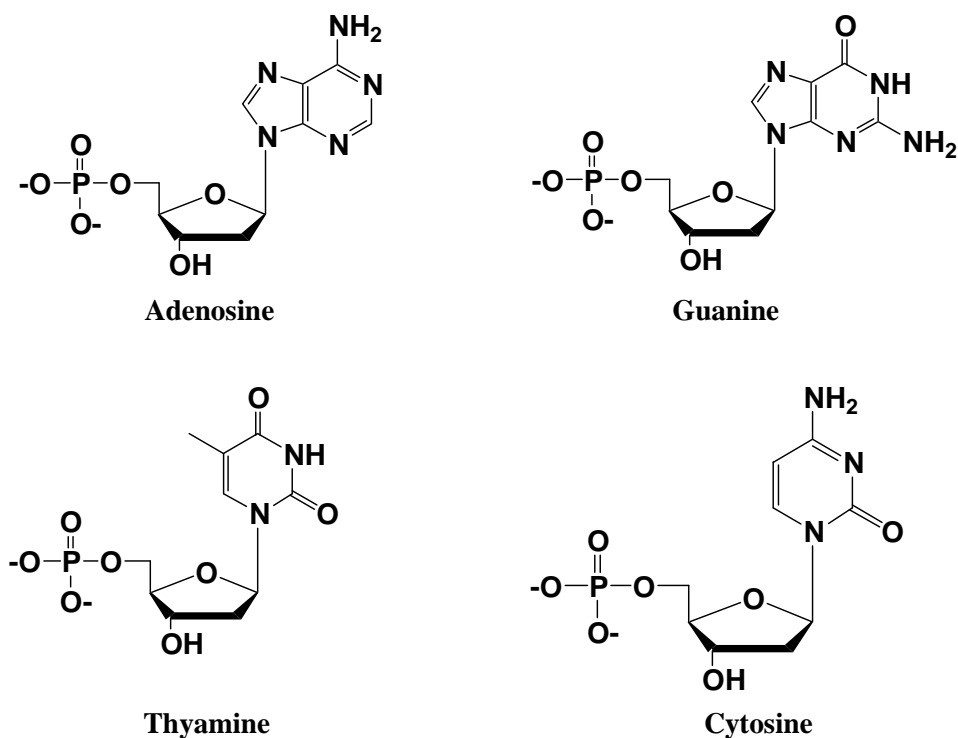


Figure 2: Structures of the DNA nucleobases

Oxidation reactions in biological systems involve the paired movement of protons and electrons as a method to move charges over long distances. In Photosystem II, the oxidation of tyrosine  $Y_z$  is coupled to transfer of its hydroxyl proton. At the same time the electron is transferred from tyrosine to the chromophore  $P_{680}$ , the proton is transferred to a neighboring histidine,  $H_{190}$ .<sup>5</sup> Oxidation of guanine also occurs through the movement of both protons and electrons. As the guanine is oxidized, the N1 proton is believed to transfer, but if the proton is transferred to the cytosine or to bulk solvent is often debated.<sup>17-20</sup> Long range electron transfer, as seen in RNR, where an electron is moved  $35\text{\AA}$ , is also believed to be coupled to proton transfer. In the protein framework, tyrosines and cysteines are potential

hydrogen bond partners of histidine and aspartate respectively.<sup>21,22</sup> As the electron hops from one electroactive residue to the next, the proton is thought to transfer to a neighboring base.

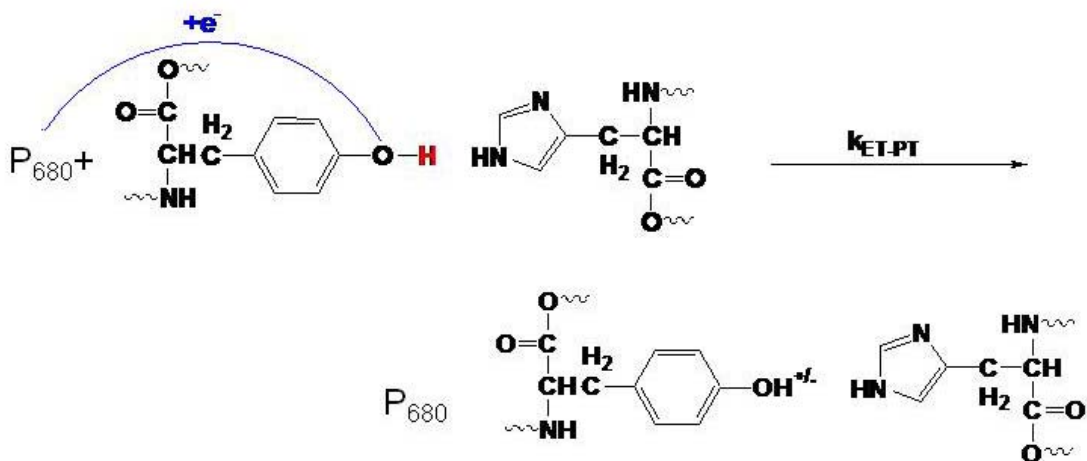
The coupled movement of protons and electrons is supported by experimental results. Studies on DNA and electroactive proteins have reported pH dependent oxidations in which the rate of electron transfer is directly proportional to the pH of solution.<sup>23</sup> Proton movement is also supported by isotope effects reported in the literature for the electroactive amino acids and the guanine nucleobase. Isotope effects in oxidation reactions, indicate the reaction proceeds through a rate-determining step involving the transfer of a proton.<sup>24</sup> It is commonly agreed that both electrons and protons are involved in these reaction mechanisms, the mechanistic details of these reactions remains unclear.<sup>1-24</sup>

**1.2 Proton Coupled Electron Transfer:** Proton coupled electron transfer (PCET) describes any reaction that involves the net movement of protons and electrons.<sup>5</sup> Oxidation of tyrosine, tryptophan, cysteine, and guanine all involve the net movement of electrons and protons, but the specific reaction mechanism is highly debated.<sup>23, 25</sup>

Oxidation can occur in one of three ways, electron transfer followed by proton transfer (ET-PT), proton transfer followed by electron transfer (PT-ET) and concerted electron proton transfer (EPT).<sup>5</sup> Each mechanism will be addressed independently and in terms of a common reaction, tyrosine Y<sub>z</sub> in photosystem II, but the general mechanism can be applied to all four substrates.

Electron Transfer Followed by Proton Transfer (ET-PT): The ET-PT mechanism involves the step-wise movement of the electron and the proton. In this case, as illustrated in figure 3, the electron transfer results in the formation of a highly acidic protonated radical. The reduction potential of the radical cation is 1.34V vs NHE, where as the reduction potential of

the  $P_{680}^+$  is 0.9V vs NHE making the transfer of an electron a thermodynamically unfavorable reaction. The second step, proton transfer, however, occurs rapidly due to the acidity (-2) of the protonated radical. The initial electron transfer to the  $P_{680}$  is uphill by +0.08eV due to the formation of a highly charged intermediate.



**Electron Transfer followed by Proton Transfer**

Figure 3: Mechanistic outline of ET-PT in PSII

Proton Transfer followed by Electron Transfer (PT-ET): Oxidation of tyrosine can also occur through another step-wise process involving initial deprotonation to the deprotonated tyrosyl anion shown in figure 4. The  $pK_a$  of the hydroxyl proton is 10.1 making initial deprotonation to the neighboring histidine residue with a  $pK_a$  of 6.6 unfavorable by +0.36eV. However, the reduction potential of the anion is 0.7V vs NHE and the reduction of the anion would occur rapidly upon deprotonation.

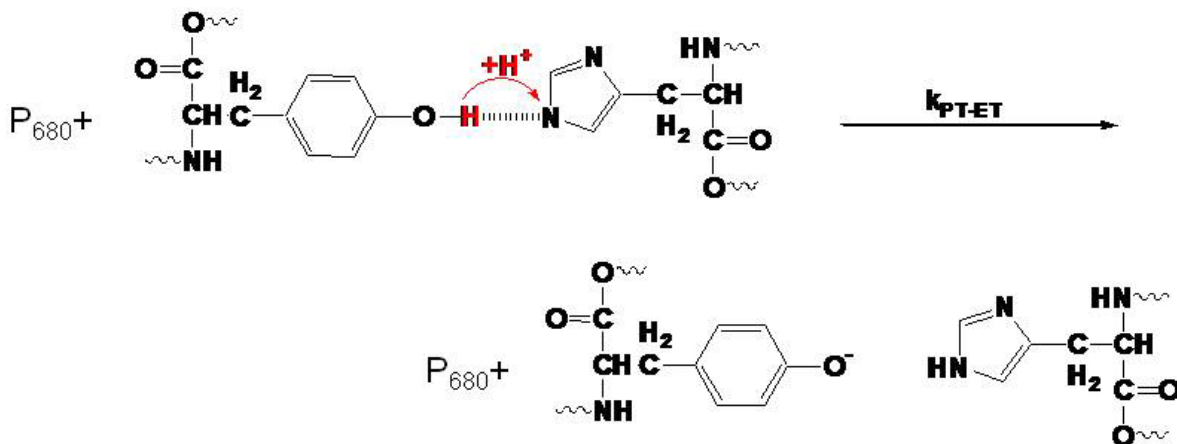


Figure 4: Mechanistic outline of the PT-ET reaction.

Concerted Electron Proton Transfer (EPT): A third type of oxidation mechanism has been proposed. As shown in figure 5, the reaction of tyrosine involves the simultaneous transfer of a proton to His190 and an electron to the  $P_{680+}$ . Microscopically more complex than the step-wise reactions, the concerted mechanism avoids the thermodynamic cost of forming a charge intermediate. The simultaneous movement of the electron and the proton is actually thermodynamically favored over the step-wise reactions by 0.1eV.

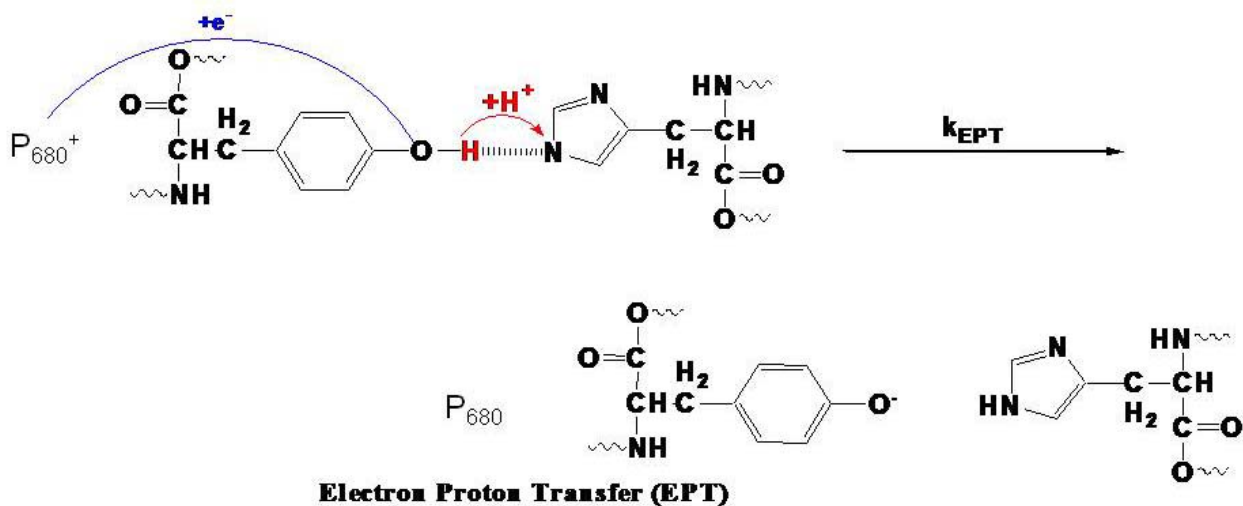


Figure 5: Mechanistic outline of the EPT reaction.

Electron proton transfer occurs through simultaneous transfer of protons and electrons. EPT results from a redox process that allows for transfer of the electron and proton from different orbital sites on the same molecule to different acceptor sites on the same molecule.<sup>5</sup> Multi-site electron proton transfer is a subset of EPT and is defined by transfer of the proton and the acceptor to different electron and proton acceptor sites.<sup>5</sup> The fundamental principles for EPT have been addressed by Hammes-Schiffer, Cukier, and others where EPT theory is based on traditional Marcus electron transfer theory.<sup>3,5,12,15,16</sup>

**1.3 Metal Mediated Electrocatalysis on ITO Electrodes:** Model systems are routinely used to investigate specific interactions inside biological species to avoid the added complications of the cellular environment.<sup>12</sup> Model systems have helped elucidate the fundamental aspects of PCET reactions with regard to the oxidation of tyrosine, cysteine, tryptophan, and guanine.<sup>23-25</sup> Experiments have been designed to study PCET reactions chemically, photochemically, and electrochemically in solution.<sup>6, 18-25</sup> Specifically, electrochemistry has the advantage because the reaction is controlled by the potential of the electrode and reaction kinetics can be monitored directly from current over-potentials.<sup>15,23</sup>

Electrochemical techniques have been used to investigate the oxidation mechanisms of guanine and DNA and have recently applied this technique to amino acids through the use of electrocatalytic oxidation<sup>26-28</sup>. In electrocatalytic oxidation, metal complexes  $M(\text{bpy})_3^{2+}$  ( $M=\text{Ru, Fe, Os}$ ) are placed in the presence of organic donors and can be studied on indium tin oxide doped electrodes in aqueous solution in a near neutral pH window.<sup>26,27</sup>

Electrocatalysis works by forming  $M(\text{bpy})_3^{2+}$  on a positively biased ITO electrode to form  $M(\text{bpy})_3^{3+}$  at the electrode surface. When no electron donor is present,  $M(\text{bpy})_3^{3+}$  will exist in solution until a negative bias is applied when the  $M(\text{bpy})_3^{2+}$  will reform in solution (Figure

6a). When an organic donor, such as tyrosine is present in solution and positive potentials are applied to the electrode,  $M(\text{bpy})_3^{3+}$  gains an electron from the electron donor to reform the  $M(\text{bpy})_3^{2+}$  in solution instead of at the electrode surface. The electrode only detects the presence of the  $M(\text{bpy})_3^{2+}$  species, and the cyclic voltammograms show significant enhancement of the oxidative wave (Figure 6b).

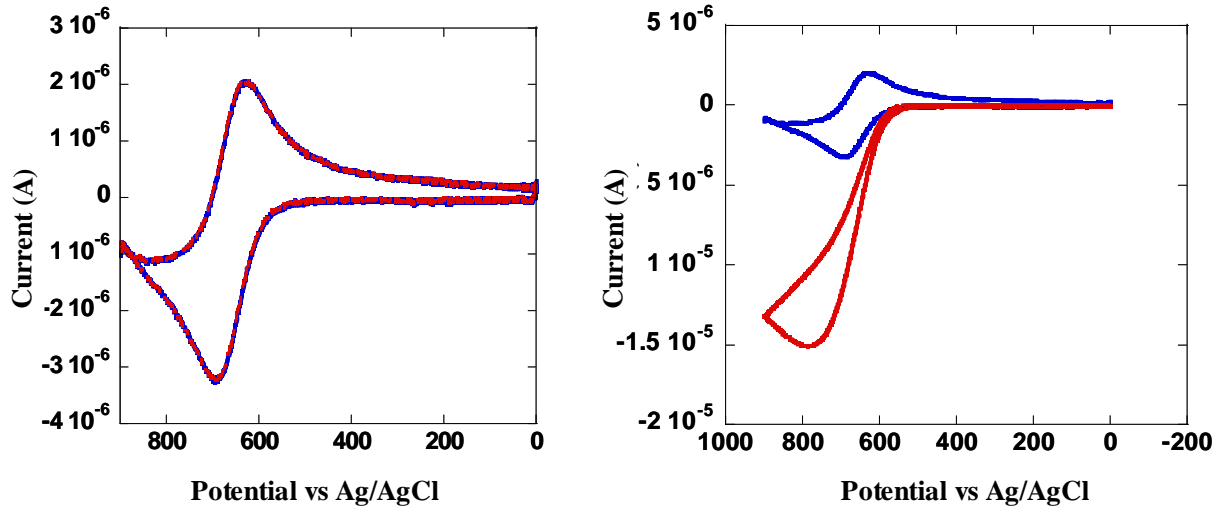


Figure 6: Cyclic voltammograms of  $\text{Os}(\text{bpy})_3^{3+}$  a) alone in phosphate buffered solution and b) in the presence of tyrosine. When an electron donor is present as in (b), electron transfer occurs from the tyrosine to the  $\text{Os}(\text{bpy})_3^{3+}$  in solution. The electrode only detects the conversion from  $\text{Os}^{2+}$  to  $\text{Os}^{3+}$  which results in enhancement of the catalytic oxidative wave.

Kinetic information can be obtained from cyclic voltammetric studies exhibiting current enhancement of the oxidative wave through digital simulation. Current and potential information is related through the Butler Volmer equation<sup>29,30</sup> shown in eq 1. Digital simulation of the oxidative wave results in rate constants consistent with the homogeneous electron transfer rate constant for the exchange between the  $M(\text{bpy})_3^{3+}$  and the electron donor in solution using equation 2, which relates reduction potential to the observed rate constant ( $k_{\text{obs}}$ ). Digital simulations are compared to experimental data as shown in figure 7.

$$\frac{i}{nFA} = k_s \left[ [A]_{x=0} \exp\left(-\alpha \frac{F}{RT} \Delta E\right) - [B]_{x=0} \exp\left((1-\alpha) \frac{F}{RT} \Delta E\right) \right] \quad (1)$$

$$\Delta G = nF(E_{\text{ox}}^{\circ} - E_{\text{red}}^{\circ}) \quad (2a)$$

$$k_{\text{obs}} = A \exp - \frac{\Delta G}{RT} \quad (2b)$$

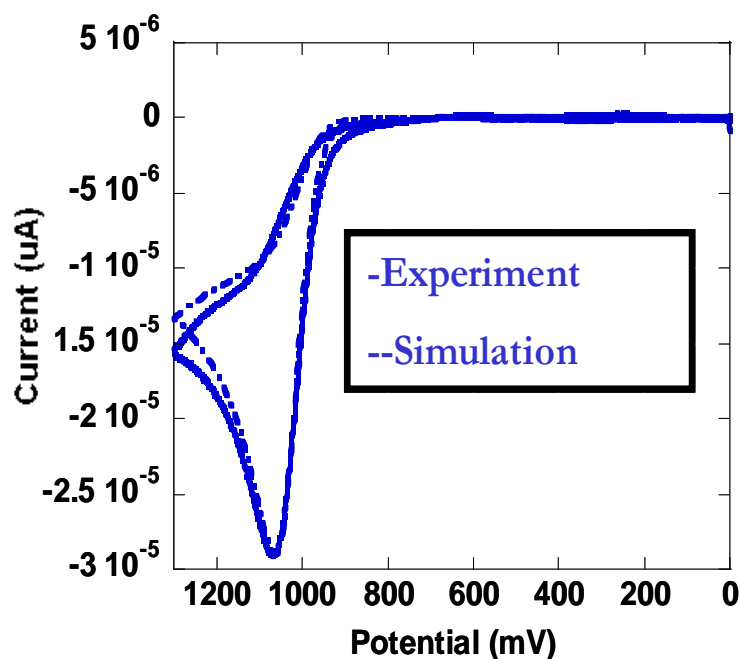


Figure 7: Electrocatalytic cyclic voltammograms of  $M(\text{bpy})_3^{3+}$  in the presence of an organic donor (solid line) and a digitally simulated cyclic voltammogram (dashed line). Digital simulations are fit to experimental data to obtain rate constants for the homogeneous electron transfer between the metal complex

**1.4 Electrocatalysis of Amino Acids and Nucleobases:** We report here, the application of this electrochemical technique to the investigation of the oxidation mechanism of the biologically relevant substrates, tyrosine, tryptophan, cysteine and guanine.

Initial application of this technique to tyrosine resulted in isolation of a new mechanism for tyrosine oxidation through competitive PT-ET and EPT. The key mechanistic finding was the formation of an association complex with the basic form of the buffer ( $\text{HPO}_4^{2-}$ ),

before oxidation through either pathway. The pathway of oxidation was determined by solution conditions with PT-ET dominating at high concentrations of base and low concentrations of acid and MS-EPT dominating at low concentrations of base and high concentrations of acid. Rate constants and isotope effects were isolated that supported the oxidation mechanism. Further studies on the tyrosine system have found that previous reported pH dependent oxidation occurs through prior association with the basic form of the buffer (in the limit of  $pK_a = 4.7-8.1$  investigated) followed by either deprotonation or electron proton transfer depending on solution conditions.

The same experimental technique was applied to amino acids, cysteine, and tryptophan and the nucleobase guanine. Guanine, was studied in several environments, including dGMP, single stranded (ssDNA), and double stranded (dsDNA). We have found that the EPT reaction mechanism is a general mechanism for tyrosine, tryptophan, cysteine, and guanine. We have found that base association and redox activity through competitive pathways of deprotonation and electron proton transfer are common in biological redox systems, and play a role in tuning the reduction potentials of these substrates.

The initial technique was applied to an unprecedented number of oxidants, bases, and reductants and resulted in rate constants and isotope effects that provide insight into the nature of electron proton transfer in biological systems. The information from this study can be applied directly to how the movement of electrons and protons can tune oxidation in proteins and DNA.

## 1.5 References:

- 1) Cukier, R. I; Nocera, D. G. **Proton Coupled Electron Transfer**, *Annu. Rev. Phys. Chem.* **1998** 49 337-69
- 2) Mayer, J. M. **Proton Coupled Electron Transfer: A Reaction Chemist's Point of View**. *Annu. Rev. Phys. Chem.* **2004** 55 363-90
- 3) Hammes-Schiffer, S. **Theoretical Perspectives on Proton Coupled Electron Transfer Reactions** *Acc. Chem. Res.* **2001** 34 273-81
- 4) Brudvig, G. W.; Thorp, H. H.; Crabtree, R. H. **Probing the Mechanism of Water Oxidation**. *Acc. Chem. Res.* **1991** 24, 311-316
- 5) Alstrum-Acevedo, J. H.; Brennaman, M. K.; Meyer, T. J. *Inorg. Chem.* **2005**, 3446802-27. Meyer, T. J.; Huynh, M-H. V.; Thorp, H. H. **The Possible Role of Proton Coupled Electron Transfer (PCET) in Water Oxidation by Photosystem II** *Angew. Chem., Int. Ed.* **2007**, 46, 5284-5304
- 6) Stubbe, J.; Nocera, D. G.; Yee, C. S.; Chang, M. C. Y. **Radical initiation in the Class I ribonucleotide reductase: long-range proton-coupled electron transfer?** *Chem Rev* **2003**, 103 2167-2202
- 7) Baraj, G. **Free Radicals and Aging** *J. Neurosci.* **2004**, 27, 595-600
- 8) Chan, P. H. **Reactive Oxygen Radicals in Signaling and Damage in the Ischemic Brain**. *J. Cereb. Blood Flow Metals.* **2001**, 21, 2-14
- 9) Fancchinetti, F.; Dawson, V. L.; Dawson, T. M. **Free Radicals as mediators of neuronal injury**. *Cell, Mol. Neurobiol.* **1998**, 18, 667-82
- 10) Mattson, M. P.; Pederson, W. A.; Duan, W.; Culmsee, C.; Camanola, S. **Cellular and molecular mechanisms underlying perturbed energy metabolism and neuronal degeneration in Alzheimer's and Parkinson's diseases**. *Ann. NY Acad. Sci.* **1999**, 893, 154-75
- 11) Steenken, S.; Javanovic, S.V **How Easily Oxidizable Is DNA? One-Electron Reduction Potentials of Adenosine and Guanosine Radicals in Aqueous Solution** *J. Am. Chem. Soc.* **1997**, 119, 617-618
- 12) Hammes-Schiffer, S.; Hatcher, E.; Ishikita, H.; Skone, J. H.; Soudackov, A. V. **Theoretical Studies of Proton Coupled Electron Transfer: Models and Concepts Relevant to Bioenergetics**. *Coord. Chem. Revs.* **2008**, 252, 384-394.

- 13) Rhile, I. J.; Markle, T. F.; Nagao, H.; DiPasquale, A. G.; Lam, O. P.; Lockwood, M. A.; Rotter, K.; Mayer, J. M. **Concerted Proton-Electron Transfer in the Oxidation of Hydrogen-Bonded Phenols** *J. Am. Chem. Soc.* **2006**, *128*, 6075-6088.
- 14) Chang, C. J.; Chang, M. C. Y.; Damrauer, N. H.; Nocera, D. G. **Models for Proton Coupled Electron Transfer in Photosystem II** *Biochim. Biophys. Acta-Bioenerg.* **2004**, *1655*, 13
- 15) Hammes-Schiffer, S.; Iordanova, N. **Theoretical Perspectives on Proton Coupled Electron Transfer Reactions** *Biochim Biophys Acta*, **2004**, *1655*, 29-36
- 16) Cukier, R. I. **Proton Coupled Electron Transfer** *J. Phys. Chem.* **1996**, *100*, 15428-15443.
- 17) Abo-Riziq, A.; Grace, L.; Nir, E.; Kabelac, M.; Hobza, P.; deVries, M.S. **Vibrational spectroscopy of the G...C base pair: experiment, harmonic and anharmonic calculations, and the nature of the anharmonic couplings.** *Proc. Natl. Acad. Sci. U.S.A.* **2005**, *102*, 20-23
- 18) Sobolewski, A.L.; Domcke, W; Hattig, C. **Tautomeric selectivity of the excited-state lifetime of guanine/cytosine base pairs: the role of electron-driven proton-transfer processes.** *Proc. Natl. Acad. Sci. U.S.A.* **2005**, *102*, 17903-06
- 19) Sun, Lixiang; Bu, Yuxiang **Marked variations of dissociation energy and H-bond character of the guanine-cytosine base pair induced by one-electron oxidation and Li<sup>+</sup> cation coupling.** *J. Phys. Chem. B.* **2005** *109*, 593-600
- 20) Ghosh, A. K.; Schuster, G. B. **Role of the guanine N1 imino proton in the migration and reaction of radical cations in DNA oligomers.** *J. Am. Chem. Soc.* **2006**, *128*, 4172-73
- 21) Ekberg, M.; Potsch, S.; Sadin, E.; Thunnissen, M.; Nordlund, P.; Sahlin, M.; Sjoberg, B.-M. **Preserved Catalytic Activity in an Engineered Ribonucleotide Reductase R2 Protein with a Nonphysiological Radical Transfer Pathway. The Importance of Hydrogen Bond Connections between the Participating Residues.** *J. Biol. Chem.* **1998**, *273*, 21003-21008
- 22) Persson, A. L.; Eriksson, M.; Katterle, B.; Potsch, S.; Sahlin, A.; Sjoberg, B.-M. **A New Mechanism-based Radical Intermediate in a Mutant R1 Protein Affecting the Catalytically Essential Glu<sup>441</sup> in *Escherichia coli* Ribonucleotide Reductase** *J. Biol. Chem.* **1997** *272*, 31533-31541
- 23) Constantin, C. **Electrochemical Approach to the Mechanistic Study of Proton Coupled Electron Transfer.** *Chem. Rev.* **2008**, *108*, 2145-2179

- 24) Weatherly, S. C.; Yang, I. V.; Thorp, H. H. **Proton-coupled electron transfer in duplex DNA: driving force dependence and isotope effects on electrocatalytic oxidation of guanine.** *J. Am. Chem. Soc.* **2001**, *123*, 1236-37
- 25) a) Sjödin, M.; Styring, S.; Akermark, B.; Sun, L.; Hammerstrom, L. **Proton-Coupled Electron Transfer from Tyrosine in a Tyrosine-Ruthenium-tris-Bipyridine Complex Comparison with Tyrosine<sub>z</sub> Oxidation in Photosystem II:** *J. Am. Chem. Soc.* **2000** *122*, 3932 b) Sjödin, M.; Styring, S.; Wolpher, H.; Xu, Y.; Sun, L.; Hammarström, L. **Switching the Redox Mechanism: Models for Proton-Coupled Electron Transfer from Tyrosine and Tryptophan** *J. Am. Chem. Soc.* **2005**, *127*, 3855-3863. c) Costenin, C.; Robert, M.; Saveant, J. **Electrochemical and Homogeneous Proton-Coupled Electron Transfers: Concerted Pathways in the One-Electron Oxidation of a Phenol Coupled with an Intramolecular Amine-Driven Proton Transfer.** *J. Am. Chem. Soc.* **2006**, *128*, 4552-53.
- 26) Johnston, D. H.; Glasgow, K. C.; Thorp, H. H. **Electrochemical Measurement of the Solvent Accessibility of Nucleobases Using Electron Transfer between DNA and Metal Complexes.** *J. Phys. Chem. B.* **2000**, *117*, 8933-3938
- 27) Armistead, P. M.; Thorp, H. H. **Oxidation Kinetics of Guanine in DNA Molecules Adsorbed onto Indium Tin Oxide Electrodes** *Anal. Chem.* **2001**, *73*, 558-564
- 28) a) Fecenko, C. J.; Meyer, T. J.; Thorp, H. H. **Electrocatalytic Oxidation of Tyrosine by Parallel Rate-Limiting Proton Transfer and Multisite Electron-Proton Transfer.** *J. Am. Chem. Soc.* **2006**, *128*, 11020-11021. b) Fecenko, C. J.; Thorp, H. H.; Meyer, T. J. **The Role of Free Energy Change in Concerted Electron Proton Transfer** *J. Am. Chem. Soc.*, **2007**, *129*, 15098-15099
- 29) Rudolph, M.; Reddy, D. P.; Feldberg, S. W. **A Simulator for Cyclic Voltammetric Responses** *Anal. Chem.* **1994**, *66*, 589A-600A.
- 30) Bard, A. J.; Faulkner, L. R. **Electrochemical Methods: Fundamentals and Applications**; John Wiley and Sons, Inc., Hoboken, NJ **2004**.

## Chapter 2

### **The Oxidation of Tyrosine through Parallel Rate-Determining Deprotonation and MS-EPT**

Reproduced with permission from the American Chemical Society  
Christine J. Fecenko, Thomas J. Meyer, H. Holden Thorp **The Oxidation of Tyrosine through Parallel Rate-Determining Deprotonation and MS-EPT.** *Journal of the American Chemical Society* **2006**, *128*, 11020-11021 © 2006 American Chemical Society

## 2.1 Abstract:

The oxidation of the amino acid tyrosine and tryptophan by complexes based on  $M(\text{bpy})_3^{3+}$  ( $M = \text{Ru}, \text{Os}$ ) was studied by monitoring the cyclic voltammetry of the metal complex in the presence of electroactive amino acids. Addition of both amino acids to aqueous solutions of the metal complexes in phosphate buffer produced electrocatalytic enhancement in the oxidative wave observed at indium tin oxide electrodes. The kinetics for the oxidation by the Ru(III) and Os(III) forms was determined by digital simulation. The oxidation kinetics for tryptophan were consistent with outer-sphere electron transfer, giving an expected dependence of the oxidation rate constant on the reduction potential of the metal complex. In contrast, oxidation of tyrosine at pH 7.5 did not give an appreciable dependence on the metal complex potential. These results were explained by a mechanism involving preassociation of tyrosine with the base form of the buffer ( $\text{HPO}_4^{2-}$ ). After association with the base, the oxidation of tyrosine can occur through three competitive oxidation pathways depending on solution conditions: electron transfer followed by proton transfer (ET-PT), rate-limiting proton transfer followed by electron transfer (PT-ET), and concerted electron proton transfer (EPT). In the absence of base, the ET-PT pathway dominates and kinetics are slow. Significant rate enhancement occurs in the presence of base. Kinetic isolate methods through alteration of acid and base concentrations in solution allow for distinction between the PT-ET and EPT pathway with the PT-ET pathway dominating at high base concentrations and low acid concentrations and the EPT pathway dominating at low concentrations of base and high concentrations of acid. Rate constants and isotope effects have been isolated under limiting conditions and support the presence of competitive kinetics in phosphate buffered solutions. These results suggest that tyrosine oxidation in enzymes can access both proton pathways

(PT-ET and EPT) depending on the solvent accessibility of the oxidized residue and the availability of a suitable proton acceptor.

## 2.2 Introduction:

Oxidation of the tyrosine phenol to its deprotonated, neutral radical is a critical step in numerous enzymatic processes.<sup>1-5</sup> In enzymes, loss of an electron is believed to accompany proton transfer to an available proton acceptor residue.<sup>6</sup> In photosystem II, for example, oxidation of  $Y_z$  is thought to occur through a proton coupled electron transfer mechanism with transfer of a proton to His 190.<sup>5,7</sup> Proton coupled electron transfer (PCET) reactions involve the net movement of a proton and an electron.<sup>7</sup> Knowledge of whether this PCET occurs via concerted electron proton transfer (EPT) or sequential electron-proton transfers is of importance in understanding how these reactions occur.<sup>2</sup> A concerted EPT avoids build-up of charged species in over the course of the reaction. However, the microscopic demands of the concerted reaction are greater because of the requirement for moving the proton and the electron simultaneously. A reaction that proceeds through a step-wise reaction involving initial deprotonation of the tyrosine would be controlled by the availability of a suitable base with less demand on the precise nature of the oxidant. Like-wise, a reaction that proceeds through a step-wise electron transfer followed by proton transfer would be controlled by the strength of the oxidant and not by the availability of a proton acceptor.

The oxidation of complex organic redox donors, such as guanine, is conveniently studied via electrocatalysis utilizing metal complexes, such as  $M(\text{bpy})_3^{2+}$  ( $M=\text{Ru}, \text{Fe}, \text{Os}$ ), ( $\text{bpy} = 2,2'$ -bipyridine) at indium tin oxide (ITO) electrodes in neutral solution.  $E^{o'}$  values for  $M(\text{bpy})_3^{3+}$  oxidants range from 0.85 V(vs NHE) ( $M = \text{Os}$ ) to 1.26 V ( $M = \text{Ru}$ ).<sup>10,11</sup> Rate constants for the homogeneous electron transfer between the organic donor and oxidant can be analyzed through digital simulation of the cyclic voltammograms.<sup>11</sup> Amino acid oxidation was studied in aqueous solution at ITO electrodes and the influence of added reductant

(tyrosine and tryptophan), oxidant  $(M(\text{bpy})_3^{3+})$ , and added base on cyclic voltammetric waveforms was analyzed by digital simulation to yield kinetic parameters for each amino acid.<sup>12</sup> The electrochemical results provide new insights into the intimate details of the coupling of electron and proton transfer in amino acid oxidation.

### **2.3 Methods and Materials:**

2.3.1 General: Deionized water was purified by passing in-house distilled water through a MilliQ (18 $\Omega$ ) deionizing system and was used to prepare all aqueous solutions. All buffers and tyrosine were purchased from Sigma-Aldrich as well. Metal complexes were prepared previously or purchased from Sigma Aldrich and purified by recrystallization. The purity of the sample was verified by UV-visible measurements and  $^1\text{H}$  NMR measurements.

2.3.2 Preparation of buffers: Buffers were prepared as a stock solution of 0.5M buffer and diluted to the appropriate concentration with MilliQ water. The concentration of buffer components was calculated based on the Henderson Hasselbach equation. The  $\text{pK}_a$  values used in the calculations are standard values for each buffer in aqueous solution. The pH was verified by using a digital pH meter (Fischer Scientific Accumet AB 15 plus) with pH adjusted by adding HCl or NaOH. Studies with no buffer were prepared by using MilliQ water alone. The pH of stock solutions was verified by using a digital pH monitor with adjustments made by adding HCl or NaOH and then diluting to the appropriate base concentration by using MilliQwater.

2.3.3 Isotope Studies: Deuteriated tyrosine was prepared by dissolving protonated tyrosine in  $\text{D}_2\text{O}$  and deprotonating by adding NaOD. The pD ( $\text{pH} + 0.4$ ) of the solution was decreased to pD 7.0 by adding DCl (5M in  $\text{D}_2\text{O}$ ). The d-tyrosine was isolated by a distillation method that left the d-tyrosine in the bottom of the reaction flask. Proton content was monitored by

$^1\text{H-NMR}$ . Deuteriated buffers were prepared similarly and isolated through distillation. The deuteriated components were subsequently re-dissolved in  $\text{D}_2\text{O}$  and used in the voltammetric studies.

2.3.4 Sample Preparation. After establishing the rate law dependence on tyrosine and metal complex concentrations, the tyrosine concentration was held constant at  $100\mu\text{M}$ , and the concentration of complex at  $20\mu\text{M}$ . Ionic strength was held constant by use of  $800\text{ mM}$  added  $\text{NaCl}$  throughout the study. The absolute concentration, base to acid ratio, was held constant in all pH studies, while the actual concentration in solution was varied from  $10\text{-}500\text{ mM}$ .

2.3.5 Electrochemistry: Electrochemical experiments were performed by using a BAS100B/W series potentiostat. Electrochemical experiments were performed in a three electrode cell. The working electrode was indium tin oxide (ITO) coated glass electrode with a reaction area of  $0.32\text{cm}^2$  was purchased from Delta Technologies (Stillwater, MN). The reference electrode was a teflon coated  $\text{Ag/AgCl}$  micro-electrode purchased from Cypress Systems, Inc (Lawrence, KS). The auxiliary electrode was platinum wire purchased from Sigma Aldrich (St. Louis, MO). The auxiliary electrode was wrapped around the base of the Teflon on the reference electrode. ITO electrodes were treated before use by sonication in MilliQ water for 15 minutes, isopropanol for 15 minutes, and two washes with MilliQ water for 15 minutes each. ITO electrodes were laid flat and allowed to dry overnight. Experimental volumes were typically  $50\mu\text{L}$ . The potential was swept in a positive potential direction from 0 to up to  $1.3\text{V}$ . The ITO electrode was conditioned for 6 consecutive scans in phosphate buffer solution before the first measurement. A final background scan was taken. A scan of buffer plus metal complex was run next, then finally a

scan of buffer and 20 $\mu$ M metal complex with 100 $\mu$ M reductant (tyrosine). After a scan of buffer with oxidant and reductant was taken, the ITO electrode was discarded and a new electrode was used for the next sample. Cyclic voltammograms (CV) were background corrected by subtracting buffer alone scans from CV's of metal and metal + reductant.

2.3.6 Digital Simulation: Digital simulations were performed by using the DigiSim software package purchased from BioAnalytical Systems (West Lafayette, IN). The diffusion coefficients used were 6.0x10<sup>-6</sup> cm<sup>2</sup>/s for Ru(bpy)<sub>3</sub><sup>2+/3+</sup>, 3.0x10<sup>-5</sup> cm<sup>2</sup>/s<sup>2</sup> for tyrosine. The reduction potential of the metal, complex (E<sup>o</sup> = 0.85 V vs NHE in 0.05M phosphate and 0.8M NaCl at 23 $\pm$ 2 $^{\circ}$ C) and the heterogeneous electron transfer rate constant (k<sub>s</sub> = 0.01cm/s) were obtained by fitting cyclic voltammograms of the metal complex alone in solution.

The general rate law for the mechanism in Scheme 1 in the text. The observed rate constant (k<sub>obs</sub>) is given by equation 1,

$$\frac{k_{obs}}{[\text{TyrOH}]} = \left( K_A K_A' k_{red} + \frac{K_A k_1 k_2}{k_{-1} [\text{H}_2\text{PO}_4^-] + k_2 [\text{Os}^{3+}]} \right) [\text{HPO}_4^{2-}] \quad (1)$$

Limiting forms of the rate law allow for kinetic isolation of each base catalyzed pathway. Under conditions of high acid and low base, the equilibrium that dictates deprotonation is pushed to the left, and reactivity through the deprotonation pathway is thermodynamically unfavored. This means the k<sub>-1</sub> <<< k<sub>2</sub> and K<sub>A</sub>[HPO<sub>4</sub><sup>2-</sup>] < 1 and results in isolation of the MS-EPT pathway independently. In this limit the MS-EPT pathway simplifies to eq 2.

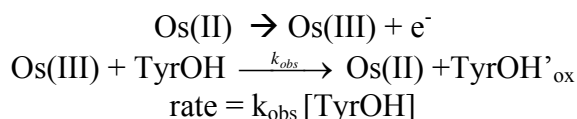
$$\frac{k_{obs}}{[\text{TyrOH}]} = K_A K_A' k_{red} [\text{HPO}_4^{2-}] \quad (2)$$

In the limit where  $k_2 \ll k_1[\text{H}_2\text{PO}_4^-]$ , the rate law simplifies to eq 4 and the PT-ET pathway dominates reactivity.

$$\frac{k_{\text{obs}}}{[\text{TyrOH}]} = k_1[\text{HPO}_4^{2-}] \quad (3)$$

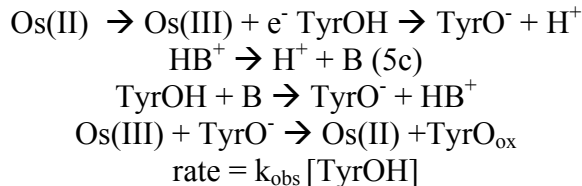
The cyclic voltammetric data were fit to DigiSim by assuming the electrochemical mechanism in Scheme 1. Oxidation of tyrosine occurs by  $1 e^-$  followed by dimerization consistent with the value of  $n = 1$  used in the fits for the MS-EPT pathway of:

Scheme 1



and the electrochemical mechanism expressed in Scheme 2 for the deprotonation pathway.

Scheme 2



Limiting conditions were achieved in the electrocatalytic analysis through alteration of acid ( $\text{H}_2\text{PO}_4^-$ ) and base ( $\text{HPO}_4^-$ ). For the MS-EPT pathway, with  $\text{H}_2\text{PO}_4^-/\text{HPO}_4^{2-}$  as buffer and with TyrOH in pseudo first order excess, this was achieved under conditions where the buffer acid concentration was in a 10:1 excess over the base form. Under these conditions  $k_{\text{obs}}$  from the simulations is given by  $k_{\text{obs}} = k_{\text{red}}K_A K_A'[\text{TyrOH}]$  with the product  $k_{\text{red}}K_A K_A'$  obtained from the slopes of plots of  $k_{\text{obs}}$  vs. [adduct]. For the PT-ET pathway, isolation was achieved at a 15:1 excess of  $\text{HPO}_4^{2-}$ . Under these conditions,  $k_{\text{obs}}$  from the simulations is given by  $k_{\text{obs}} = K_A k_1$ . At higher concentrations of TyrOH,  $> 0.001\text{M}$ , saturation kinetics are observed allowing separation of  $K_A' k_{\text{red}}$  and  $K_A$ . At high concentrations of both TyrOH and

$\text{Os}(\text{bpy})_3^{2+}$ , onset of a second region of saturation kinetics allows for the separation of  $k_{\text{red}}$  and  $K_A'$ .

2.3.7  $^{31}\text{P}$  NMR:  $^{31}\text{P}$  NMR was used to independently verify the existence of the proposed association complex between TyrOH and  $\text{HPO}_4^{2-}$  in Scheme 1. Solutions containing the  $\text{HPO}_4^{2-}/\text{H}_2\text{PO}_4^-$  buffer ( $1.0 \times 10^{-4}$ - $1.0 \times 10^{-3}$  M) and tyrosine in pseudo first order excess ( $2.0 \times 10^{-2}$  M) were prepared in  $\text{D}_2\text{O}$ . A background  $^{31}\text{P}$  NMR spectrum was taken with phosphate alone in solution and another with added tyrosine. A single  $^{31}\text{P}$  chemical shift was observed whose chemical shift was concentration dependence consistent with the rapid exchange limit. Spectra were recorded and an small increase in chemical shift observed for solutions of increasing tyrosine concentration with measurements made up to a 1:1 ratio of tyrosine to dibasic phosphate. The association constant was calculated based on literature sources outlining the calculation of association constants from NMR data (Equation 4).

$$\frac{1}{\Delta\delta_{\text{obs}}} = \frac{1}{K_A (\delta_{\text{complex}} - \delta_{\text{TyrOH}})} \cdot \frac{1}{[\text{HPO}_4^{2-}]} + \frac{1}{\delta_{\text{complex}} - \delta_{\text{TyrOH}}} \quad (4)$$

2.3.8 Mixing studies:  $\text{Os}(\text{bpy})_3^{3+}$  in water was prepared by bubbling  $\text{Cl}_2$  gas through the solution. The solution changed from dark green to red. Chlorine gas was bubbled through the reaction vessel to maintain  $\text{Os}(\text{bpy})_3^{3+}$  and avoid re-reduction to  $\text{Os}(\text{bpy})_3^{2+}$ , before use in UV/visible experiments, the reaction cell is purged with argon gas to ensure removal of excess  $\text{Cl}_2$ .  $\text{Os}(\text{bpy})_3^{3+}$  decomposition was monitored by UV/visible analysis and was not found to be on the time scale of the experiment under all solution conditions. The reaction was monitored by UV/vis measurements and disappearance of the absorption at  $\lambda_{\text{max}} = 490$  nm for  $\text{Os}(\text{bpy})_3^{2+}$ . Once oxidation was complete, the solutions containing  $\text{Os}(\text{bpy})_3^{3+}$  were used as a stock solution. The initial concentration of complex was determined by UV/vis

measurements and the known molar extinction coefficient at 490 nm ( $\epsilon=12,400\text{M}^{-1}\text{cm}^{-1}$ ).

Excess chlorine gas was removed from solution through purging the solution with argon gas.

In the absence of added bases, oxidation of TyrOH by  $\text{Os}(\text{bpy})_3^{3+}$  is too slow for electrochemical monitoring. Under these conditions rate constants and rate laws for TyrOH oxidation were monitoring spectrophotometrically following conventional mixing by using pseudo first order conditions in TyrOH as in the electrochemical experiments. Solutions of  $1.0 \times 10^{-3}\text{M}$ - $10^{-4}\text{M}$  TyrOH were mixed with varying amounts of  $\text{Os}(\text{bpy})_3^{3+}$  ( $1.0 \times 10^{-5}\text{M}$ - $1.0 \times 10^{-4}\text{M}$ ) and the time of conversion from Os(III) to Os(II) monitored spectrophotometrically at 490 nm. Kinetic parameters were determined through using Equation 5. Values of  $k_{\text{ET}}' = k_{\text{ET}}K_{\text{A}}$  were obtained from the slopes of plots of  $k_{\text{obs}}$  vs [TyrOH].

$$\text{Ln} \left[ \frac{(\text{Abs}_{\infty} - \text{Abs}_t)}{(\text{Abs}_{\infty} - \text{Abs}_0)} \right] = k_{\text{obs}} t \quad (5)$$

## 2.4 Results and Discussion:

2.4.1 Electrocatalysis Studies in Phosphate: The addition of tyrosine and tryptophan to aqueous solutions of the  $\text{M}(\text{bpy})_3^{2+}$  complexes  $\text{Os}(\text{bpy})_3^{2+}$ ,  $\text{Fe}(\text{bpy})_3^{2+}$ ,  $\text{Ru}(4,4'\text{-dimethyl-bpy})_3^{2+}$ ,  $\text{Ru}(\text{bpy})_2(4,4'\text{-dimethyl-bpy})^{2+}$ , and  $\text{Ru}(\text{bpy})_3^{2+}$  resulted in enhancement of the oxidative wave. For tryptophan, the dependence of  $k$  on the redox potential of the metal complex oxidant over the range 0.83 to 1.25 V (vs. NHE) displayed a predicted Marcus dependence with  $\text{RTln}k_{\text{obs}}$  increasing with  $E^{\circ}$  with a slope of 0.42 (Figure 1), consistent with outer-sphere, one-electron oxidation.<sup>13, 14</sup> By contrast, oxidation of tyrosine at pH 7.5 proceeded with no detectable dependence on the redox potential of the oxidant (Figure 1), suggesting that electron transfer was not involved in the rate-determining step. Further,

increases in the phosphate buffer concentration increased the catalytic current (Figure 2) up to 50 mM with limiting currents observed at phosphate concentrations around 80 mM.

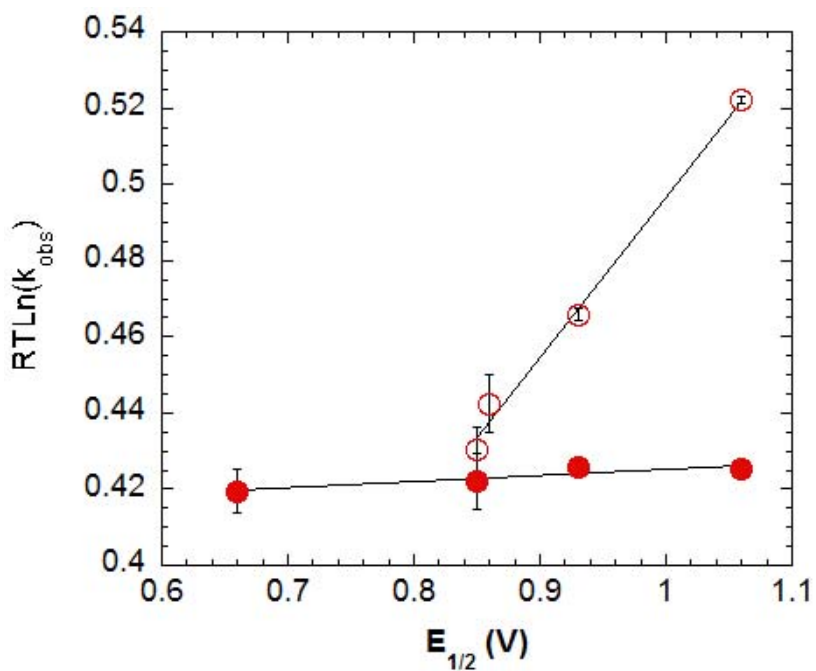


Figure 1: Plot of  $RT\ln(k_{obs})$  vs midpoint potential of the oxidant at pH 6.0 (open circles) and pH 7.5 (closed circles) at  $23\pm 2^\circ\text{C}$  in 0.8M NaCl. At pH 7.5, as the oxidant potential increased, there was no effect on the rate of reaction as indicated by a minimal slope of 0.025. At pH 6.0, the slope of the line equals 0.25, and the increase in slope indicates the metal complex is playing a role in reaction rate.

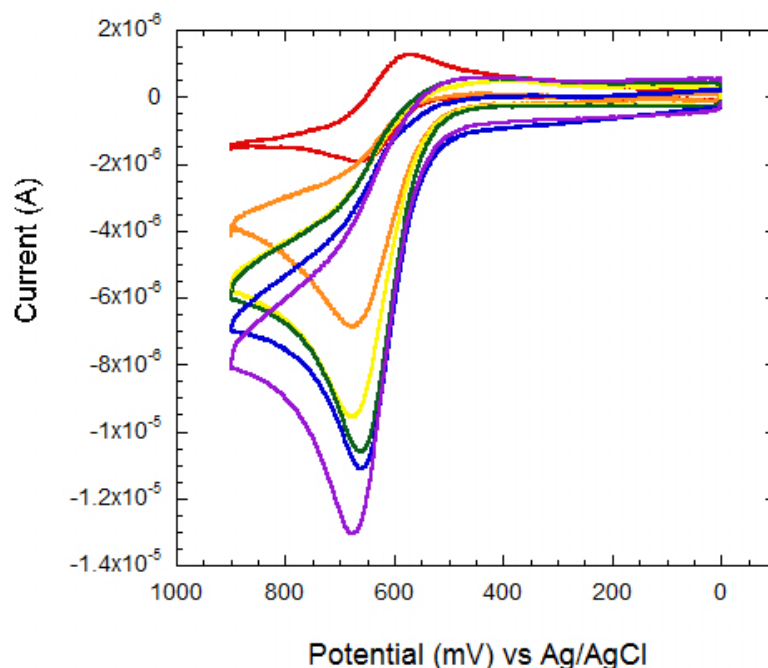
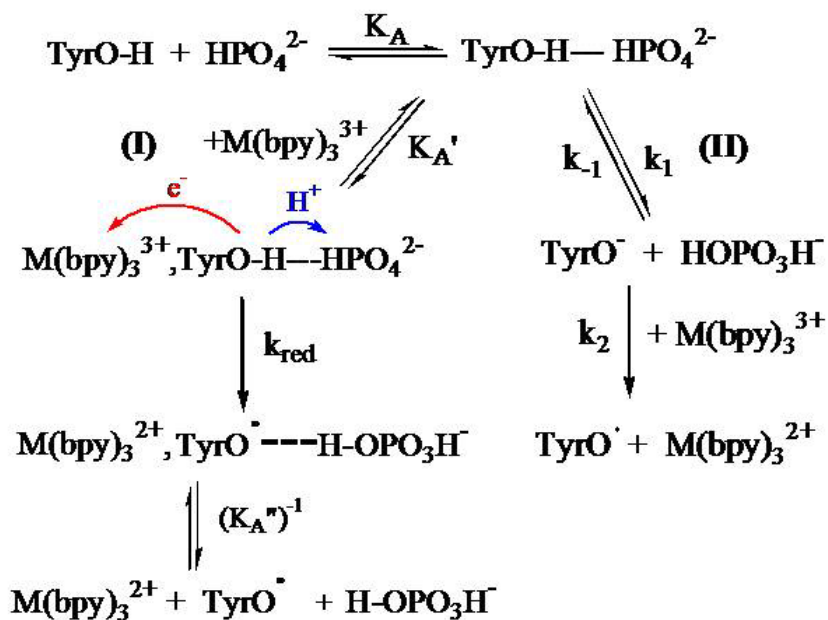


Figure 2: Cyclic voltammograms of  $\text{Os}(\text{bpy})_3^{2+}$  (0.02mM) in the presence of 0.1mM tyrosine and increasing concentrations of phosphate buffer (10-50mM) at pH 7.5 at  $23\pm 2^\circ\text{C}$  in 0.8 NaCl

2.4.2 Kinetic Studies on Tyrosine: The reaction of tyrosine with  $\text{Os}(\text{bpy})_3^{2+}$  was investigated over a wide range of tyrosine and complex concentrations and buffer ratios. The results of this study revealed the rate law in eq 6a in which  $[\text{TyrOH}]_T$  is the total concentration of tyrosine. This rate law is consistent with the mechanism in Scheme 1 with the observed rate described by eq 6b. In Scheme 3 oxidation of a hydrogen-bonded tyrosine intermediate occurs by parallel pathways, one involving EPT ( $K_A k_{\text{red}}$ ) and the other, initial deprotonation ( $k_1, k_2$ ). Rate and equilibrium constants for the two bases are listed in Table 1.

Scheme 3



$$\frac{d[\text{Os}^{2+}]}{dt} = \left[ \frac{K_A [\text{TyrOH}]_T [\text{HPO}_4^{2-}]}{1 + K_A [\text{H}_2\text{PO}_4^-]} \right] [\text{Os}^{3+}] \left( K_A' k_{\text{red}} + \frac{k_1 k_2}{k_{-1} [\text{H}_2\text{PO}_4^-] + k_2 [\text{Os}^{3+}]} \right) \quad (6a)$$

$$\frac{d[\text{Os}^{2+}]}{dt} = k_{\text{obs}} [\text{TyrOH}] [\text{Os}^{3+}] \quad (6b)$$

Base	pK <sub>A</sub>	K <sub>A</sub> (M <sup>-1</sup> )	k <sub>1</sub> (s <sup>-1</sup> )	k <sub>-1</sub> (M <sup>-1</sup> s <sup>-1</sup> )	k <sub>2</sub> (M <sup>-1</sup> s <sup>-1</sup> )	K <sub>A</sub> ' (M <sup>-2</sup> )	k <sub>red</sub> (s <sup>-1</sup> )
HPO <sub>4</sub> <sup>2-</sup>	7.2	30.0±0.1	3.3±0.1×10 <sup>5</sup>	7.8±0.4×10 <sup>9</sup>	1.7±0.3×10 <sup>7</sup>	22.2±0.1	9.6±0.5×10 <sup>4</sup>

Table 1: Table of rate and equilibrium constants in phosphate buffer with 0.8M NaCl at 23±2°C

The rate law in eq 6 was verified through several observations. Saturation kinetics were observed at concentrations of base greater than 50mM indicating the formation of the association complex with HPO<sub>4</sub><sup>2-</sup>. In the limit with k<sub>-1</sub>≪k<sub>2</sub>, and the term k<sub>1</sub> dominates, the oxidative current is zero order in metal complex (Figure 3). (3) In the limit where k<sub>-1</sub>≫k<sub>2</sub>,

$K_A k_{\text{red}}$  dominates the rate law, and the dependence of the rate constant ( $k_{\text{obs}}$ ) on the reduction potential ( $E^{\circ}$ ) reappears. This observation is reflected in plots of  $\text{RTln}(k_{\text{obs}})$  vs  $E^{\circ}$  shows an increasing trend with a slope of  $m=0.25$  (Figure 4). When the reaction with added  $\text{HPO}_4^{2-}$  was performed in  $\text{D}_2\text{O}$  a quadratic dependence on the mole fraction of  $\text{D}_2\text{O}$  was found indicating the involvement of 2 protons in the reaction. Under these kinetic limits,  $\text{H}_2\text{O}/\text{D}_2\text{O}$  isotope effects of  $1.7\pm 0.1$  and  $1.0\pm 0.1$  for  $K_A$  and  $K_A'$  were observed and  $2.1\pm 0.6$  and  $1.2\pm 0.4$  for  $k_{\text{red}}$  and  $k_1$  summarized in table 2. Bulk electrolysis in  $\text{HPO}_4^{2-}/\text{H}_2\text{PO}_4^-$  occurs with  $n = 1$  consistent with radical coupling following one-electron oxidation. The catalytic effect of added base is considerable and studies in the absence of buffer were too slow to study on the electrochemical time scale. Oxidation of TyrOH by  $\text{Os}(\text{bpy})_3^{2+}$  followed by spectrophotometric monitoring in 0.8 M NaCl at room temperature ( $\text{pH} = 7$ ) occurs with  $k \sim 1.7 \times 10^2 \text{ M}^{-1}\text{s}^{-1}$ , which is slower by  $\sim 10^4$  than  $K_A K_A' k_{\text{red}}$  in Scheme 1 with added  $\text{HPO}_4^{2-}$  at neutral pH.

Base	$\text{pK}_A$	EIE $K_A$	KIE $k_1$	KIE $k_{\text{red}}$
$\text{HPO}_4^{2-}$	7.2	$1.7\pm 0.4$	$1.2\pm 0.4$	$2.1\pm 0.6$

Table 2: Table of kinetic and equilibrium isotope effects in deuterated phosphate buffer with 0.8M NaCl at  $23\pm 2^\circ\text{C}$ .

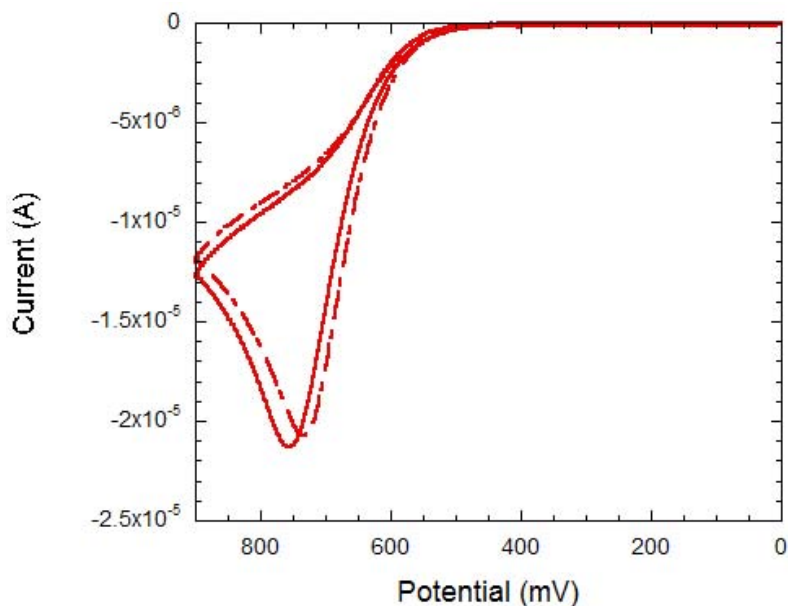


Figure 3: Cyclic voltammograms of 20 $\mu$ M (solid) and 40 $\mu$ M Os(bpy) $_3^{2+}$  in the presence of 0.1mM tyrosine in 50mM phosphate buffer (pH 8.5, [HPO $_4^{2-}$ /H $_2$ PO $_4^-$ ] = 15/1) at 23 $\pm$ 2 $^\circ$ C in 0.8M NaCl

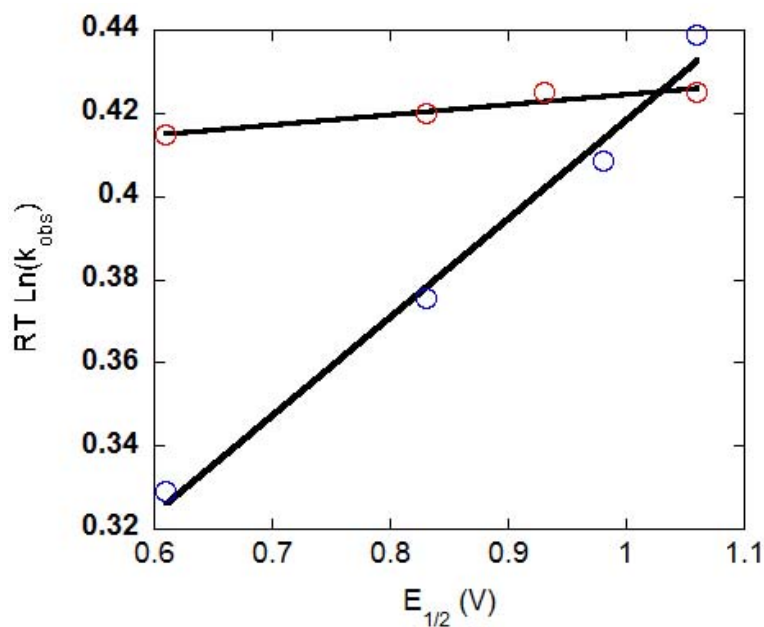


Figure 4: Plot of  $RT \ln(k_{obs})$  vs reduction potential ( $E^0$ ) of the oxidant at pH 6.0 (open circles) and pH 7.5 (closed circles) at 23 $\pm$ 2 $^\circ$ C in 0.8M NaCl. At pH 7.5, as the oxidant potential increased, there was no effect on the rate of reaction as indicated by a minimal slope of 0.025. At pH 6.0, the slope of the line equals 0.25, and the increase in slope indicates the metal complex is playing a role in reaction rate.

These results demonstrate that catalyzed oxidation of tyrosine in water occurs at a significant rate following association with the base form of the  $\text{H}_2\text{PO}_4^-/\text{HPO}_4^{2-}$  buffer, presumably forming H-bonded association complexes. Once formed, the association complexes can react either via concerted loss of electrons and protons (EPT),  $k_{\text{red}}$ , or by rate-limiting proton transfer followed by electron transfer (PT-ET) oxidation of the phenoxide anion, Scheme 1.

## 2.5 Conclusions:

In the EPT pathway, electron and proton transfers occur to separate acceptors, ( $\text{Os}(\text{bpy})_3^{3+}$  and  $\text{HPO}_4^{2-}$  in Scheme 1), and the reaction can be described as occurring by Multi Site-Electron Proton Transfer (MS-EPT).<sup>5</sup> It is important as a possible model for the tyrosine-histidine pair in photosystem II.<sup>5, 7, 15</sup>

Recent results on the oxidation of hydrogen-bonded phenols in acetonitrile also support a concerted reaction<sup>16</sup> as do voltammetric results on hydrogen bonded phenols in nonpolar solvent.<sup>17</sup> By contrast, in closely related studies, intramolecular oxidation of a phenol linked to a  $\text{Ru}(\text{bpy})_3^{2+}$  derivative has been found to respond to changes in the external pH at low concentrations of added buffer.<sup>18, 19</sup> Recent results, however, by Hammarstrom, Hammes-Schiffer and others have resulted in a rate law consistent with MS-EPT through a base acceptor in solution at high concentrations of buffer.<sup>19</sup>

Recent work on tryptophan supports an outersphere mechanism in phosphate buffer solution due to the high  $\text{pK}_a$  of tryptophan ( $\text{pK}_a = 16.4$ ). The free energy of EPT is thermodynamically unfavorable under the solution conditions described here-in due to the lack of a proton acceptor with a high enough  $\text{pK}_a$  to accept a proton from the imidazole group on the tryptophan.<sup>20</sup>

The observation of competing pathways suggests that enzymes may have the ability to tune kinetic pathways based on solvent accessibility of the oxidized tyrosine.<sup>12</sup> Such tunability may be critical in regulating enzyme kinetics and in allowing enzyme mechanisms to respond to proton gradients.

## 2.6 References:

1. Cukier, R. I.; Nocera, D. G. **Proton Coupled Electron Transfer** *Annu. Rev. Phys. Chem.* **1998**, *49*, 337-369.
2. Mayer, J. M. **Proton Coupled Electron Transfer: A Reaction Chemist's Perspective.** *Annu. Rev. Phys. Chem.* **2004**, *55*, 363-390.
3. Hammes-Schiffer, S. **Theoretical Perspectives on Proton Coupled Electron Transfer Reactions.** *Acc. Chem. Res.* **2001**, *34*, 273-281.
4. Brudvig, G. W.; Thorp, H. H.; Crabtree, R. H. **Probing the Mechanism of Water Oxidation in Photosystem II.** *Acc. Chem. Res.* **1991**, *24*, 311.
5. Alstrum-Acevedo, J.H.; Brennaman, M.K.; Meyer, T.J.; **Chemical Approaches to Artificial Photosynthesis.** *Inorg. Chem.* **2005**, *44*, 6802-6827; Meyer, T. J.; Huynh, M.-H. V.; Thorp, H. H. **The Possible Role of Proton Coupled Electron Transfer in Water Oxidation by Photosystem II** *Angew. Chem. Int. Ed.* **2007**, *46*, 5284-5304
6. Stubbe, J.; Nocera, D. G.; Yee, C. S.; Chang, M. C. Y. **Radical initiation in the Class I ribonucleotide reductase: long-range proton-coupled electron transfer?** *Chem. Rev.* **2003**, *103*, 2167-2202.
7. Tommos, C.; Babcock, G. T. **The protein environment appears to regulate the biological function of tyrosyl radicals** *Acc. Chem. Res.* **1998**, *31*, 18-25.
8. Johnston, D. H.; Glasgow, K. C.; Thorp, H. H. **Electrochemical Measurement of the Solvent Accessibility of Nucleobases Using Electron Transfer between DNA and Metal Complexes.** *J. Am. Chem. Soc.* **1995**, *117*, 8933-8938.
9. Napier, M. E.; Hull, D. O.; Thorp, H. H. **Electrocatalytic Oxidation of DNA-Wrapped Carbon Nanotubes.** *J. Am. Chem. Soc.* **2005**, *127*, 11952-11953.
10. Sistare, M. F.; Holmberg, R. C.; Thorp, H. H. **Electrochemical Studies of Polynucleotide Binding and Oxidation by Metal Complexes: Effects of Scan Rate, Concentration, and Sequence.** *J. Phys. Chem. B* **1999**, *103*, 10718-10728.
11. Armistead, P. M.; Thorp, H. H. **Oxidation Kinetics of Guanine in DNA Molecules Adsorbed onto Indium Tin Oxide Electrodes** *Anal. Chem.* **2000**, *72*, 3764-3770.
12. Di Bilio, A. J.; Crane, B. R.; Wehbi, W. A.; Kiser, C. N.; Abu-Omar, M. M.; Carlos, R. M.; Richards, J. H.; Winkler, J. R.; Gray, H. B. **Properties of Photogenerated Tryptophan and Tyrosyl Radicals in Structurally Characterized Proteins Containing Rhenium(I) Tricarbonyl Diimines.** *J. Am. Chem. Soc.* **2001**, *123*, 3181-3182.

13. Bock, C. R.; Connor, J. A.; Gutierrez, A. R.; Meyer, T. J.; Whitten, D. G.; Sullivan, B. P.; Nagle, J. K. **Estimation of excited-state redox potentials by electron-transfer quenching. Application of electron-transfer theory to excited-state redox processes.** *J. Am. Chem. Soc.* **1979**, *101*, 4815-4824.
14. Marcus, R. A. **Chemical and Electrochemical Electron Transfer** *Theory Annu. Rev. Phys. Chem.* **1964**, *15*, 155-196.
15. L. Biczok, L.; Gupta, N; Linschitz, H. **Coupled Electron-Proton Transfer in Interactions of Triplet C<sub>60</sub> with Hydrogen-Bonded Phenols: Effects of Solvation, Deuteration, and Redox Potentials.** *J. Am. Chem. Soc.* **1997**, *119*, 12601-12609
16. Rhile, I. J.; Mayer, J. M. **One-Electron Oxidation of a Hydrogen-Bonded Phenol Occurs by Concerted Proton-Coupled Electron Transfer** *J. Am. Chem. Soc.* **2004**, *126*, 12718-12719.
17. Costentin, C.; Robert, M.; Saveant, J. **Electrochemical and Homogeneous Proton-Coupled Electron Transfers: Concerted Pathways in the One-Electron Oxidation of a Phenol Coupled with an Intramolecular Amine-Driven Proton Transfer.** *J. Am. Chem. Soc.* **2006**, *128*, 4552-53.
18. Sjödin, M.; Styring, S.; Wolpher, H.; Xu, Y.; Sun, L.; Hammarström, L. **Switching the Redox Mechanism: Models for Proton-Coupled Electron Transfer from Tyrosine and Tryptophan** *J. Am. Chem. Soc.* **2005**, *127*, 3855-3863.
19. a) Irebo, T.; Reece, S. Y.; Sjödin, M.; Nocera, D. G.; Hammarström, L. **Proton-Coupled Electron Transfer of Tyrosine Oxidation: Buffer Dependence and Parallel Mechanisms** *J. Am. Chem. Soc.* **2007**, *129*, 15462-15464. b) Costentin, C.; Robert, M.; Saveant, J. M. **Concerted Proton-Electron Transfer Reactions in Acts as Proton Donor or Acceptor?** *J. Am. Chem. Soc.* **2007**, *129*, 5870-5879. c) Ishikita, H.; Soudackov, A. V.; Hammes-Schiffer, S. **Buffer-Assisted Proton-Coupled Electron Transfer in a Model Rhenium-Tyrosine Complex.** *J. Am. Chem. Soc.* **2007**, *129*, 11146-11152.
20. a) Gagliardi, C.; Thorp, H. H.; Meyer, T. J. **2008**, unpublished results. b) Fecenko, C. J.; Thorp, H. H.; Meyer, T. J. **The Role of Free Energy Change in Concerted Electron Proton Transfer.** *J. Am. Chem. Soc.* **2007**, *129*, 15098-15099.

## Chapter 3

### **Coupled Electron-Proton Transfer Pathways in Tyrosine Oxidation**

Reproduced with permission of the American Chemical Society  
Christine F. Murphy, H. Holden Thorp, Thomas J. Meyer **Coupled Electron-Proton  
Transfer Pathways in Tyrosine Oxidation** *J. Am. Chem. Soc.* **2009**, *submitted*. © American  
Chemical Society 2009

### 3.1 Abstract

Catalytic enhancements occur in cyclic voltammograms for the oxidative waves for,  $[M(\text{bpy})_3]^{2+} \rightarrow [M(\text{bpy})_3]^{3+}$  (bpy is 2,2'-bipyridine; M = Fe, Ru, Os), in the presence of tyrosine with added aqueous buffers at ITO electrodes. Analysis of these data over a wide range of tyrosine, metal complex, and buffer concentrations and buffer ratios reveal a complex catalytic mechanism involving prior association between the base form of the buffer (B) and tyrosine,  $\text{TyrOH} \rightleftharpoons \text{B}$ . Complex formation is followed by: 1) Initial loss of a proton to give  $\text{TyrO}^-$  followed by its oxidation by electron transfer (PT-ET); 2) Further association with oxidant  $[M(\text{bpy})_3]^{3+}$  followed by simultaneous transfer of a proton to the base and electron to the oxidant in a Multiple Site-Electron Proton Transfer (MS-EPT) step. All of the rate and equilibrium constants in this mechanism have been resolved for the series of oxidants and a family of buffer bases ranging from from acetic acid ( $\text{pK}_a = 4.7$ ) to Tris ( $\text{pK}_a = 8.1$ ). The kinetics of oxidation of both tyrosine and tyrosyl anion by  $[M(\text{bpy})_3]^{3+}$  in the absence of buffer have also been investigated.

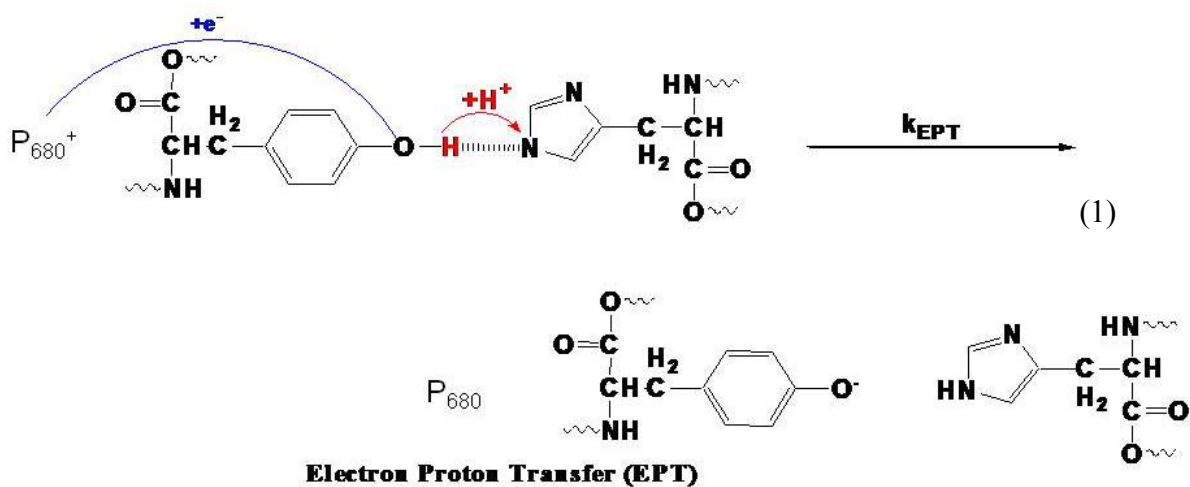
The results of these studies reveal the existence of multiple competing pathways for tyrosine oxidation: electron transfer followed by proton transfer (ET-PT); proton transfer followed by electron transfer (PT-ET), concerted electron-proton transfer (EPT) with an added base or  $\text{OH}^-$  as proton acceptor. Depending on reaction conditions all of these pathways can be competitive.

Because of the high reduction potential for the tyrosine radical cation,  $\text{TyrOH}^{\cdot+}$ , mechanisms involving initial oxidation in the absence of an EPT base are inhibited and addition of added bases leads to a strong catalytic effect. As shown by H/D kinetic isotope effect and  $\Delta G$

dependences, at the microscopic level EPT is dominated by the quantum nature of the coupled proton transfer.

### 3.2 Introduction

Tyrosine oxidation is a critical pathway in many enzymatic reactions . and been studied extensively in model reactions.<sup>1-16</sup> In some reactions it has been suggested that loss of an electron from tyrosine is accompanied by proton transfer to a neighboring base by coupled or concerted electron-proton transfer (EPT).<sup>3-21</sup> This is the suggested pathway, for example, in Photosystem II with oxidation of Tyr161 by oxidized chlorophyll  $P_{680}^+$  thought to be accompanied by proton transfer to His190. In this Multiple Site-Electron Proton Transfer (MS-EPT) pathway an electron is transferred to  $P_{680}^+$  in concert with proton transfer to His190 (Eq 1).



Although EPT pathways are mechanistically more complex than either electron transfer or proton transfer, they offer the advantage of avoiding high-energy intermediates in the prevailing medium. For example,  $\Delta G^{0'} \sim -0.36\text{eV}$  for EPT in eq 1 as opposed to  $\Delta G^{0'} \sim +0.08\text{eV}$  for initial electron transfer. The overall free energy change of the reaction is

recovered in the proton transfer step following electron transfer with  $\Delta G^{\circ}$  (25 °C in eV) = -0.059(pH - pK<sub>a</sub>(TyrOH<sup>+</sup>)) with pK<sub>a</sub>(TyrOH<sup>+</sup>) = -2.<sup>22</sup>

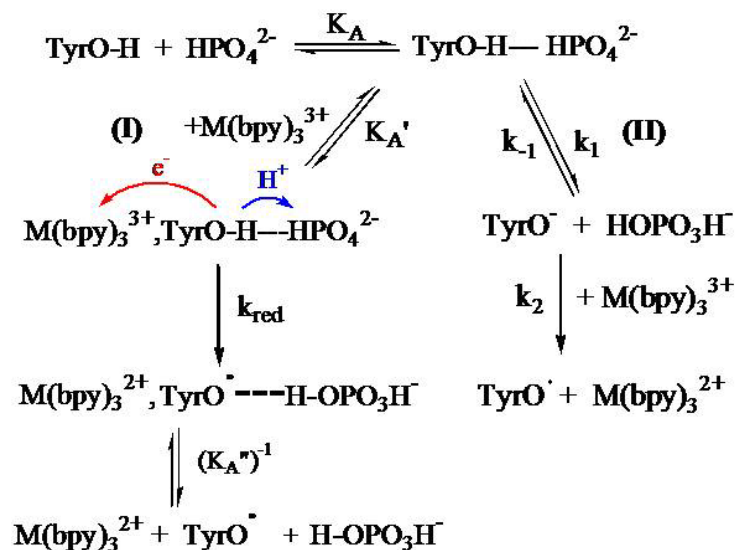
There is growing recognition of the importance of EPT pathways in both chemistry and biology and current interest in identifying the full scope of this reactivity and the factors at the microscopic level that dictate reaction rates and barriers. Theoretical insight is available largely from the work of Cukier and Hammes-Schiffer and their coworkers.<sup>4,6,17,19</sup> There are controversies. One is the origin of pH dependences in Proton Coupled Electron Transfer (PCET) reactions with added buffers and whether it arises from the pH dependence of the driving force for electron transfer<sup>5,7,8,10</sup> or from coupled proton transfer to the basic form of the buffer.<sup>15,16,23-25</sup>

We investigated tyrosine oxidation by metal complex oxidants M(bpy)<sub>3</sub><sup>3+</sup> (M = Fe, Ru, Os) with added phosphate buffers (H<sub>2</sub>PO<sub>4</sub><sup>-</sup>/ HPO<sub>4</sub><sup>2-</sup>) by a catalytic cyclic voltammetric technique and established the mechanism in Scheme 1.<sup>15</sup> In this mechanism prior association with the basic form of the buffer is followed by competitive pathways for tyrosine oxidation involving proton transfer followed by electron transfer (PT-ET) or Multiple Site-Electron Proton Transfer (MS-EPT) in which electron transfer occurs to the oxidant and proton transfer to the base.

In this and the following paper we document a detailed study of tyrosine oxidation with a family of added buffer bases by application of the electrochemical approach. We present experimental evidence that Scheme 1 is a common mechanism for tyrosine oxidation by a series of metal complex oxidants and variety of bases. We also discuss implications and microscopic insights gained from an extensive and unprecedented data set for MS-EPT over

an extensive range of  $\Delta G$  values including experimental evidence for a quantum effect in the O-H transfer.

Scheme 1



### 3.3 Methods and Materials:

**3.3.1 General:** All chemicals were purchased from Sigma Aldrich (St. Louis, MO) and used without further modification. Solutions for kinetic studies were prepared by using MilliQ water. Buffers (acetate, succinate, histidine, phosphate, and tris) were purchased from Sigma Aldrich. Buffers were prepared as stock solutions at a concentration of 0.5M and were brought to the appropriate pH by adding appropriate amounts of stock NaOH or HCl solutions. Ionic strength was maintained with added 0.8M NaCl as supporting electrolyte. Background voltammetric scans were limited to potentials where there was no contribution from the NaCl electrolyte.

**3.3.2 Isotope Studies:** Deuterated solutions were prepared using deuterium oxide (99 % D) purchased from Sigma Aldrich (St. Louis, MO). Tyrosine and buffer compounds were dissolved in D<sub>2</sub>O and protons were removed by the addition of NaOD (99% D Sigma Aldrich). Solutions were then redeuterated with the addition of DCl (99% D Sigma Aldrich).

After pD equilibration, deuterium oxide was removed by distillation leaving deuterated solid. Deuterium content was confirmed by NMR. Deuterated solutions were then redissolved in fresh D<sub>2</sub>O and pD (pH + 0.4) of buffered solutions were adjusted to the appropriate pD using NaOD and DCl. The ionic strength was maintained with added 0.8M NaCl as supporting electrolyte. As with protonated solution studies the voltammetric range was limited to potentials where there was little contribution of NaCl.

3.3.3 Electrochemistry: Electrochemical experiments were performed by using a BAS100B/W series potentiostat in a three electrode cell described previously.<sup>26</sup> The working electrode was indium tin oxide coated glass (ITO) with a reaction area of 0.32 cm<sup>2</sup> purchased from Delta Technologies (Stillwater, MN). The reference electrode was a teflon coated Ag/AgCl microelectrode purchased from Cypress Systems, Inc (Lawrence, KS). The auxiliary electrode was platinum wire, purchased from Sigma Aldrich (St. Louis, MO), wrapped around the teflon base of the reference electrode. ITO electrodes were treated before use by sonication in MilliQ water, then isopropanol each for 15 minutes, followed by two washes with MilliQ water for 15 minutes each. ITO electrodes were laid flat and allowed to dry overnight. Each electrochemical experiment was performed on a solution volume of 50  $\mu$ L. To collect a cyclic voltammogram (CV), the potential was swept in a positive potential direction from 0-1.3 V. The ITO electrode was conditioned for 6 consecutive scans in phosphate buffer solution before the first measurement. A final background CV was collected. A CV of buffer with added metal complex was then scanned and, finally, a scan of buffer and 20  $\mu$ M metal complex with 100  $\mu$ M tyrosine. After a scan of buffer with oxidant and reductant was taken, the ITO electrode was discarded and a new electrode was used for the next sample. CV's were background corrected by subtracting

buffer scans from CV's of metal complex and metal complex with tyrosine. Cyclic voltammetric measurements were conducted for the series of buffer bases with added buffer in aqueous 0.8 M NaCl solutions at 23±2°C.

**3.3.4 Rate Law:** A rate law for the mechanism in Scheme 1, but generalized to any acceptor base B (B = HPO<sub>4</sub><sup>2-</sup> in Scheme 1), is shown in eq 2a. Cyclic voltammograms consistent with this mechanism were simulated digitally by the electrochemical mechanism in Scheme 2.

The quantity  $k_{\text{obs}}$ , derived from the simulations, was obtained over a variety of conditions in added complex, tyrosine, buffer ratio, and buffer concentrations.

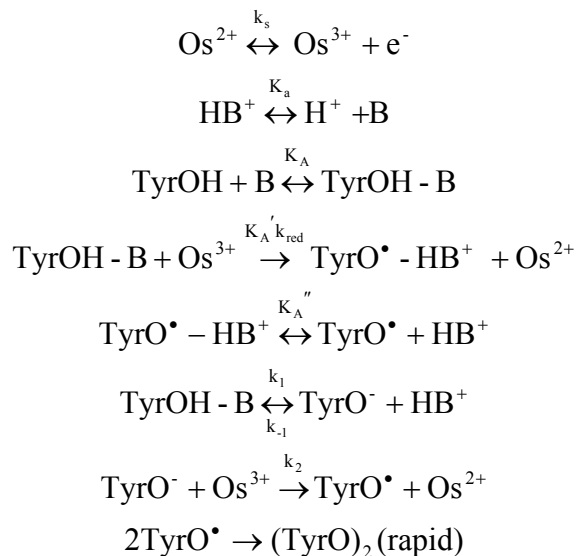
The quantities in eq 2a not defined in Scheme 1 are <sup>+</sup>HB and B for buffer acid and base and [TyrOH]<sub>T</sub> for total tyrosine concentration both free and in the TyrOH---B association complex, TyrOH---OPO<sub>2</sub>OH<sup>2-</sup> in Scheme 1 and M<sup>3+</sup> for M(bpy)<sub>3</sub><sup>3+</sup>. Under pseudo-first order conditions in both TyrOH and buffer base the rate law becomes eq 2b with  $k_{\text{obs}}$  given by eq 3. Eq 3 is applicable over a wide range of concentrations of buffer, buffer base, complex and tyrosine but is not the general rate law, see below. It does not include direct oxidation of TyrOH and its anion, TyrO<sup>-</sup>. Also, at relatively high concentrations of complex, buffer base and tyrosine, evidence is found for an additional saturation kinetics.

$$-\frac{d[M^{3+}]}{dt} = \left[ \frac{K_A [TyrOH]_T [B]}{1 + K_A [B]} \right] \left( k_{\text{red}} K_A' + \frac{k_1 k_2}{k_{-1} [{}^+HB] + k_2 [M^{3+}]} \right) [M^{3+}] \quad (2a)$$

$$-\frac{d[M^{3+}]}{dt} = k_{\text{obs}} [TyrOH]_T [M^{3+}] \quad (2b)$$

$$\frac{k_{\text{obs}}}{[TyrOH]_T} = \left( k_{\text{red}} K_A K_A' + \frac{K_A k_1 k_2}{k_{-1} [{}^+HB] + k_2 [M^{3+}]} \right) \left[ \frac{K_A [B]}{1 + K_A [B]} \right] \quad (3)$$

Scheme 2



Limiting conditions were used to simplify the mechanism in Scheme 1 by kinetically isolating either the MS-EPT or PT-ET pathways.

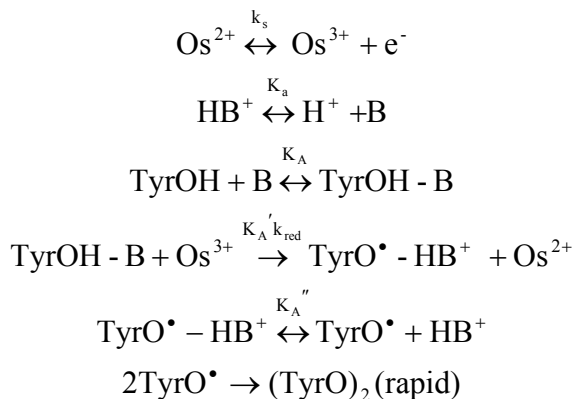
At high buffer ratios,  $[^+\text{HB}]/[\text{B}] > 10$ , the MS-EPT pathway dominates and eq 3 becomes eq 4a or, if  $K_A[\text{B}] < 1$ , eq 4b.

$$\frac{k_{\text{obs}}}{[\text{TyrOH}]_T} = \left( k_{\text{red}} K_A' \right) \left[ \frac{K_A [\text{B}]}{1 + K_A [\text{B}]} \right] \quad (4a)$$

$$\frac{k_{\text{obs}}}{[\text{TyrOH}]} = k_{\text{red}} K_A K_A' [\text{B}] \quad (4b)$$

Under these conditions the electrochemical mechanism simplifies to Scheme 3.

Scheme 3



At relatively high concentrations of [TyOH] and [B] the TyOH---B adduct, TyOH---OPO<sub>2</sub>OH<sup>2-</sup> in Scheme 1, dominates with [TyOH]<sub>T</sub> ~ [TyOH---B]. Under these conditions the rate law in eq 2b becomes eq 4a. As noted below, at high concentrations of complex, TyrOH, and buffer base there is evidence for additional saturation kinetics arising from association complex formation between TyOH---B and M(bpy)<sub>3</sub><sup>3+</sup> with EPT occurring within the complex, M(bpy)<sub>3</sub><sup>3+</sup>, TyOH---B  $\xrightarrow{k_{red}}$  M(bpy)<sub>3</sub><sup>2+</sup>, TyO<sup>•</sup>---<sup>+</sup>H-B. Under these conditions with TyOH---B in high, pseudo first order excess, the rate law becomes eq 6a with k<sub>obs</sub> given by eq 6b.

$$-\frac{d[\text{M}^{3+}]}{dt} = k_{\text{obs}} [\text{TyrOH}]_T [\text{M}^{3+}] = k_{\text{obs}} [\text{TyrOH} \cdots \text{B}] [\text{M}^{3+}] \quad (5)$$

$$\begin{aligned}
 -\frac{d[\text{M}^{3+}]}{dt} &= k_{\text{red}} [\text{M}^{3+}, \text{TyrOH} \cdots \text{B}] = \frac{k_{\text{red}} K_A' [\text{TyrOH} \cdots \text{B}] [\text{M}^{3+}]}{1 + K_A' [\text{TyrOH} \cdots \text{B}]} = \\
 &= \frac{k_{\text{red}} K_A' [\text{TyrOH}]_T [\text{M}^{3+}]}{1 + K_A' [\text{TyrOH}]_T} = k_{\text{obs}} [\text{M}^{3+}]
 \end{aligned} \quad (6a)$$

$$k_{\text{obs}} = \frac{k_{\text{red}} K_A' [\text{TyrOH}]_T}{1 + K_A' [\text{TyrOH}]_T} \quad (6b)$$

At low buffer ratios,  $[^+HB]/[B] < 10$ , the PT-ET pathway dominates and the rate law in in eq 2 becomes eq 7a or, in solutions dilute in B with  $K_A[B] < 1$  and  $[TyrOH]_T \sim [TyrOH]$  and tyrosine in pseudo first order excess, eq 7b.

$$-\frac{d[M^{3+}]}{dt} = \left[ \frac{K_A [TyrOH]_T [B]}{1 + K_A [B]} \right] \left( \frac{k_1 k_2}{k_{-1} [^+HB] + k_2 [M^{3+}]} \right) [M^{3+}] \quad (7a)$$

$$-\frac{d[M^{3+}]}{dt} = \left( \frac{k_1 k_2}{k_{-1} [^+HB] + k_2 [M^{3+}]} \right) [M^{3+}] [B] [TyrOH] \quad (7b)$$

At high buffer concentrations with  $k_2 [M^{3+}] \ll k_{-1} [^+HB]$ , the rate law further simplifies to eq 8a and with  $K_A[B] < 1$  and  $[TyrOH]_T \sim [TyrOH]$ , eq 7b with  $k_{obs}$  given in eqs 9a and 9b.

$$-\frac{d[M^{3+}]}{dt} = \left[ \frac{K_A [TyrOH]_T [B]}{1 + K_A [B]} \right] \left( \frac{k_1 k_2}{k_{-1} [^+HB]} \right) [M^{3+}] = k_{obs} [M^{3+}] [TyrOH]_T \quad (8a)$$

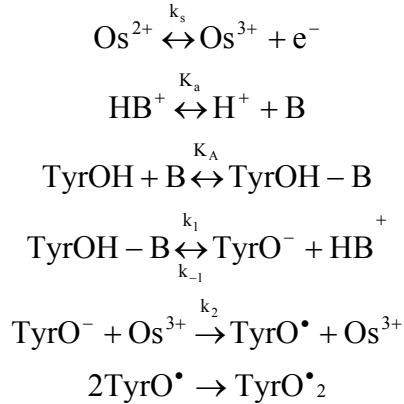
$$-\frac{d[M^{3+}]}{dt} = k_{obs} [M^{3+}] [TyrOH] \quad (8b)$$

$$\frac{k_{obs}}{[TyrOH]_T} = \left( \frac{k_1 k_2}{k_{-1} [^+HB]} \right) \left[ \frac{K_A [B]}{1 + K_A [B]} \right] \quad (9a)$$

$$\frac{k_{obs}}{[TyrOH]} = \left( \frac{k_1 k_2}{k_{-1} [^+HB]} \right) K_A [B] \quad (9b)$$

The electrochemical mechanism in this limit is shown in Scheme 4.

#### Scheme 4



At low buffer concentrations in the limit  $k_2[M^{3+}] \gg k_1[{}^+HB]$ , the rate law in eq 7a becomes independent of  $[M(bpy)_3^{3+}]$  giving eq 10a or with  $K_A[B] < 1$  and  $[TyrOH]_T \sim [TyrOH]$ , eq 9b and the corresponding expressions for  $k_{obs}$  in eq 11a and 11b.

$$-\frac{d[M^{3+}]}{dt} = \left[ \frac{K_A[TyrOH]_T[B]}{1 + K_A[B]} \right] \left( \frac{k_1 k_2}{k_2} \right) = k_{obs}[TyrOH]_T \quad (10a)$$

$$-\frac{d[M^{3+}]}{dt} = \left( \frac{k_1 k_2 K_A}{k_2} \right) [TyrOH][B] = k_{obs}[TyrOH][B] \quad (10b)$$

$$k_{obs} = k_1 \left[ \frac{K_A[B]}{1 + K_A[B]} \right] \quad (11a)$$

$$k_{obs} = k_1 K_A [B] \quad (11b)$$

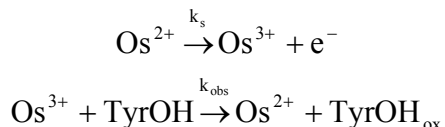
3.3.5 Digital Simulation. Digital simulations were performed by using the DigiSim software package purchased from BioAnalytical Systems (West Lafayette, IN). The DigiSim software uses the Butler-Volmer equation 12 to relate current-time data as a function of applied potential to evaluate homogeneous rate constants for oxidation of tyrosine by  $M^{III}(bpy)_3^{3+}$ .<sup>30</sup>

$$i = i_o \left( \exp\left(\frac{(1-\alpha)F\eta}{RT}\right) - \exp\left(\frac{-\alpha F\eta}{RT}\right) \right) \quad (12)$$

Literature values<sup>7</sup> for the diffusion coefficients of  $6.0 \times 10^{-6} \text{ cm}^2/\text{s}$  for  $Os(bpy)_3^{3+/2+}$  and  $3.0 \times 10^{-5} \text{ cm}^2/\text{s}^2$  for tyrosine were used in the simulations.<sup>27-29</sup> The reduction potential of the metal complex ( $E^{0'} = 0.85 \text{ V}$  vs NHE in 0.05 M phosphate and 0.8 M NaCl at  $23 \pm 2^\circ\text{C}$ ) and heterogeneous electron transfer rate constants ( $k_s = 0.01 \text{ cm/s}$ ) were obtained by fitting cyclic voltammograms of the metal complex alone.

A simple electron transfer mechanism was used in saturation studies and is illustrated in scheme 5. In this mechanism  $k_{\text{obs}}$  is the rate constant for the overall reaction.

Scheme 5



3.3.6  $K_A$  by  $^{31}\text{P}$  NMR:  $^{31}\text{P}$  NMR was used to obtain  $K_A$  independently for complex formation between TyrOH and  $\text{HPO}_4^{2-}$ , Scheme 1. Solutions containing the  $\text{H}_2\text{PO}_4^-/\text{HPO}_4^{2-}$  buffer ( $1.0 \times 10^{-4}$ - $1.0 \times 10^{-3}$  M) and tyrosine ( $2.0 \times 10^{-2}$  M) were prepared in  $\text{D}_2\text{O}$ . A background  $^{31}\text{P}$  NMR spectrum was recorded with phosphate alone in solution and another with added tyrosine. A single  $^{31}\text{P}$  chemical shift was observed whose chemical shift was concentration dependence consistent with the rapid exchange limit. Spectra were recorded and a small increase in chemical shift was observed as tyrosine concentration was increased with measurements made up to a 1:1 ratio of tyrosine to  $\text{HPO}_4^{2-}$ . The association constant was calculated by using eq 13.<sup>32</sup>

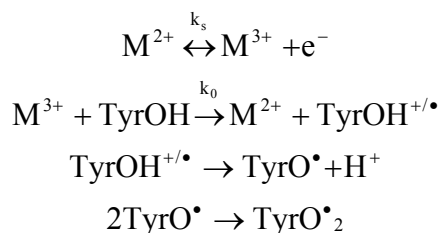
$$\frac{1}{\Delta\delta_{\text{obs}}} = \left( \frac{1}{K_A (\delta_{\text{complex}} - \delta_{\text{TyrOH}})} \right) \frac{1}{[\text{HPO}_4^{2-}]} + \frac{1}{\delta_{\text{complex}} - \delta_{\text{TyrOH}}} \quad (13)$$

3.3.7 Electron Transfer Oxidation of Tyrosine and Tyrosine Anion. The outer sphere oxidation mechanism of the tyrosyl radical cation was investigated electrochemically in acidic sodium chloride solution at pH 3.0 using  $\text{M}(\text{bpy})_3^{3+}$  oxidants with a reduction potential range of 1.06V-1.25V vs NHE. Under these conditions,  $\text{M}(\text{bpy})_3^{3+}$  oxidants (Fe and Ru) varied over a potential range of 1.06V-1.25V vs NHE, and the catalytic oxidative current was analyzed. The rate law for the reaction is given in Eq 14. The kinetics of the reaction were extremely slow, and catalysis was not visualized for oxidants below 0.85V vs NHE. In the

electrochemical studies,  $1.0 \times 10^{-4} \text{ M}$  TyrOH was reacted with  $2.0 \times 10^{-5} \text{ M}$   $\text{M}(\text{bpy})_3^{3+}$  in acidic aqueous solution at pH 3.0 in 0.8M NaCl at  $25 \pm 2^\circ \text{C}$ . Cyclic voltammograms were analyzed using digital simulation of the mechanism reported in Scheme 6 for a one electron outer sphere oxidation, followed by rapid proton equilibration and radical coupling. The rate constant,  $k_o$ , is the outer sphere rate constant for the formation of the tyrosyl radical cation.

$$-\frac{d[\text{M}^{3+}]}{dt} = k_o [\text{TyrOH}][\text{M}^{3+}] \quad (14)$$

Scheme 6



Oxidation of TyrOH by  $\text{Os}(\text{bpy})_3^{3+}$  was investigated in acidic solution pH 3.0 through spectrophotometric monitoring using pseudofirst order kinetics consistent with Eq. Solution conditions were as follows:  $1.0 \times 10^{-3}$ -  $5.0 \times 10^{-4} \text{ M}$  TyrOH and  $2.0 \times 10^{-5} \text{ M}$   $\text{Os}(\text{bpy})_3^{3+}$  in 0.8M NaCl at  $23 \pm 2^\circ \text{C}$ . The rate constant  $k_{\text{obs}}$  was determined for a variety of TyrOH concentrations and  $k_o$  is reported from  $k_{\text{obs}}/[\text{TyrOH}]$ .

$$\text{Ln} \left[ \frac{\text{Abs}_\infty - \text{Abs}_t}{\text{Abs}_\infty - \text{Abs}_o} \right] = k_{\text{obs}} dt \quad (15a)$$

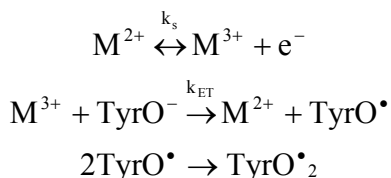
$$\frac{k_{\text{obs}}}{[\text{TyrOH}]} = k_o \quad (15b)$$

Reactivity of the anion was investigated in an aqueous NaOH solution with 0.8M NaCl at  $23 \pm 2^\circ \text{C}$ . A stock solution of 1.0mM of tyrosine was brought up to pH 12 where the phenolic proton should be completely removed. The rate law for the oxidation of tyrosyl anion is reported in Eq 16. Cyclic voltammetric studies were completed in NaOH solution using 0.8M NaCl supporting electrolyte at  $23 \pm 2^\circ \text{C}$  investigating the catalytic current over a

potential range of 0.85-1.25V vs NHE. The cyclic voltammograms were analyzed through digital simulation and fit to the mechanism reported in Scheme 7. The rate constant,  $k_{ET}$ , is the outer sphere rate constant for reaction of the tyrosyl anion with the metal complex.

$$-\frac{d[M^{3+}]}{dt} = k_{ET}[TyrO^-][M^{3+}] \quad (16)$$

Scheme 7



### 3.4 Results

#### 3.4.1 Oxidation of Tyrosine and Tyrosine Anion by $M(bpy)_3^{3+/2+}$ . Oxidation of tyrosine by

$M(bpy)_3^{3+}$  is first order in both. The reaction of  $Os(bpy)_3^{3+}$  was monitored spectrophotometrically under pseudo first order conditions in tyrosine by following the reappearance of  $M(bpy)_3^{2+}$  at its MLCT absorption maximum in the visible, 490 nm for  $Os(bpy)_3^{3+}$ . The reaction was too slow to be monitored by the catalytic cyclic voltammetric technique.

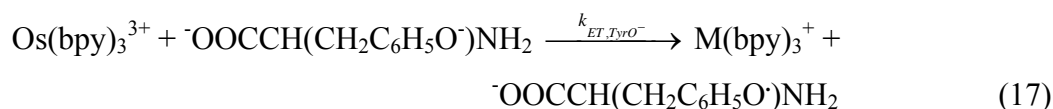
The absorbance over time scans for the appearance of  $Os(bpy)_3^{2+}$  was consistent with the outersphere rate constant  $k_o$  of  $1.7 \times 10^2 M^{-1} s^{-1}$ .

The driving force investigation was consistent with the rate law,  $-d[M(bpy)_3^{3+}]/dt = k_{o,TyrOH} [M(bpy)_3^{3+}][TyrOH]$  for  $M(bpy)_3^{3+}$  oxidants (Fe, Ru). The rate constant  $k_o$  was obtained by digital simulation of cyclic voltammograms of  $1.0 \times 10^{-4} M$  TyrOH with  $2.0 \times 10^{-5} M$   $M(bpy)_3^{3+}$  in pH 3.0 acidic solution in 0.8M NaCl at  $23 \pm 2^\circ C$ . The driving force investigation over the  $E^0$  potential range of 1.06-1.25V resulted in a slope of 0.5 predicted for a single electron outer sphere transfer. Rate constants and  $E^{o'}(M(bpy)_3^{3+/2+})$  values for the metal complex couples are listed in Table 1.

Oxidant	E <sup>0</sup> V vs NHE	k <sub>o</sub> M <sup>-1</sup> s <sup>-1</sup>
Ru(bpy) <sub>3</sub> <sup>3+</sup>	1.25	3.0x10 <sup>5</sup>
Ru(bpy)(dmb) <sub>2</sub> <sup>3+</sup>	1.11	-
Ru(dmb) <sub>3</sub> <sup>3+</sup>	1.06	1.8x10 <sup>4</sup>
Fe(bpy) <sub>3</sub> <sup>3+</sup>	1.04	9.7x10 <sup>3</sup>
Os(bpy) <sub>3</sub> <sup>3+</sup>	0.85	1.6x10 <sup>2</sup>

Table 1: Rate constants and E<sup>0</sup> values for metal complex couples in acid solution pH 3.0 NaCl. The rate constant for Os(bpy)<sub>3</sub><sup>3+</sup> was determined spectrochemically at pH 3.0 in NaCl at 23±2°C

The rate constant for tyrosine anion oxidation by M(bpy)<sub>3</sub><sup>3+</sup>, eq 17, was obtained in the cyclic voltammetry measurements, see below. The anion was prepared by deprotonating a 1.0x10<sup>-3</sup>M stock solution of TyrOH at pH 12. Cyclic voltammograms of 1.0x10<sup>-4</sup>M TyrO<sup>-</sup> with 2.0x10<sup>-5</sup>M M(bpy)<sub>3</sub><sup>3+</sup> in NaOH solution with 0.8M NaCl at 23±2°C were digitally simulated using the mechanism reported in scheme 5. The rate constant isolated for TyrO<sup>-</sup> with Os(bpy)<sub>3</sub><sup>3+</sup> was determined to be 1.7±0.5x10<sup>7</sup>M<sup>-1</sup>s<sup>-1</sup>.



3.4.2 Determination of Rate Law. HPO<sub>4</sub><sup>2-</sup> as the EPT Base. ITO electrodes were used in the catalytic cyclic voltammetry measurements of oxidation of tyrosine by M(bpy)<sub>3</sub><sup>3+</sup>. As noted elsewhere, direct electrochemical oxidation of amino acids and guanine derivatives at these electrodes is greatly inhibited.<sup>28,29,31</sup> Experiments currently in progress show that direct

oxidation at glassy carbon electrodes does occur with added buffers and these results will be reported elsewhere.<sup>33</sup>

Cyclic voltammograms illustrating the catalytic effect on  $\text{Os}(\text{bpy})_3^{3+}$  oxidation of tyrosine by added  $\text{H}_2\text{PO}_4^-/\text{HPO}_4^{2-}$  buffer in 0.8M NaCl at  $23\pm 2^\circ\text{C}$  are illustrated in Figure 1. Application of the Three examples are shown: a)  $1.0\times 10^{-4}$  M TyrOH with  $2.0\times 10^{-5}$  M  $\text{Os}(\text{bpy})_3^{3+}$ , b) with 0.05  $\text{H}_2\text{PO}_4^-/\text{HPO}_4^{2-}$  M buffer at pH 6.0,  $[\text{H}_2\text{PO}_4^-]/[\text{HPO}_4^{2-}] = 15:1$ , under conditions where the MS-EPT pathway dominates, eq 9 in Scheme 1 (red), and c) with 0.05 M buffer at pH 8.5,  $[\text{H}_2\text{PO}_4^-]/[\text{HPO}_4^{2-}] = 1/15$ , under conditions where the PT-ET pathway dominates, eq 10 (blue).

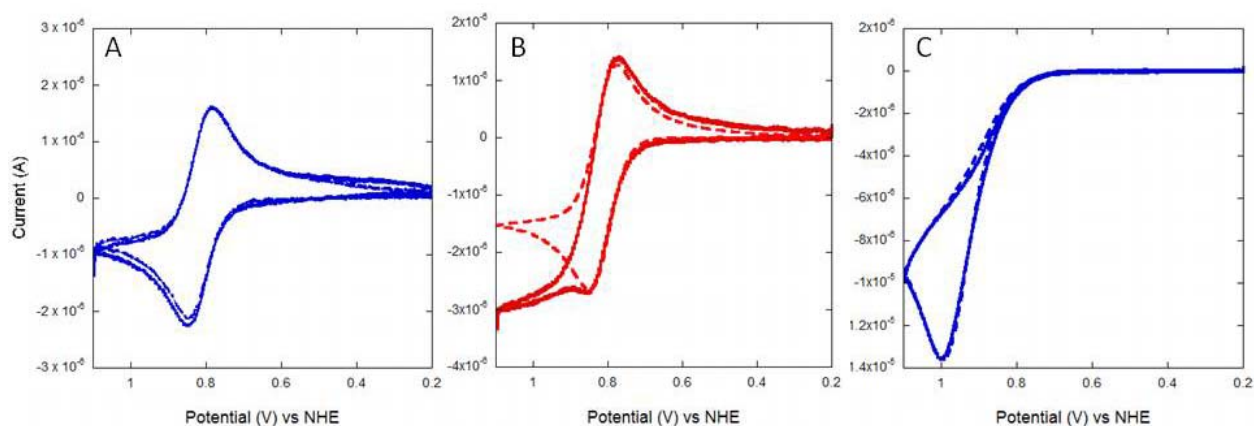


Figure 1. A) Cyclic voltammogram of  $\text{Os}(\text{bpy})_3^{3+}$  alone ( $2.0\times 10^{-5}$ M, red) and in the presence of TyrOH (blue) in 0.8 M NaCl. A digital simulation of the voltammogram is shown as the dashed line fit to eq 12 with  $E^{0'} = 0.85\text{V}$ ,  $k_s=0.01\text{cm A}=0.32\text{cm}^2$  B) As in A) with 0.05M phosphate buffer at pH 6.0,  $[\text{H}_2\text{PO}_4^-]/[\text{HPO}_4^{2-}] = 15/1$  under conditions where the MS-EPT mechanism in Scheme 1 dominates. The dashed line is a digital simulation of the waveform to the mechanism in Scheme 3 with  $K_A=30.0\text{M}^{-1}$ ,  $K_A k_{\text{red}}=9.6\times 10^4$ . C) As in B) with 0.05 M buffer at pH 8.5,  $[\text{H}_2\text{PO}_4^-]/[\text{HPO}_4^{2-}] = 15/1$ , under conditions where the PT-ET mechanism in Scheme 1 dominates. The dashed line is a digital simulation of the waveform to Scheme 4 with the parameters  $K_A=30.0\text{M}^{-1}$ ,  $k_1=3.3\times 10^5\text{s}^{-1}$ ,  $k_2=1.0\times 10^7\text{M}^{-1}\text{s}^{-1}$

Cyclic voltammetric waveforms were simulated digitally by use of Digisim and the Butler-Volmer relation in eq 12 and applied to the general electrochemical mechanism in Scheme 2 or the limiting mechanisms in Schemes 3 and 4. Diffusion coefficients of  $6.0\times 10^{-6}$

$\text{cm}^2/\text{s}$  for  $\text{Os}(\text{bpy})_3^{3+/2+}$  and  $3.0 \times 10^{-5} \text{cm}^2/\text{s}^2$  for tyrosine were used in the simulations with  $n = 1$  confirmed by bulk oxidation in pH 7.0 phosphate buffered solution.<sup>33</sup> Comparisons between digitally simulated and actual voltammograms are shown in Figure 1 under limiting conditions where the MS-EPT pathway in Scheme 1 dominates and where the PT-ET pathway dominates.

The simulations were used to obtain  $k_{\text{obs}}$  at a variety of concentrations of metal complex oxidant, tyrosine, buffer, and buffer ratios. Kinetic isolation of the pathways in Scheme 1 was used to establish the rate law in eq 3 with the example of  $\text{HPO}_4^{2-}$  as base featured below.

#### 3.4.3 Pre-association between TyrOH and B. Determination of $K_A$ and $k_{\text{red}}K_A'$ : At high

buffer ratios,  $[\text{HB}^+]/[\text{B}] > 10$ , with the MS-EPT pathway dominating, saturation kinetics in  $[\text{B}]$  are predicted by eq 3a. In Figure 2 is shown a plot of  $k_{\text{obs}}/[\text{TyrOH}]_{\text{T}}$ , with  $[\text{TyrOH}]_{\text{T}}$  the total tyrosine concentration, which illustrates the behavior predicted by eq 3a. From the inverse-inverse plot of  $[\text{TyrOH}]_{\text{T}}/k_{\text{obs}}$  in the inset: slope =  $(k_{\text{red}}K_AK_A')^{-1} = 5.8 \times 10^{-9}$ ; intercept =  $(k_{\text{red}}K_A')^{-1}$ ; intercept/slope =  $2.1 \times 10^{-7} K_A = 30.0 \text{ M}^{-1}$  and  $k_{\text{red}}K_A' = 4.8 \times 10^6 \text{ M}^{-1} \text{ s}^{-1}$ .

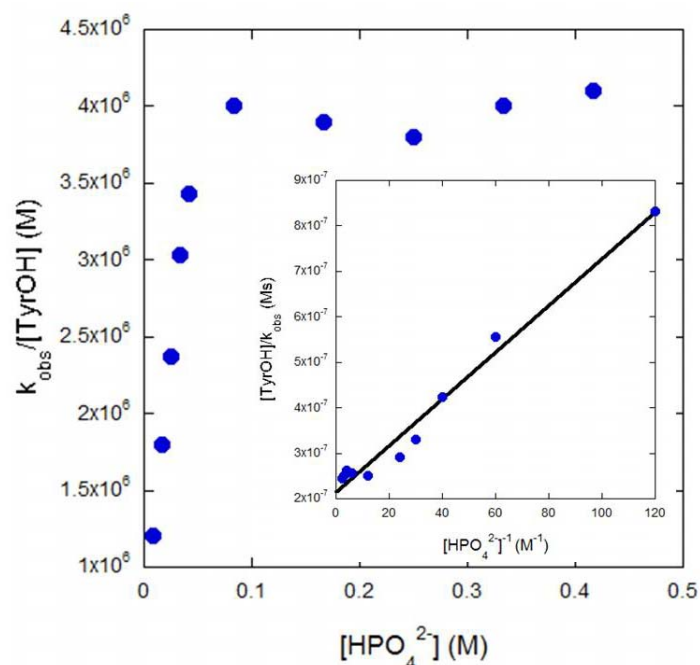


Figure 2: Plot of  $k_{\text{obs}}/[\text{TyrOH}]$  vs  $[\text{HPO}_4^{2-}]$  in a  $\text{H}_2\text{PO}_4^-$ - $\text{HPO}_4^{2-}$  buffer at pH 7.5 ( $[\text{H}_2\text{PO}_4^-]/[\text{HPO}_4^{2-}] = 5$ ) for the oxidation of TyrOH by  $\text{Os}(\text{bpy})_3^{3+}$  illustrating saturation kinetics at  $[\text{HPO}_4^{2-}] > 100\text{mM}$ ; 0.8 NaCl at  $23 \pm 2^\circ\text{C}$ . In the inset is shown a plot of  $[\text{TyrOH}]_T/k_{\text{obs}}$  vs.  $[\text{HPO}_4^{2-}]^{-1}$  with slope = 0.05 and intercept = 1.8; eq 13. The inset plot is of  $k_{\text{obs}}/[\text{HPO}_4^{2-}]$  vs  $[\text{H}_2\text{PO}_4^-]^{-1}$  with  $1.0 \times 10^{-4}\text{M}$  and  $2.0 \times 10^{-5}\text{M}$   $\text{Os}(\text{bpy})_3^{3+}$  in 0.8M NaCl at  $23 \pm 2^\circ\text{C}$  in phosphate buffered solution. The nonzero intercept and slope are consistent with the rate law in Eq 1.

3.4.4 Dependence on  $[\text{TyrOH}]$  and  $[\text{B}]$  with  $\text{B} = \text{HPO}_4^{2-}$ : In the limit  $K_A[\text{B}] < 1$ ,  $[\text{TyrOH}]_T \sim [\text{TyrOH}]$  and eq 3a becomes eq 3b. In Figure 3 are shown plots of  $k_{\text{obs}}$  vs  $[\text{TyrOH}]$  at fixed  $[\text{HPO}_4^{2-}]$  and of  $k_{\text{obs}}$  vs  $[\text{HPO}_4^{2-}]$  at fixed  $[\text{TyrOH}]$  illustrating the predicted dependences on buffer base and TyrOH. From the slopes of the two,  $k_{\text{red}}K_AK_A' = 2.0 \times 10^7\text{M}^{-1}\text{s}^{-1}$  (Figure 3A) and  $3.0 \times 10^7\text{M}^{-2}\text{s}^{-1}$  (Figure 3B).

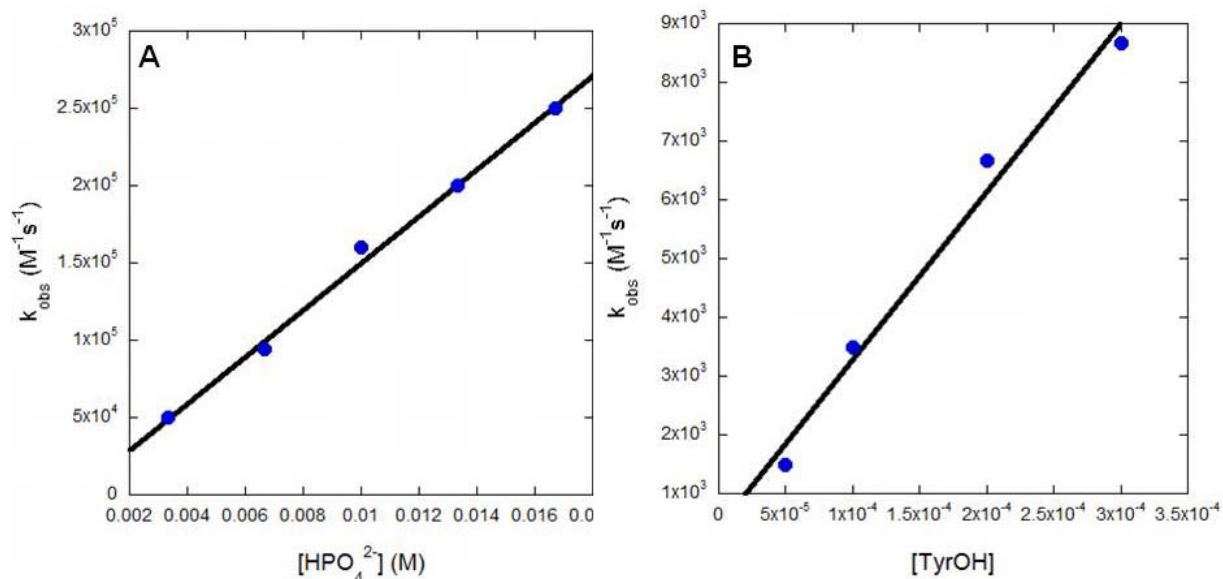


Figure 3: A) Plot of  $k_{\text{obs}}$  vs  $[\text{HPO}_4^{2-}]$  at pH 6.5  $\{\text{H}_2\text{PO}_4^-/\text{HPO}_4^{2-}=3/1\}$  at  $1.0 \times 10^{-3}$  M TyrOH in 0.8 M NaCl at  $23 \pm 2^\circ\text{C}$ . B) Plot of  $k_{\text{obs}}$  vs  $[\text{TyrOH}]$  at pH 6.0  $\{\text{H}_2\text{PO}_4^-/\text{HPO}_4^{2-}=15:1\}$  at 500 mM total buffer.

#### 3.4.5 Independent determination of $K_A$ by $^{31}\text{P}$ NMR: As described in Experimental, $^{31}\text{P}$

NMR was applied to the independent determination of  $K_A$  for the TyrOH- $\text{HPO}_4^{2-}$  association complex. As shown by the data in Figure 4, the predicted variation in inverse chemical shift with

$[\text{HPO}_4^{2-}]^{-1}$  in the fast exchange limit is observed over the range  $1.0 \times 10^{-4} - 1.0 \times 10^{-2}$  M in  $\text{HPO}_4^{2-}$ . From the slope, 0.05, and intercept, 1.7, of the plot,  $K_A = 34 \pm 2 \text{ M}^{-1}$ , in good agreement with the electrochemically derived value under the same conditions.

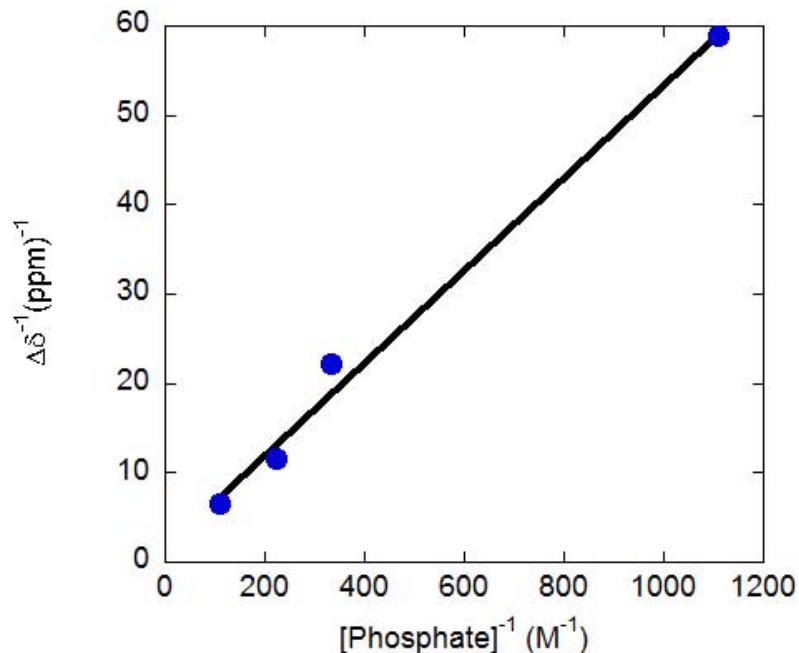


Figure 4: Plot of  $\frac{1}{\Delta\delta_{\text{obs}}}$  vs.  $\frac{1}{[\text{HPO}_4^{2-}]}$  according to eq 11 for the  $^{31}\text{P}$  NMR chemical shift of  $\text{HPO}_4^{2-}$  at  $23\pm 2^\circ\text{C}$ . From the slope of the line,  $K_A = 34\pm 2\text{M}^{-1}$ .

3.4.6 Pre-association between  $\text{TyrOH}\cdots\text{HPO}_4^{2-}$  and  $[\text{M}(\text{bpy})_3^{3+}]$ ; determination of  $K_A'$ : At high concentrations of TyrOH and B with  $K_A[\text{TyrOH}]$  or  $K_A[\text{B}] > 1$ , the TyrOH---B adduct becomes the dominant form of TyrOH in solution. At high concentrations of the adduct there is experimental evidence for an additional kinetic saturation region with prior association of the adduct with metal complex oxidant before the EPT step, Scheme 1, eq 5. The predicted decrease in  $k_{\text{obs}}$  with  $[\text{M}^{3+}]$  showing saturation behavior is shown in Figure 5. From the plot of  $k_{\text{obs}}^{-1}$  vs  $[\text{Os}(\text{bpy})_3^{3+}]^{-1}$  in the inset, consistent with eq 5b with  $k_{\text{red}} = 9.6\times 10^4\text{s}^{-1}$  and  $K_A' = 37.8\text{M}^{-1}$ .

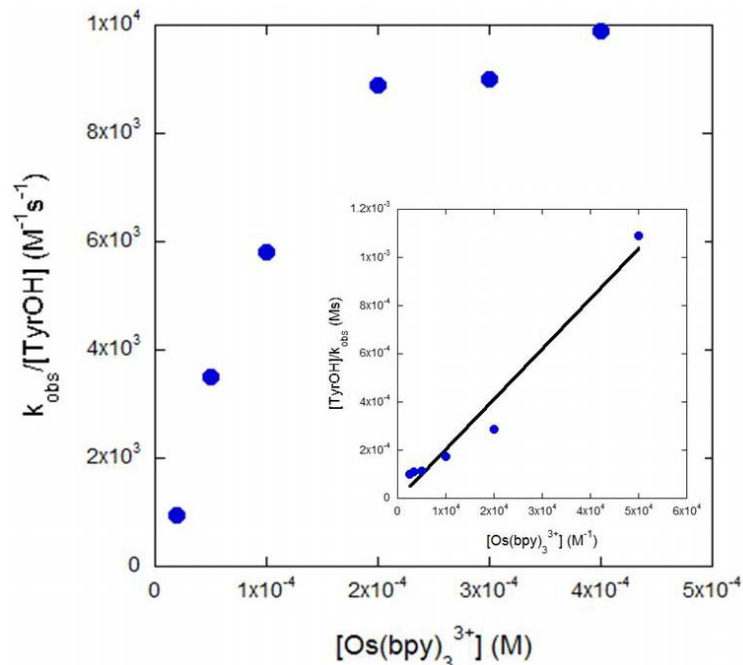


Figure 5: Plot of  $k_{\text{obs}}$  vs  $[\text{Os}(\text{bpy})_3^{3+}]$  in oxidation of TyrOH by  $\text{Os}(\text{bpy})_3^{3+}$  exhibiting saturation kinetics in complex at  $[\text{TyrOH}] > 5.0 \times 10^{-4} \text{ M}$ , 0.5 M in  $\text{H}_2\text{PO}_4^- - \text{HPO}_4^{2-}$  at pH 6.0 ( $[\text{HPO}_4^{2-}] = 0.07 \text{ M}$  under conditions of complete TyrOH-  $\text{HPO}_4^{2-}$  complex formation in 0.8 NaCl at  $23 \pm 2^\circ \text{C}$ . In the inset is shown a plot of  $k_{\text{obs}}^{-1}$  vs  $[\text{Os}(\text{bpy})_3^{3+}]^{-1}$  for which slope =  $3.8 \times 10^{-8}$  and intercept =  $2.1 \times 10^{-6}$ .

#### 3.4.7 Rapid pre-equilibrium formation of TyrO<sup>-</sup> followed by rate limiting oxidation:

determination of  $k_2$  and  $k_1/k_{-1}$ : At low buffer ratios with  $[\text{H}^+]/[\text{B}] < 10$  the PT-ET pathway is dominant in Scheme 1. At relatively high buffer concentrations with  $k_2[\text{M}^{3+}] \ll k_{-1}[\text{H}^+]$ , the dominant mechanism becomes equilibrium proton loss giving TyrO<sup>-</sup> followed by its rapid oxidation by  $[\text{M}(\text{bpy})_3^{3+}]$ , Scheme 1 and eqs 10 and 11. In Figure 6 is shown a plot of  $k_{\text{obs}}/[\text{TyrOH}]$  vs.  $[\text{B}]/[\text{H}^+]$  with  $K_A[\text{B}] < 1$ ,  $[\text{TyrOH}]_{\text{T}} \sim [\text{TyrOH}]$  consistent with eq 8b. From this plot: slope =  $(k_1 k_2 K_A / k_{-1}) = 7.3 \times 10^6 \text{ M}^{-1} \text{ s}^{-1}$ . The rate constant ratio  $k_1/k_{-1}$  is the equilibrium constant for proton transfer to B,  $\text{TyrOH} + \text{B} = \text{TyrO}^- + \text{H-B}$ . It is given by the known  $\text{pK}_a$  values by use of eq 18. For  $\text{HPO}_4^{2-}$  as base with  $\text{pK}_a(\text{H}_2\text{PO}_4^-) = 7.2$ ,  $K = 6.0 \times 10^{-4}$ . With this value and  $K_A = 30.0 \text{ M}^{-1}$ ,  $k_2 = 1.7 \times 10^7 \text{ M}^{-1} \text{ s}^{-1}$  with  $k_2$  the rate constant for electron

transfer oxidation of TyrO<sup>-</sup> by M(bpy)<sub>3</sub><sup>3+</sup>. This value compares favorably with the value  $k_2 = 1.0 \times 10^7 \text{ M}^{-1}\text{s}^{-1}$  obtained for the direct oxidation of TyrO<sup>-</sup> by Os(bpy)<sub>3</sub><sup>3+</sup>.

$$K = \frac{k_1}{k_{-1}} = \frac{k_{\text{TyrOH}}}{k_{\text{HB}^+}} \quad (18)$$

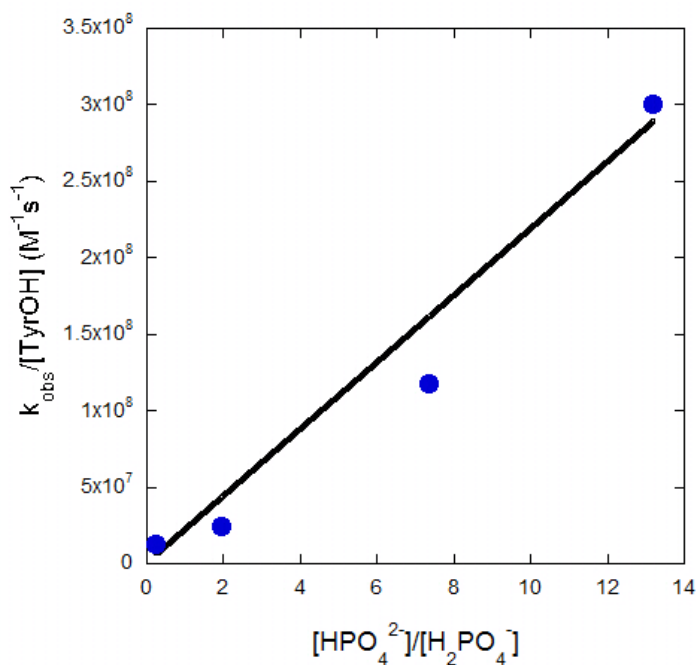


Figure 6: Plot of  $k_{\text{obs}}/[\text{TyrOH}]$  vs.  $[\text{B}]/[\text{HB}^+]$   $\{[\text{HPO}_4^{2-}]/[\text{H}_2\text{PO}_4^-]\}$  according to eq 8b from 0.002 to 1.3 M H<sub>2</sub>PO<sub>4</sub><sup>-</sup>-HPO<sub>4</sub><sup>2-</sup> buffer in 0.8M NaCl at 23±2°C.

3.4.8 Rate limiting proton transfer; determination of  $k_2$  and  $k_{-1}$ : At low buffer concentrations in the limit  $k_2[\text{M}^{3+}] \gg k_{-1}[\text{HB}^+]$ , the rate law becomes independent of  $[\text{M}(\text{bpy})_3^{3+}]$ , eq 11 with rate limiting proton transfer from TyrOH to B. The appearance of this region in the kinetics is shown by the data in Figure 7.

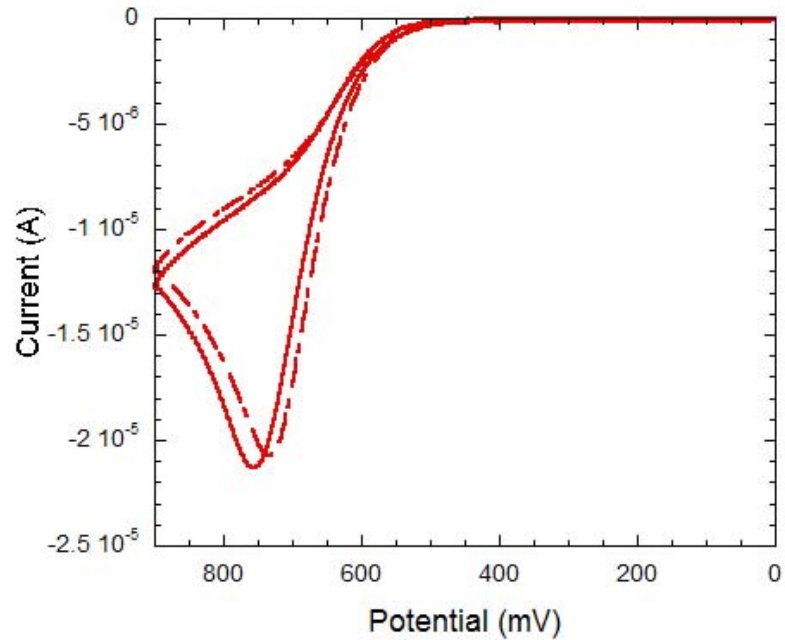


Figure 7: Cyclic voltammograms for tyrosine oxidation by  $\text{Os}(\text{bpy})_3^{3+}$  at  $20\mu\text{M}$  (solid) and  $40\mu\text{M}$   $\text{Os}(\text{bpy})_3^{2+}$  (dashed) with  $0.1\text{mM}$  tyrosine in  $50\text{mM}$  phosphate buffer at  $\text{pH} = 8.5$ , ( $[\text{HPO}_4^{2-}]/[\text{H}_2\text{PO}_4^-] = 15/1$ ) at  $23\pm 2^\circ\text{C}$  in  $0.8\text{M}$   $\text{NaCl}$ .

In Figure 8 is shown a plot of  $k_{\text{obs}}$  vs.  $[\text{B}]$  consistent with eq 10b. From the plot in Figure 8: slope =  $2.0 \times 10^7 \text{M}^{-1} \text{s}^{-1}$  and intercept =  $3.9 \times 10^5 \text{s}^{-1}$  with  $K_A = 30.0$ ,  $k_1 = 3.3 \times 10^5 \text{s}^{-1}$ . With this value of  $k_1$  and the rate constant ratio  $k_1/k_{-1} = 4 \times 10^{-5}$ ,  $k_{-1} = 7.8 \times 10^9 \text{M}^{-1} \text{s}^{-1}$ .

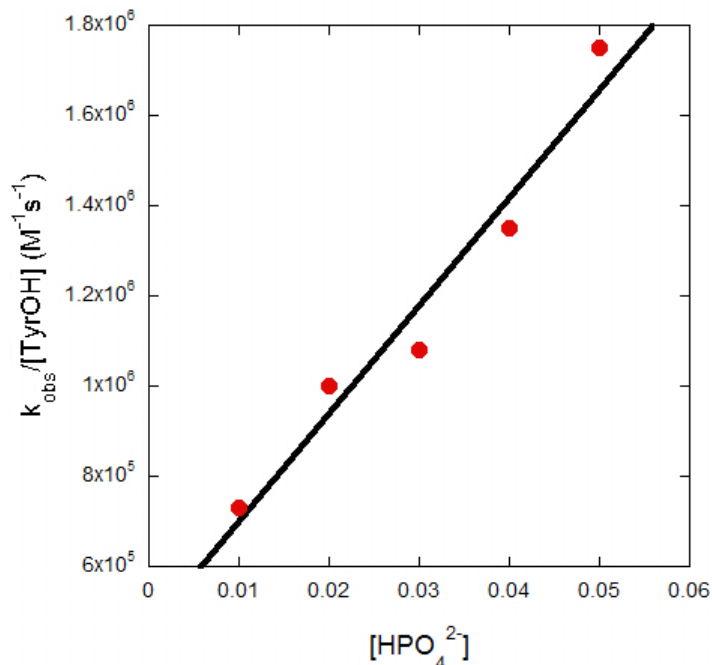


Figure 8. Plot of  $k_{\text{obs}}/[\text{TyrOH}]$  vs  $[\text{HPO}_4^{2-}]$  for  $1.0 \times 10^{-4} \text{M}$  TyrOH with  $2.0 \times 10^{-5} \text{M}$  Os(bpy)<sub>3</sub><sup>3+</sup> at pH 8.5 in phosphate buffer with 0.8M NaCl at  $23 \pm 2^\circ \text{C}$ .

3.4.9 Complete rate expression; validity of Schemes 1 and 2 and eq 2: With all of the rate and equilibrium parameters in Scheme 1 and eq 2 evaluated it is possible to test the validity of the mechanism and rate expression in general over a wide range in buffer, complex, and tyrosine concentrations and buffer ratios by application of the digital simulations. An example of a fit to data at pH = 7.5 with both MS-EPT and PT-ET pathways playing a significant role is shown in Figure 9. Kinetic and equilibrium parameters obtained from the kinetic analysis and used in the digital simulations are listed in Table 1.

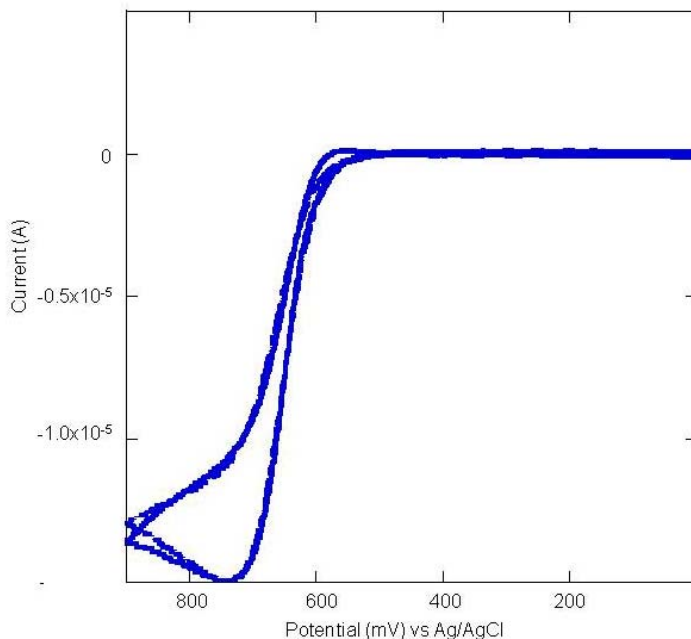


Figure 9: Cyclic voltammogram and digital simulation of  $\text{Os}(\text{bpy})_3^{3+}$  oxidation of tyrosine at  $1.0 \times 10^{-4}$  M tyrosine,  $2.0 \times 10^{-5}$  M  $\text{Os}(\text{bpy})_3^{3+}$ , and 0.05 M phosphate buffer,  $[\text{H}_2\text{PO}_4^-]/[\text{HPO}_4^{2-}] = 1/5$ , in 0.8M NaCl at  $23 \pm 2^\circ\text{C}$ . The simulation (dashed line) was fit to the electrochemical mechanism in Scheme 2 and rate constants reported in table 1 for phosphate.

Base	$\text{pK}_a$	$\text{K}_A$ ( $\text{M}^{-1}$ )	$k_1$ ( $\text{s}^{-1}$ )	$k_{-1}$ ( $\text{M}^{-1}\text{s}^{-1}$ )	$k_2$ ( $\text{M}^{-1}\text{s}^{-1}$ )	$\text{K}_A'$ ( $\text{M}^{-1}$ )	$k_{\text{red}}$ ( $\text{s}^{-1}$ )
Acetate	4.7	$11.7 \pm 0.9$	$1.4 \pm 0.2 \times 10^4$	$1.0 \pm 0.3 \times 10^8$	$1.7 \pm 0.2 \times 10^7$	$45 \pm 0.8$	$5.0 \pm 0.3 \times 10^3$
Succinate	5.6	$22.2 \pm 0.5$	$5.0 \pm 0.2 \times 10^4$	$3.7 \pm 0.9 \times 10^8$	$1.0 \pm 0.9 \times 10^7$	$31.2 \pm 0.2$	$2.5 \pm 0.2 \times 10^4$
Histidine	6.6	$26.3 \pm 0.3$	$1.4 \pm 0.1 \times 10^5$	$2.9 \pm 0.1 \times 10^9$	$1.4 \pm 0.1 \times 10^7$	$37.8 \pm 0.2$	$6.9 \pm 0.3 \times 10^4$
Phosphate	7.2	$30.0 \pm 0.1$	$3.3 \pm 0.1 \times 10^5$	$7.8 \pm 0.4 \times 10^9$	$1.7 \pm 0.3 \times 10^7$	$22.2 \pm 0.1$	$9.6 \pm 0.5 \times 10^4$
Tris	8.1	$37.8 \pm 0.5$	$1.1 \pm 0.1 \times 10^5$	$2.4 \pm 0.2 \times 10^9$	$1.1 \pm 0.2 \times 10^7$	$22.6 \pm 0.4$	$1.0 \pm 0.3 \times 10^6$

Table 2: Rate and equilibrium constants (Scheme 1) for oxidation of tyrosine by  $\text{Os}(\text{bpy})_3^{2+}$  for bases from acetate to tris with a  $\text{pK}_a$  range of 4.5-8.1 in 0.8 M NaCl at  $23 \pm 2^\circ\text{C}$ .

3.4.10 H/D Isotope Effects: The role of exchange of  $\text{D}_2\text{O}$  for  $\text{H}_2\text{O}$  on the kinetic parameters

in Scheme 1 was also investigated. Because of the overlap of contributions from both MS-

EPT and PT-EPT pathways over a wide region of buffer concentrations and ratios, the isotope effects were investigated under limiting conditions for the two pathways; pH 6.0 for MS-EPT and 8.5 for PT-ET. In these experiments kinetic parameters were derived from digital simulation of cyclic voltammograms as described in the previous section.

Cyclic voltammetry experiments were repeated in both pure (99 atom %) D<sub>2</sub>O isotope and in solutions containing equal mole fractions of both D<sub>2</sub>O and H<sub>2</sub>O in order to establish proton inventories for the two pathways, eq 19. In this equation  $k_{\text{obs,X}}$ ,  $k_{\text{obs,D}}$ , and  $k_{\text{obs,H}}$  are the observed rate constants obtained from the simulations at mole fraction  $\chi_{\text{D}}$ , in D<sub>2</sub>O and in H<sub>2</sub>O.<sup>21,35-37</sup>

Plots of  $k_{\text{obs,X}}/k_{\text{obs,H}}$  vs.  $\chi_{\text{D}}$  under both sets of limiting conditions are shown in Figure 10 for oxidation of tyrosine by Os(bpy)<sub>3</sub><sup>3+</sup> with added H<sub>2</sub>PO<sub>4</sub><sup>-</sup>-HPO<sub>4</sub><sup>2-</sup> buffer.

$$\frac{k_{\text{obs,X}}}{k_{\text{obs,H}}} = 1 + \chi_{\text{D}} (k_{\text{obs,D}} - k_{\text{obs,H}} - 1) \quad (19)$$

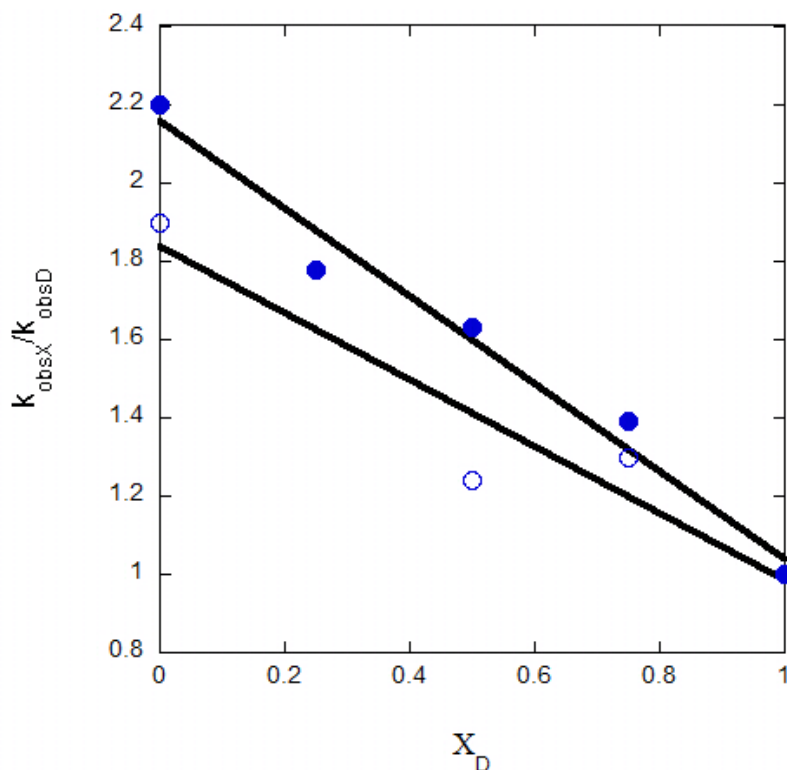


Figure 10: Plot of  $k_{obs,X}/k_{obs,H}$  vs.  $\chi_D$  according to eq 13 under limiting conditions for MS-EPT oxidation of tyrosine by  $Os(bpy)_3^{2+}$ ,  $H_2PO_4^-/HPO_4^{2-} < 1/10$ , at pH = 6.0 (open) and for limiting PT-ET.  $H_2PO_4^-/HPO_4^{2-} > 10/1$  closed

The procedure described in the previous section for isolation of the separate rate and equilibrium constants in Scheme 1 was repeated in both  $D_2O$  and the 1:1  $D_2O:H_2O$  mixture. Isotope effects for the separate parameters in Scheme 1 are reported in Table 2.

Base	pK <sub>a</sub>	EIE K <sub>A</sub>	KIE k <sub>1</sub>	KIE k <sub>red</sub>
Acetate	4.7	1.5±0.2	3.5±0.1	2.8±0.3
Succinate	5.6	1.8±0.1	2.8±0.2	2.5±0.4
Histidine	6.6	1.4±0.1	2.4±0.2	2.3±0.3
Phosphate	7.2	1.7±0.4	1.2±0.4	2.1±0.6
Tris	8.1	1.2±0.3	1.1±0.3	1.9±0.1

Table 2: Equilibrium and kinetic H/D isotope effects for tyrosine oxidation by  $Os(bpy)_3^{2+}$  in 0.8M NaCl at 23±2°C.

Although not shown, plots of  $k_X/k_H$  vs.  $\chi_D$  for the individual rate constants,  $k_1$ ,  $k_{-1}$ ,  $k_2$ , and  $k_{red}$ , were all linear consistent with transfer and involvement of a single proton.<sup>21,35-37</sup>

3.4.11 General Buffer Base Catalysis: The cyclic voltammetric technique was also applied to tyrosine oxidation by a series of metal complexes  $M(bpy)_3^{3+}$  ( $M = Fe, Ru, Os$ ) and buffer bases. In the complete study 5 buffers and four metal complex oxidants were investigated. In these studies catalytic enhancements arising from tyrosine oxidation by  $M(bpy)_3^{3+}$  was investigated over a broad range of tyrosine, buffer ratio, and base forms of the buffer at concentrations between 0.002M and 0.48M. The  $pK_a$  values for the bases range from 4.7 for acetate buffer to 8.1 for Tris in the series, Table 3, and  $E^{0'}$  values for the metal complex oxidants from 0.85 to 1.25V, vs NHE, Table 3 .

Base	$pK_a$
Acetate	4.7
Succinate	5.6
Histidine	6.6
Phosphate	7.2
Tris	8.1

Table 3: Each of the 5 bases reported with  $pK_a$  used in electrochemical equation.

The range of accessible buffers was limited by the  $pK_a$  of tyrosine (10.1 and by the influence on pH the response of the ITO electrodes. The surface of ITO has a phosphonated surface that responds to pH conditions of the solution. It is most effective at neutral or near neutral pH. As the pH nears this  $pK_a$ (TyrOH), the kinetic analysis is complicated by direct oxidation of TyrO<sup>-</sup> as it forms in equilibrium amounts.

Data for the series of oxidants in addition to  $\text{Os}(\text{bpy})_3^{3+}$  with the complete set of buffers are collected in Table 3. In reporting these data only values for  $k_{\text{red}}$ , the EPT step, and  $k_2$ , the rate constant for oxidation of tyrosine anion are reported. The other values are independent of oxidant,  $k_1, k_{-1}$ , or given the nearly common molecular radii through the series of complexes, were the same within experiment error of those reported in Table 1.

Oxidant	$E^{\circ}$ (V vs NHE)	$k_{\text{red}}$ ( $\text{s}^{-1}$ )	$k_2$ ( $\text{M}^{-1}\text{s}^{-1}$ )
$\text{Os}(\text{bpy})_3^{3+}$	0.85	$9.6 \times 10^4$	$1.7 \times 10^7$
$\text{Fe}(\text{bpy})_3^{3+}$	1.06	$1.8 \times 10^6$	$6.1 \times 10^7$
$\text{Ru}(\text{dmb})_3^{3+}$	1.11	$2.7 \times 10^6$	$1.6 \times 10^8$
$\text{Ru}(\text{bpy})_3^{3+}$	1.25	$4.4 \times 10^7$	$7.2 \times 10^8$

Table 4: Rate constants reported for oxidants over a potential rang of 0.85V vs NHE for  $\text{Os}(\text{bpy})_3^{3+}$  to 1.25V vs NHE for  $\text{Ru}(\text{bpy})_3^{3+}$

### 3.5 Discussion:

We report here on tyrosine oxidation in the presence of a series of buffers at a variety of pH's. For the buffers used the dominant form of the amino acid is as the zwitterion, Scheme 1 over the pH range 4.7 to 8.1. Oxidation of tyrosine under these conditions is known to occur with radical coupling following  $1e^-$  oxidation<sup>33,38,39</sup> consistent with  $n = 1$  in the cyclic voltammetry simulations with  $n$  the electrochemical stoichiometry. There was evidence in the voltammograms at higher pH's with Tris as the buffer for possible complications arising from reaction of the deprotonated amino acid,  $\text{M}(\text{bpy})_3^{3+}, ^-$   $\text{OOCCH}(\text{CH}_2\text{C}_6\text{H}_5\text{OH})\text{NH}_2$ .

The electrochemical simulations were carried out at ITO (Sn(IV) doped  $\text{In}_2\text{O}_3$ ) electrodes. Direct oxidation of tyrosine at these electrodes is kinetically inhibited although studies currently in progress show that oxidation does occur at glassy carbon. Kinetic

inhibition of the direct oxidation allowed for indirect, chemically catalyzed oxidation by added oxidants  $M(\text{bpy})_3^{3+}$  to be investigated. The  $M(\text{bpy})_3^{3+/2+}$  couples are kinetically reversible at ITO and, following electrochemical oxidation to  $M(\text{bpy})_3^{3+}$ , oxidize tyrosine in solution near the electrode resulting in a catalytic component to the  $M(\text{bpy})_3^{3+/2+}$  couple.

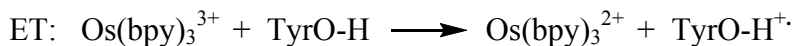
3.5.1 Pathways for tyrosine oxidation. The results presented here and in earlier communications,<sup>15</sup> demonstrate the existence of a general catalytic effect in the oxidation of tyrosine by  $\text{Os}(\text{bpy})_3^{3+}$  and related metal complex oxidants in the presence of added buffers. The catalytic effect is significant. For example, there is an increase over background reactivity of  $10^5$  in a 0.05 M 1:5  $\text{H}_2\text{PO}_4^-/\text{HPO}_4^{2-}$  buffer at pH 7.5 compared to an unbuffered solution at pH= 7. A catalytic enhancement of  $\sim 10^2$  over background is observed for an acetate buffer at the same buffer ratio at pH = 5.4. For Tris under comparable conditions the enhancement was  $10^6$ .

The kinetic analysis shows that the origin of the catalysis with added buffers is prior association of the base form of the buffer with tyrosine Scheme 1. This activates tyrosine both toward proton transfer to added buffer base B and toward Multiple Site-Electron Proton Transfer (MS-EPT) with proton transfer to B coupled with electron transfer to  $M(\text{bpy})_3^{3+}$ .

As shown by the kinetic studies on oxidation of TyrOH and TyrO<sup>-</sup> by  $M(\text{bpy})_3^{3+}$ , additional background pathways for tyrosine oxidation also exist. A summary of pathways is given in Scheme 5 for the generalized buffer <sup>+</sup>HB/B with  $\text{Os}(\text{bpy})_3^{3+}$  as the example oxidant. In the calculations that follow:  $\text{pK}_a(\text{H}_2\text{O}) = 15.7$ ,  $\text{pK}_a(\text{H}_3\text{O}^+) = -1.74$ ,  $\text{pK}_a(\text{TyrOH}) = 10.1$ ,  $\text{pK}_a(\text{TyrOH}^+) = -2$ ,  $E^{0'}(\text{TyrOH}^{+/0}) = 1.34$  V vs. NHE,  $E^{0'}(\text{Os}(\text{bpy})_3^{3+/2+}) = 0.85$  V.  $F$  is the Faraday, 1 eV/V in SI units.

***Scheme 8. Pathways for Tyrosine Oxidation (23<sup>0</sup>C, I = 0.8M NaCl)***

**ET-PT(rate limiting electron transfer followed by proton transfer)**



$$\Delta G^{\circ} = 1.34\text{eV}$$

$$k = 1.7 \times 10^2 \text{ M}^{-1}\text{s}^{-1}$$



$$\Delta G^{\circ} = 0.059(\text{pK}_a(\text{TyrO-H}^{\cdot+}) - \text{pH}) \text{ (eV at } 25^{\circ}\text{C)}$$

**PT-ET (rate limiting proton transfer followed by electron transfer)**



$$\Delta G^{\circ} = 0.059(\text{pK}_a(\text{TyrOH}) - \text{pK}_a(\text{B})) \text{ (eV at } 25 \text{ C)}$$

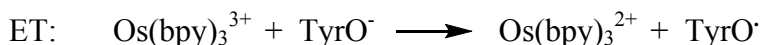
$$k(\text{B} = \text{HPO}_4^-) = 3.0 \times 10^5 \text{ s}^{-1} \text{ (Table 1)}$$



$$\Delta G^{\circ} = 0.059(\text{pK}_a(\text{TyrOH}) - \text{pK}_a(\text{H}_2\text{O})) = -0.33 \text{ eV}$$



$$\Delta G^{\circ} = 0.059(\text{pK}_a(\text{TyrOH}) - \text{pK}_a(\text{H}_3\text{O}^+)) = +0.70 \text{ eV}$$



$$\Delta G^{\circ} = -1.5 \text{ eV}$$

$$k = 1.7 \times 10^7 \text{ M}^{-1}\text{s}^{-1}$$

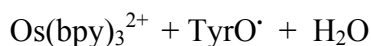
**MS-EPT (Multi-site electron-proton transfer)**



$$\Delta G^{\circ} = -F\{E^{\circ\circ}(\text{Os(bpy)}_3^{3+/2+}) - E^{\circ\circ}(\text{TyrOH}^{\cdot+/0})\} + 0.059\{\text{pK}_a(\text{TyrOH}^{\cdot+}) - \text{pK}_a(\text{B})\}$$

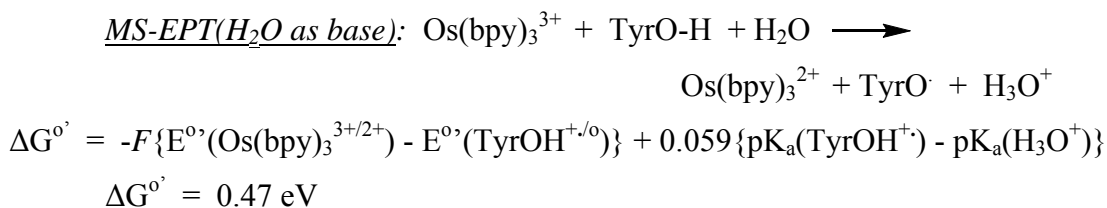
$$\Delta G^{\circ} = -0.22 \text{ eV} \text{ (B} = \text{HPO}_4^-, \text{ Table 1)}$$

$$k_{\text{red}} K_A K_A' = 9.6 \times 10^4 \text{ M}^{-1}\text{s}^{-1} \text{ (B} = \text{HPO}_4^-, \text{ Table 1)}$$



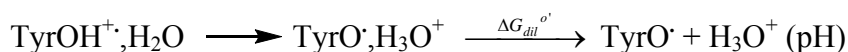
$$\Delta G^{\circ} = -F\{E^{\circ\circ}(\text{Os(bpy)}_3^{3+/2+}) - E^{\circ\circ}(\text{TyrOH}^{\cdot+/0})\} + 0.059\{\text{pK}_a(\text{TyrOH}^{\cdot+}) - \text{pK}_a(\text{H}_2\text{O})\}$$

$$\Delta G^{\circ} = -0.57 \text{ eV}$$



**ET-PT.** Oxidation of tyrosine by  $\text{Os}(\text{bpy})_3^{3+}$  by initial electron transfer is relatively slow with  $k = 1.7 \times 10^2 \text{ M}^{-1}\text{s}^{-1}$ . Slow electron transfer is due to the uphill nature of the electron transfer step with  $\Delta G^{o'} = 1.34 \text{ eV}$ .

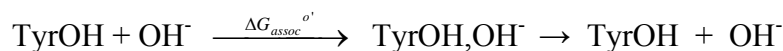
Electron transfer greatly enhances acidity with  $\text{pK}_a$  decreasing from 10.1 for TyrOH to -2 for  $\text{TyrOH}^+$ .<sup>22</sup> The free energy change in the net reaction is recovered in a subsequent proton loss to solvent which occurs first by proton transfer to an associated water molecule or water cluster,



Initial proton loss occurs with  $\Delta G^{o'} = 0.059(\text{pK}_a(\text{TyrOH}^+) - \text{pK}_a(\text{H}_3\text{O}^+)) = -0.02 \text{ eV}$ . It is followed by dilution of the released proton to the prevailing pH,

$$\Delta G^{o'} = 0.059(\text{pK}_a(\text{TyrOH}^+) - \text{pH}) \text{ (eV at 25 C)}.$$

**PT-ET.** Proton loss to  $\text{OH}^-$  is favorable given the relative  $\text{pK}_a$ 's of TyrOH and  $\text{H}_2\text{O}$ . It occurs by initial association, the reverse of dilution, with  $\Delta G_{assoc}^{o'} = 0.059(\text{pK}_a(\text{TyrOH}) - \text{pH}) \text{ (eV at 25 C)}$ ,



and is followed by proton loss,

$$\Delta G^{o'} = 0.059(\text{pK}_a(\text{TyrOH}) - \text{pK}_a(\text{H}_2\text{O})) = -0.33 \text{ eV (at 25 C)}$$

Water is not a good proton acceptor with an energy penalty of +0.22 eV for initial proton transfer to  $\text{H}_2\text{O}$  followed by electron transfer. The use of water as a proton acceptor is

expected to be important as a competitive pathway only for strong acids or if the following ET reaction is slow.

**MS-EPT.** MS-EPT with coupled electron transfer to the complex and proton transfer to a base (B, OH<sup>-</sup>, or H<sub>2</sub>O) is microscopically more complex than either simple electron transfer or proton transfer and will be discussed in detail in the next section. MS-EPT is at a microscopic disadvantage due to an enhanced barrier arising from the requirement for proton transfer. There are also important orbital requirements for an MS-EPT pathway and a need for low energy proton orbital binding sites at both the proton donor and reduced acceptor.

MS-EPT plays a role because of its significant energy advantage. This can be seen in the  $\Delta G^{\circ}$  values for MS-EPT in Table 8. These data reveal that  $\Delta G^{\circ}$  for MS-EPT with B as the proton acceptor varies from -0.11 to 0.09eV with  $\Delta G^{\circ} = -0.59$  eV for OH<sup>-</sup> as acceptor base. Because of limits imposed by the pK<sub>a</sub> of TyrOH, we were unable to establish saturation kinetics for OH<sup>-</sup> as EPT base in the electrochemical experiment. As discussed in the next paper, it does function as an EPT base and is highly activating toward tyrosine oxidation

The analysis for MS-EPT with H<sub>2</sub>O as the proton acceptor shows that this is an energetically unfavorable pathway except for very strong acids given pK<sub>a</sub>(H<sub>3</sub>O<sup>+</sup>) = -1.74. For oxidation of TyrOH by Os(bpy)<sub>3</sub><sup>3+</sup>,  $\Delta G^{\circ} = +0.49$  eV for initial ET and +0.22 eV for MS-EPT with proton transfer to water. Even though  $\Delta G$  is more favorable for ET, it is expected to dominate reactivity because of the microscopic demands imposed by proton transfer.<sup>3,19,21</sup>

3.5.2 Kinetic Parameters. Kinetic and equilibrium parameters in Scheme 1 for the series of buffers, <sup>+</sup>HB/B, are listed in Table 1 and H/D isotope effects in Table 2.

*Association complex formation and H-bonding,  $K_A$ .* The association constants between TyrOH and the EPT bases,  $K_A$ , in Table 1 are significantly larger than predicted by simple, non-interactive association and the Fuoss equation in eq 20.<sup>40</sup> It calculates the statistic probability of contact without provision for special interactions such as H-bonding. In eq 20,  $N_A$  is Avogadro's number and  $d$  the close contact, distance of separation in the association complex between contacting spheres. Based on radii of 7 Å for  $M(\text{bpy})_3^{3+}$  and 3.5 to 2.6 Å for the bases, calculated values of  $K_A$  range from 1-4.<sup>40</sup> Experimental values are greater by a factor of 10 presumably reflecting the energetic importance of H-bonding between TyrOH and the added base.

$$K_A = \frac{4\pi N_A d^3}{3000} \quad (20)$$

From the data in Table 1, the free energy of formation of the association complex,  $-RT\ln K_A$  increases with the basicity of B as measured by its free energy of proton affinity,  $RT\ln K_a(^+\text{HB})$ , Figure 11. The slope of the linear correlation in Figure 11 is 0.14.

The increase in  $K_A$  with increasing base provides additional evidence for the importance of H-bonding with its magnitude increasing with  $RT\ln(K_a(^+\text{HB}))$ . There are implications in this observation for EPT reactivity. Increased H-bonding to stronger bases is accompanied by increasing symmetrization in the TyrO-H---B hydrogen bond resulting in a shorter proton transfer distance as the base strength of B increases. Proton transfer is inherently quantum mechanical given the high frequency of the  $\nu(\text{OH})$  vibrational modes coupled to the transfer event.<sup>41,42</sup> Symmetrization is important in increasing vibrational overlap, which decreases the proton transfer distance and enhancing rates of both proton transfer and MS-EPT and decreasing H/D kinetic isotope effects.

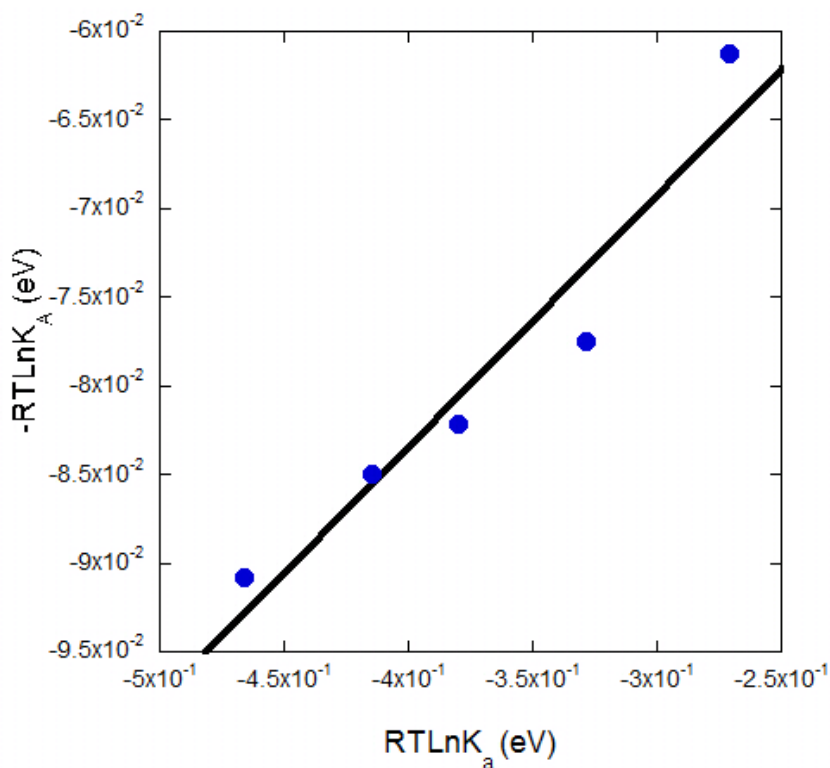


Figure 11: Plot of  $-RT\ln(K_A)$  vs.  $RT\ln(K_a(^+HB))$  from data in Table 1 in 0.8M NaCl aqueous solution at 23 °C. with 0.05M concentrations of various bases.

From the data in Table 2 there are small equilibrium isotope effects for  $K_A$ , which vary from 1.2 to 1.8 without any systematic trend in the data. The fact that  $K_A(H_2O)/K_A(D_2O) > 1$  shows that H is favored over D in the H-bonded association complex before proton transfer occurs presumably due to a zero point energy effect.

*Proton transfer to B.*  $k_1$ . Rate constants for proton transfer,  $\text{TyrO-H} \xrightarrow{k_1} \text{TyrO}^- \text{---}^+ \text{H-B}$ , also increase with the base strength of the acceptor base. This trend is shown by the plot of  $-RT\ln k_1$  vs.  $RT\ln K_a(\text{HB}^+)$  in Figure 12. The slope of the best fit straight line in Figure 12 is 0.78. The observed increase in  $k_1$  with base strength of B is also an additional, expected consequence of the symmetrization of the  $\text{TyrOH} \text{---} \text{B}$  H bond decreasing the barrier to proton transfer.

The role of proton transfer distance in the TyrO-H---B H-bond also appears in the variations in H/D kinetic isotope effects (KIE) for proton transfer in Table 2. These data reveal a systematic increase in  $k(\text{H}_2\text{O})/k(\text{D}_2\text{O})$  for  $k_1$  from 3.5 for B = acetate with  $\text{pK}_a(^+\text{H-B}) = 4.7$  to for B = Tris with  $\text{pK}_a(^+\text{H-B}) = 8.1$  as  $\Delta G$  for proton transfer decreases from +0.32 to +0.12 eV. The variation with  $\text{pK}_a$  is consistent with a shorter proton transfer distance for stronger bases where H-bonding is stronger and the H-bond more symmetric.<sup>43-51</sup>

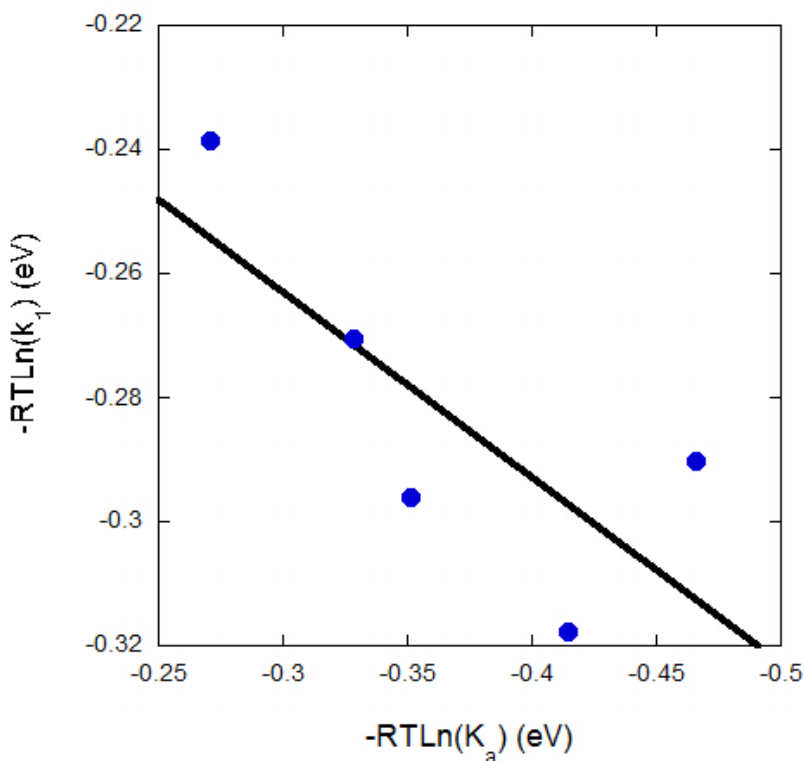
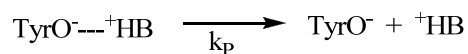
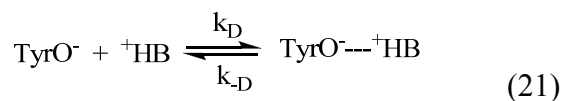


Figure 12: Plot of  $\text{RT} \ln k_1$  vs  $\text{RT} \ln K_a$  showing a linear dependence of  $k_1$  on the  $\text{pK}_a$  of the basic form of the buffer reporting a slope of 0.4.

*Back proton transfer to B.  $k_{-1}$ .* The mechanism for back proton transfer,  $k_{-1}$  in Scheme 1, is expanded in eq 21 into pre-association between TyrO<sup>-</sup> and <sup>+</sup>H-B followed by proton transfer,  $k_p$ . Assuming the steady state approximation for the association complex, TyrO<sup>-</sup>---HB<sup>+</sup>,  $k_{-1}$  is given by eq 22. In the limit  $k_p \gg k_{-D}$ ,  $k_{-1} = k_D$  and re-protonation is diffusion limited. In the limit that  $k_p \ll k_{-D}$ ,  $k_{-1} = k_p(k_D/k_{-D})$  a rapid pre-equilibrium precedes proton transfer.



$$k_{-1} = \frac{k_p k_D}{k_{-D} + k_p} \quad (22)$$

In Figure 13 is shown a plot of  $RT\ln(k_{-1})$  vs.  $\Delta G^{0'}$  for back proton transfer with  $\Delta G^{0'}$  calculated from,  $\Delta G^{0'} = -0.059(\text{pK}_a(\text{TyrOH}) - \text{pK}_a({}^+\text{HB}))$ . The data are striking in providing evidence for “inverted region proton transfer” for acetic and succinic acids with  $\Delta G^{0'} = -0.31$  and  $-0.26$  eV with the rate constant for proton transfer decreasing as the reaction becomes more favorable. Other examples have been reported in the recent chemical literature.<sup>42-44</sup> Given the magnitudes of the rate constants and the implied diffusion controlled limit of  $3\text{-}7 \times 10^9 \text{ M}^{-1}\text{s}^{-1}$  by the data in Table 1,  $k_{-1} = k_p(k_D/k_{-D})$  with the free energy dependence appearing in the proton transfer step.

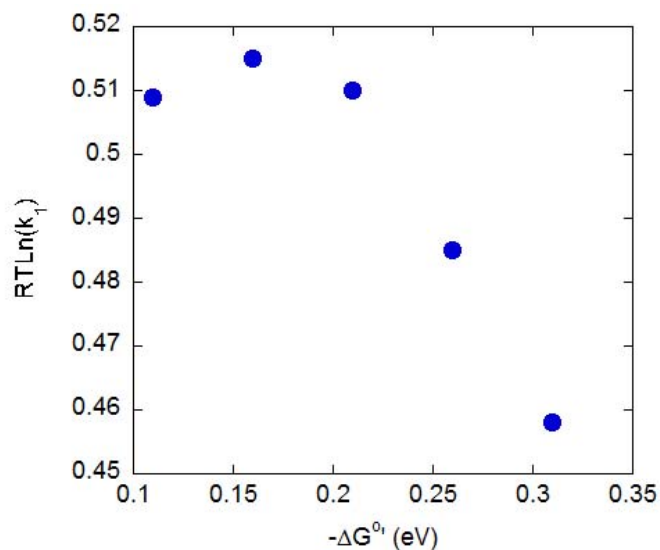


Figure 13. Variation of  $RT\ln k_{-1}$  for back proton transfer on  $-\Delta G^{0'}$  for the reaction taken from the data in Table 2.

Multi Site-Electron Proton Transfer. One goal of this study was to identify and verify Scheme 1. A second was to use the combination of four metal complexes oxidants and five acceptor bases to provide experimental insight into the microscopic details for this pathway.

*Relationship between proton transfer and EPT.* One issue to explore experimentally was the separate proton and electron transfer components of MS-EPT,  $k_1$  and  $k_{\text{red}}$  in Scheme 1. Two sets of data give insight into this. In Figure 14, are shown plots of  $RT \ln k_1$  vs  $RT \ln k_{\text{red}}$  for the series of  $M(\text{bpy})_3^{3+}$  oxidants with  $k_1$  the rate constant for proton transfer from TyrOH to B within the association complex between them and  $k_{\text{red}} = k_{\text{EPT}}$  the rate constant for coupled electron-proton transfer, eq 23. In Figure 17 the correlations are for the four separate oxidants increasing in reduction potential from 0.85 V for the  $\text{Os}(\text{bpy})_3^{3+}/\text{Os}(\text{bpy})_3^{2+}$  couple (green) to 1.25V for the  $\text{Ru}(\text{bpy})_3^{3+}/\text{Ru}(\text{bpy})_3^{2+}$  couple (red) with EPT bases of increasing base strength from acetate (4.7) to Tris (8.1), Table 3.

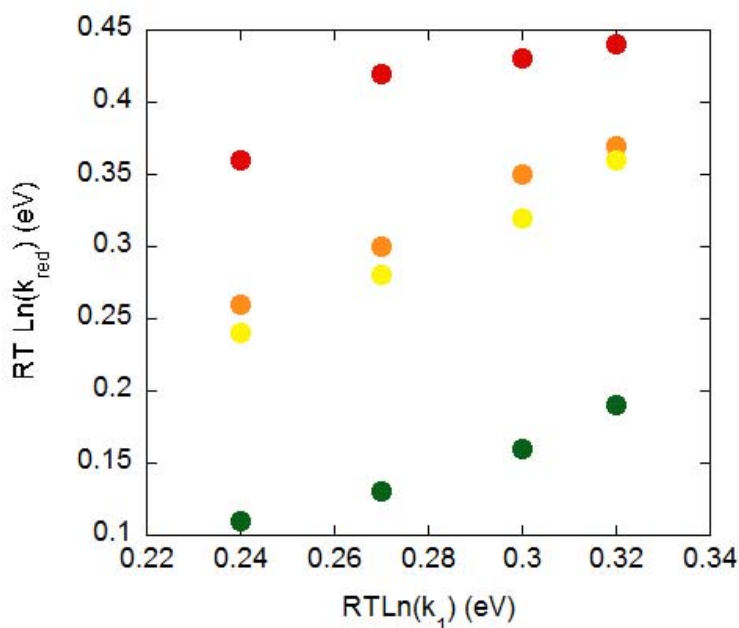
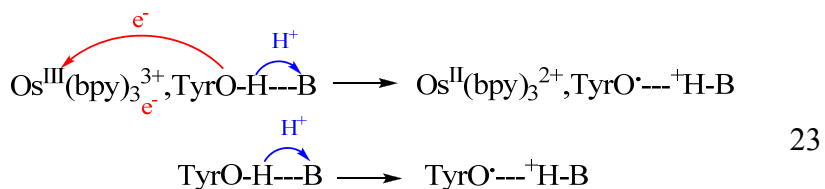


Figure 14: Illustrating the variation of  $RT \ln k_1$  for proton transfer with  $RT \ln(k_{\text{red}})$  for EPT ( $k_{\text{red}} = k_{\text{EPT}}$ ) in 0.8 M NaCl at  $23 \pm 2$  °C. Green points  $\text{Os}(\text{bpy})_3^{2+/3+}$ , yellow points  $\text{Fe}(\text{bpy})_3^{3+/2+}$ , orange points  $\text{Ru}(\text{dmb})_3^{3+/2+}$ , and red points  $\text{Ru}(\text{bpy})_3^{3+/2+}$ .



As expected by the comparison of microscopic detail in eq 23, proton transfer and EPT respond similarly to increases in the acceptor ability of the base. For each separate oxidant, there is a direct correlation between  $\text{RTln}(k_1)$  and  $\text{RTln}(k_{\text{EPT}})$  with slopes of  $\sim 1.3$ . This is true for EPT for oxidants whose reduction potentials vary over a range of 0.4 V.

The equal sensitivities of the separate correlations to  $\text{pK}_a(^+\text{HB})$  shows that the two processes, proton transfer to B and MS-EPT, are equally responsive to the electronic, environmental, and other factors that dictate the separate barriers to PT and EPT.

*Driving force dependence.* A second experiment probe into the separate roles of electron and proton transfer is available from the  $\Delta G^{\circ}$  dependence of EPT arising from the separate variations in  $\text{pK}_a(^+\text{HB})$  and redox potential of the oxidant. If the microscopic description of MS-EPT as involving concerted electron and proton transfer is correct, eq 23, the same  $\Delta G^{\circ}$  dependence should exist by varying either electron or proton acceptor.

Plots of  $\text{RTln}(k_{\text{EPT}})$  vs.  $\Delta G_{\text{EPT}}^{\circ}$  are shown in Figures 15a and 15b with  $\Delta G_{\text{EPT}}^{\circ}$  varied in two ways, with succinate dianion as the common base and the series of oxidants in Figure 15a and with  $\text{Os}(\text{bpy})_3^{3+}$  as the common oxidant and the series of bases, Figure 15b. Values of  $\Delta G_{\text{EPT}}^{\circ}$  were calculated by using eq 24.

$$\Delta G_{\text{EPT}}^{\circ} = E^{\circ}(\text{TyrOH}^{+/\cdot}) - E^{\circ}(\text{M}(\text{bpy})_3^{3+/2+}) - 0.059(\text{pK}_a(^+\text{HB}) - \text{pK}_a(\text{TyrOH}^+)) \tag{24}$$

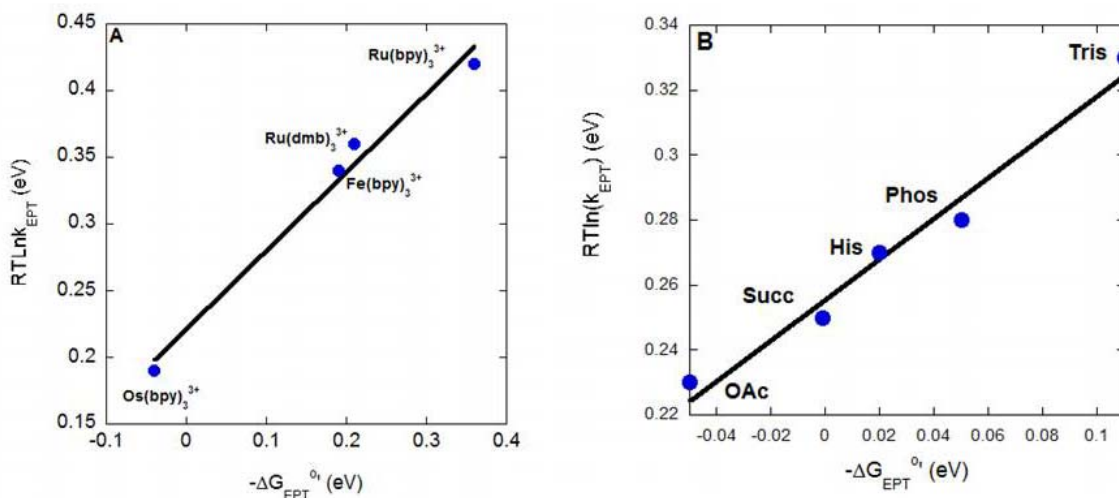


Figure 15: Variation of  $RT\ln(k_{red})$  with  $-\Delta G_{EPT}^0$  in eV in 0.8 M NaCl at 23°C: A) by varying  $E^{0'}(M^{3+/2+})$  for the oxidant (slope = 0.61) and B) by varying the  $pK_a$  of the acceptor base (slope = 0.61).

These data are significant in revealing that the key factor dictating rate constants for EPT is the driving force and not how it is varied. This conclusion is reached independent of the structural details of the base which includes in the series both N and O bases.

**3.5.3 Free Energy Dependence of Multi Site-Electron Proton Transfer.** As discussed in an earlier communication, detailed analysis of the dependence of  $k_{EPT}$  on  $\Delta G_{EPT}^0$  is complicated by the quantum nature of the proton transfer which requires application of the sum over vibrational states approach of Hammes-Schiffer, et. al, eq 25.<sup>55-58</sup> A quantum treatment is required for the high frequency  $\nu(O-H)$  and  $\nu(N-H)$  modes involved in the proton transfer with quantum spacings  $> 3000\text{ cm}^{-1}$  well above the background thermal energy at room temperature,  $\sim 200\text{ cm}^{-1}$ . In the limit of adiabatic proton transfer and non-adiabatic electron transfer,  $k_{EPT}$  is given by eq 25. In this equation  $V_{ET}$  is the electron transfer matrix element,  $\lambda$  is the sum of the solvent and intramolecular reorganization energies treated classically, and  $\varphi_{\mu}$  and  $\varphi_{\nu}$  are the proton vibrational wave functions for the proton before and after EPT occurs. The summations are over initial levels  $\mu$  in their Boltzmann populations,  $P(\mu)$ , and from each initial vibrational level  $\mu$  to final level  $\nu$ . As noted above, this equation is valid in

the limit of nonadiabatic electron transfer with weak electronic coupling and neglects small variations in  $\lambda$  for the individual vibronic channels.

$$\mathbf{k}_{\text{EPT}} = \frac{2\pi}{\hbar} \sum_{\mu} P_{\mu} \sum_{\nu} V_{\text{ET}}^2 \langle \varphi_{\mu} | \varphi_{\nu} \rangle^2 \left( 4\pi\lambda RT \right)^{-1/2} \exp \left[ - \frac{(\lambda + \Delta G^{o'} + (\mu - \nu)\hbar\omega)^2}{4\pi\lambda RT} \right] \quad (25)$$

If EPT is dominated by the  $\mu = 0 \rightarrow \nu = 0$  vibronic channel, eq 25 can be written as eq 26a with  $\Delta G^{o'} = \Delta G_{\text{EPT}}^{o'}$ . The quantity  $k_0$  is the EPT rate constant at  $\Delta G^{o'} = 0$ .

$$RT \ln(k_{\text{EPT}}) = RT \ln(k_0) + \frac{\Delta G^{o'}}{2} \left( 1 + \frac{\Delta G^{o'}}{2\lambda} \right) \quad (26a)$$

$$\mathbf{k}_0 = \frac{2\pi}{\hbar} V_{\text{ET}}^2 \langle \varphi_{\mu} | \varphi_{\nu} \rangle^2 \exp \left[ - \frac{\lambda}{4RT} \right] \quad (26b)$$

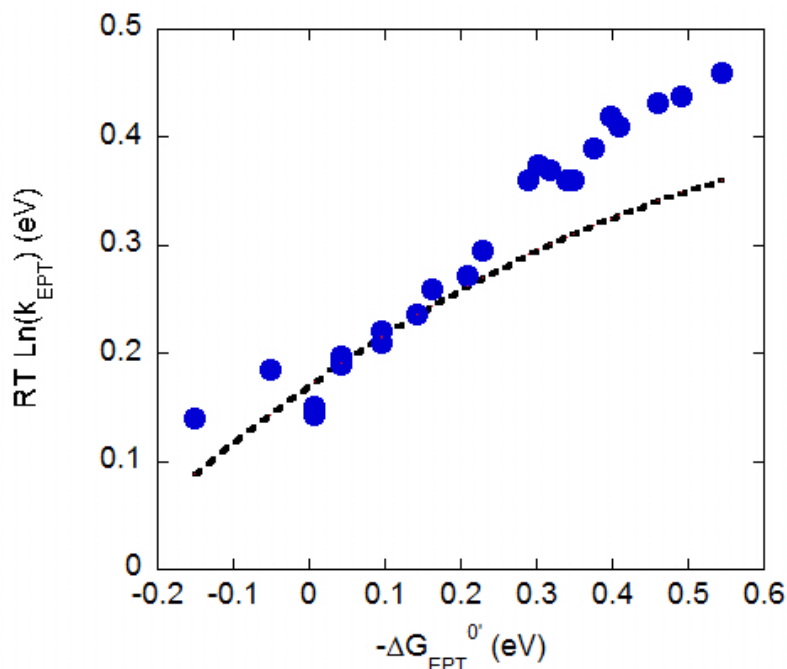


Figure 16: Variation of  $RT \ln(k_{\text{red}})$  vs  $-\Delta G^{o'}$  in eV by varying both  $E^{o'}$  for the oxidant and  $pK_a$  for the acceptor base, see text. The dashed line is a plot of  $RT \ln(k_{\text{red}}) = RT \ln(k_0) + \Delta G^{o'}/2 (1 + \Delta G^{o'}/2\lambda)$  according to eq 26a with  $k_0 = 8.9 \times 10^2 \text{ s}^{-1}$  from Figure 15a and b and  $\lambda = 0.90 \text{ eV}$  from ref 58.

In Figure 16 is shown a plot of  $RT \ln(k_{\text{EPT}})$  vs  $-\Delta G^{o'}$  for the complete data set including all bases and all oxidants with the dashed line an attempted fit to eq 26a. The

quantity,  $k_0 = 8.9 \times 10^2 \text{ s}^{-1}$ , was evaluated from these data as the average of  $k_{\text{red}}$  values at  $\Delta G^{\circ} = 0 \text{ eV}$  and  $\lambda = 0.9 \text{ eV}$  taken from an analysis of a related, intramolecular tyrosine oxidation.

58

It is clear that the limiting expression with EPT occurring solely through the  $\mu, \nu = 0$  vibronic channel is unable to account for the experimental  $\Delta G$  dependence. This failure points to the importance of quantum effects and vibronic transitions above the lowest levels where  $\phi_{\mu}, \phi_{\nu}$  vibrational overlap is enhanced.

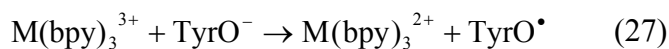
The importance of quantum effects appears at other places in the data. One is in the  $k(\text{H}_2\text{O})/k(\text{D}_2\text{O})$  kinetic isotope effect (KIE) data in Table 2 for oxidation of TyrOH by  $\text{Os}(\text{bpy})_3^{3+}$ . The same trends in KIE with  $\Delta G^{\circ}$  are observed for proton transfer and MS-EPT, Table 2. In both sets of data KIE decreases as  $\Delta G^{\circ}$  becomes more favorable with a maximum KIE reached for acetate as base with  $\Delta G^{\circ} \sim 0$ , Table 2. As noted in an earlier section, this is a consequence of increasing symmetrization of the TyrO-H---B hydrogen bond as the base strength of B increases which decreases the proton transfer distance increasing vibrational overlap integrals, eq 25.

The most dramatic quantum effect appears in the apparent structure in the plot of  $RT \ln(k_{\text{EPT}})$  vs  $\Delta G^{\circ}$  in Figure 16. This appears to be an inherent quantum effect, a “quantum beat”, arising from the high frequency  $\sim 3000 \text{ cm}^{-1}$  modes involved in the TyrO-H---B  $\rightarrow$  TyrO<sup>-</sup>---<sup>+</sup>H-B transfer.<sup>59</sup>

#### 3.5.4 Free Energy Dependence of TyrOH and TyrO<sup>-</sup> Oxidation by Electron Transfer.

Following proton loss from TyrOH in Scheme 1, TyrO<sup>-</sup> is oxidized by  $\text{M}(\text{bpy})_3^{3+}$ , eq 27 followed by radical coupling. As expected, and as shown by the data in Table 2,  $k_2$  values derived for this step are independent of the base within experimental error, which is true for

all four oxidants. This value is agreement with the value  $k_2 = k_{\text{ET},\text{TyrO}^-} = 1.7 \pm 0.5 \times 10^7 \text{ M}^{-1}\text{s}^{-1}$  measured by electrochemical investigation of the tyrosyl anion.



It is apparent from these data that  $k_2$  increases as  $-\Delta G^{0'}$  increases. From the classical Marcus-Hush theory for electron transfer within a structurally homologous series of reactions, the electron transfer rate constant,  $k_{\text{ET}}$ , is predicted to vary with driving force,  $-\Delta G_{\text{ET}}$ , as shown in 27.<sup>60-61</sup>

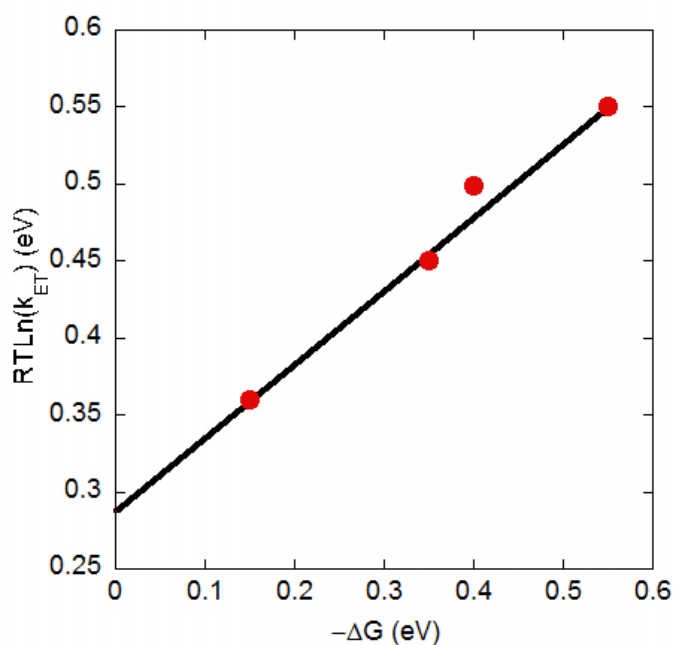


Figure 17: Plot of  $RT \ln(k_{\text{ET}})$  vs  $-\Delta G^{0'}$  for tyrosine anion oxidation by  $\text{M}(\text{bpy})_3^{3+}$ , eq 27, in 0.8M NaCl at  $23 \pm 2^\circ\text{C}$ . Individual data points are the average value of 5 individual trials.

$$RT \ln(k_2) = RT \ln(k_{\text{ET}}(0)) + RT \ln(K_A) + \frac{\Delta G_{\text{ET}}}{2} \left(1 + \frac{\Delta G_{\text{ET}}}{2\lambda}\right) \quad (28a)$$

$$k_{\text{ET}}(0) = v_{\text{ET}} K_A (4\pi RT \lambda)^{1/2} \exp\left[-\frac{(\Delta G_{\text{ET}} + \lambda)^2}{4\lambda RT}\right] \quad (28b)$$

In these equations  $v_{\text{ET}}$  is the frequency factor for electron transfer,  $K_A$  the equilibrium constant for association between  $\text{M}(\text{bpy})_3^{3+}$  and  $\text{TyrO}^-$ , and  $\lambda$  the sum of intramolecular and

solvent reorganization energies.<sup>60,61</sup>  $\Delta G_{ET}$  is the free change for electron transfer within the association complex between reactants,  $M(\text{bpy})_3^{3+}, \text{TyrO}^- \xrightarrow{k_{ET}} M(\text{bpy})_3^{2+}, \text{TyrO}^\cdot$ . It is related to the overall free energy change,  $\Delta G^{o'}$ , as shown in eq 29 with  $K_A$  the association constant between the electron transfer reactants and  $K_{-A}$  for the products,  $M(\text{bpy})_3^{2+}$  and  $\text{TyrO}^\cdot$ .  $k_{ET}(0)$  is the electron transfer rate constant at  $\Delta G_{ET} = 0$ .

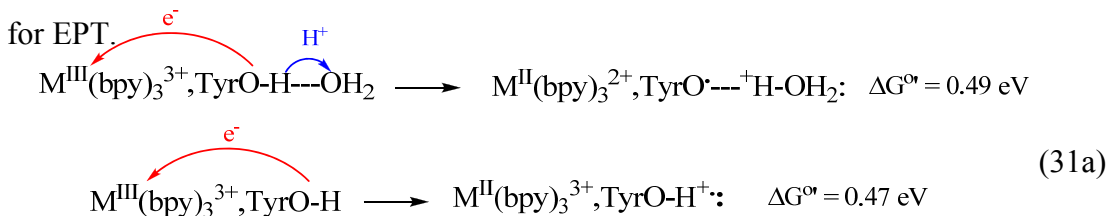
$$\Delta G_{ET} = \Delta G^{o'} - 0.059 \log(K_A - K_{-A}) \quad (\text{in eV at } 25^\circ\text{C}) \quad (29)$$

Eq 29 predicts a quadratic dependence of  $\ln(k_{ET})$  on  $\Delta G_{ET}$  with  $k_{ET}$  increasing as  $-\Delta G_{ET}$  increases. In the limit  $|\Delta G_{ET}| \ll \lambda$ ,  $k_{ET}$  is predicted to vary with  $\Delta G_{ET}/2$ , eq 30.

$$RT \ln(k_2) = RT \ln k_{ET}(0) K_A - \frac{\Delta G_{ET}}{2} \quad (30)$$

As shown in Figure 17, a plot of  $RT \ln(k_{ET})$  vs.  $\Delta G^{o'}$  is linear with a slope of 0.5 as predicted by eq 30. From the value of  $RT \ln(k_2)$  at  $\Delta G^{o'} = 0$ ,  $k_2 = k_{ET}(0) K_A = 9.0 \times 10^4 \text{ M}^{-1} \text{ s}^{-1}$ . In the correlation in Figure 17 in eq 27 was neglected and assumed to be negligible. the correction for the difference in  $\Delta G$  of association between precursor and successor complexes is neglected and assumed to be negligible.

In the oxidation of tyrosine by  $M(\text{bpy})_3^{3+}$  an ambiguity exists with regard to mechanism and whether initial oxidation occurs by electron transfer or MS-EPT with a water molecule or cluster as acceptor. The two possibilities are shown in eq 31 following pre-association of oxidant and tyrosine. From Scheme 5 the  $\Delta G$  changes are comparable clearly pointing to ET as the redox step given the greater microscopic demands and enhanced barrier for EPT.



(31b)

In Figure 18 is shown a Marcus-Hush plot for  $M(bpy)_3^{3+/}$  oxidation of tyrosine. From the extrapolated value of the experimental rate constants to  $\Delta G^0$ ,  $k_{ET}(0)K_A = 9.0 \times 10^4 \text{ M}^{-1}\text{s}^{-1}$ .

### 3.6 Conclusions

A number of significant conclusions emerge from this study concerning tyrosine oxidation and, by inference, other phenols:

- *There are multiple, competing pathways for tyrosine oxidation:* i) electron transfer followed by proton transfer (ET-PT), ii) proton transfer followed by electron transfer (PT-ET), iii) coupled electron-proton transfer (EPT) with an added base as proton acceptor, and iv) EPT with  $\text{OH}^-$  as proton acceptor. Depending on conditions these may all be competitive. ET-PT dominates in acidic solution and EPT/ET-PT at high concentrations of added bases with the distribution between them depending on the buffer ratio. Hydroxide is the most effective MS-EPT base for tyrosine playing a role even at  $\text{pH} = 7$ .<sup>23</sup>
- *There are important implications in these results for tyrosine oxidation in biology.* Because of the high reduction potential for the tyrosine radical cation,  $\text{TyrOH}^+$ , mechanisms involving initial oxidation in the absence of an EPT base are inhibited. As for histidine 190 in Photosystem II and for tyrosine in Ribonucleotide Reductase, local intervention of an acceptor base can greatly facilitate tyrosine oxidation with the TyrOH-His pair acting as a reversible electron transfer relay,  $\text{TyrO-H---His} \xrightarrow{-e^-}$   $\text{TyrO}^{\cdot-}\text{---}^+\text{H-His} \xrightarrow{+e^-}$   $\text{TyrO-H---His}$ . In the absence of a proton acceptor base tyrosine oxidation is inhibited while in an environment with an exogenous base, such as a phosphate buffer, it is facilitated.

- *At the microscopic level, EPT is dominated by the quantum nature of the coupled proton transfer.* Importantly, **this includes as a dominating theme local structure and minimizing the proton transfer distance.** Classical approximations may be appropriate for remaining low frequency modes and the solvent.

### 3.7 References

- 1) Tommos, C.; Babcock, G. T. **Proton and Hydrogen Currents in Photosynthetic Water Oxidation.** *Biochim. et Biophys. Acta.* **2000**, *1458*, 199-219
- 2) Babcock, G.T.; Rodriguez, I. D.; Hoganson, C.; Sandusky, P.O.; El-Deeb, M. **Redox Active Amino Acids in Photosystem II and in Other Enzyme Systems.** *Royal Society of chemistry*, **1991**, *94*, 55-58
- 3) Meyer, T. J.; Huynh, M-H. V.; Thorp, H. H. **The Possible Role of Proton Coupled Electron Transfer (PCET) in Water Oxidation by Photosystem II** *Angew. Chem., Int. Ed.* **2007**, *46*, 5284-5304
- 4) Hammes-Schiffer, S.; Soudackov, A. V. **Proton-Coupled Electron Transfer in Solutions, Proteins, and Electrochemistry,** *J. Phys. Chem. B.* **2008**, *112*, 14108-14123
- 5) Irebo, T.; Reece, S. Y.; Sjödin, M.; Nocera, D. G.; Hammarström, L. **Proton-Coupled Electron Transfer of Tyrosine Oxidation: Buffer Dependence and Parallel Mechanisms** *J. Am. Chem. Soc.* **2007**, *129*, 15462-15464.
- 6) Ishikita, H.; Soudackov, A. V.; Hammes-Schiffer, S. **Buffer-Assisted Proton-Coupled Electron Transfer in a Model Rhenium-Tyrosine Complex.** *J. Am. Chem. Soc.* **2007**, *129*, 11146-11152.
- 7) Sjödin, M.; Styring, S.; Akermark, B.; Sun, L.; Hammarström, L. **Proton-Coupled Electron Transfer from Tyrosine in a Tyrosine-Ruthenium-tris-Bipyridine Complex Comparison with Tyrosine<sub>Z</sub> Oxidation in Photosystem II:** *J. Am. Chem. Soc.* **2000** *122*, 3932
- 8) Sjödin, M.; Styring, S.; Wolpher, H.; Xu, Y.; Sun, L.; Hammarström, L. **Switching the Redox Mechanism: Models for Proton-Coupled Electron Transfer from Tyrosine and Tryptophan** *J. Am. Chem. Soc.* **2005**, *127*, 3855-3863.
- 9) Stubbe, J.; Nocera, D. G.; Yee, C. S.; Chang, M. C. Y. **Radical initiation in the Class I ribonucleotide reductase: long-range proton-coupled electron transfer?** *Chem Rev* **2003**, *103* 2167-2202.
- 10) Reece, S. Y.; Nocera, D. G. **Direct Oxidation Using the MLCT Excited States of Rhenium Polypyridyl Complexes.** *J. Am. Chem. Soc.*, **2005**, *127* 9448-9458.
- 11) Markle, T. F.; Rhile, I. J.; DiPasquale, A. G.; Mayer, J. M. **Probing Concerted Proton Coupled Electron Transfer in Phenol-imidazoles.** *Proc. Natl. Acad. Sci. U. S. A.* **2008**, *105*, 8185-8190

- 12) Markle, T. F.; Mayer, J. M. **Concerted Proton-Electron Transfer in Pyridyl Phenols: The Importance of the Hydrogen Bond.** *Angew. Chem. Int. Ed.* **2008**, *47*, 738-740
- 13) Mayer, J. M.; Rhile, I. J.; Larsen, F. B.; Mader, E. A.; Markle, T. F.; DiPasquale, A. G. **Models for Proton Coupled Electron Transfer in PSII.** *Photosynth. Res.* **2006**, *87*, 21-24
- 14) Rhile, I. J.; Mayer, J. M. **One Electron Oxidation of a Hydrogen Bonded Phenol Occurs by Concerted Proton Coupled Electron Transfer.** *J. Am. Chem. Soc.* **2004**, *126*, 12718-12719.
- 15) Fecenko, C. F.; Meyer, T. J.; Thorp, H. H. **Electrocatalytic Oxidation of Tyrosine through Rate-Limiting Proton Transfer and MS-EPT** *J. Am. Chem. Soc.* **2006**, *128*, 11020-11021
- 16) Fecenko, C. J.; Thorp, H. H.; Meyer, T. J. **The Role of Free Energy Change in Coupled Electron Proton Transfer** *J. Am. Chem. Soc.* **2007**, *129*, 15098-15099
- 17) Cukier, R. I.; Nocera, D. G. **Proton Coupled Electron Transfer,** *Annu. Rev. Phys. Chem.* **1998** *49* 337-69
- 18) Mayer, J. M. **Proton Coupled Electron Transfer: A Reaction Chemist's Point of View.** *Annu. Rev. Phys. Chem.* **2004** *55* 363-90
- 19) Hammes-Schiffer, S. **Theoretical Perspectives on Proton Coupled Electron Transfer Reactions** *Acc. Chem. Res.* **2001** *34* 273-81
- 20) Brudvig, G. W.; Thorp, H. H.; Crabtree, R. H. **Probing the Mechanism of Water Oxidation.** *Acc. Chem. Res.* **1991** *24*, 311-316
- 21) A) Alstrum-Acevedo, J. H.; Brennaman, M. K.; Meyer, T. J. **Chemical Approaches to Artificial Photosynthesis 2.** *Inorg. Chem.* **2005**, *344* 6802-27. B) Huynh, M.-V. H.; Meyer, T. J. **Proton Coupled Electron Transfer.** *Chem. Rev.* **2007** *107* 5004-5064
- 22) Dixon, W. T.; Murphy, D. **Determination of Acidity Constants of Some Phenol Radical Cations by Means of Electron Spin Resonance.** *J. Chem. Soc. Faraday Trans. 2.* **1976**. *72*, 1221-1230.
- 23) Murphy, C.F.; Brenneman, M. K.; Thorp, H. H.; Meyer, T. J. **pH Dependent or Base Assisted Tyrosine Oxidation?** *J. Am. Chem. Soc.* **2009**, *manuscript in prep.*

- 24) Costenin, C.; Robert, M.; Saveant, J. Electrochemical and Homogeneous Proton-Coupled Electron Transfers: Concerted Pathways in the One-Electron Oxidation of a Phenol Coupled with an Intramolecular Amine-Driven Proton Transfer. *J. Am. Chem. Soc.* **2006**, 128, 4552-53.
- 25) Costentin, C.; Robert, M.; Saveant, J. M. Concerted Proton-Electron Transfer Reactions in Acts as Proton Donor or Acceptor? *J. Am. Chem. Soc.* **2007**, 129, 5870-5879.
- 26) Willit, J. L.; Bowden, E. F., Adsorption and redox thermodynamics of strongly adsorbed cytochrome c on tin oxide electrodes *J. Phys. Chem.* **1990** 94, 8241-8245
- 27) Das, T. N.; Huie, R. E.; Neta, P. Reduction Potentials of  $\text{SO}_3^{\cdot-}$ ,  $\text{SO}_5^{\cdot-}$ , and  $\text{S}_4\text{O}_6^{3\cdot-}$  Radicals in Aqueous Solution *J. Phys. Chem. A.* **1999** 103 3581-88
- 28) A) Johnston, D. H.; Glasgow, K. C.; Thorp, H. H. **Electrochemical Measurement of the Solvent Accessibility of the Nucleobases Using Electron Transfer between DNA and Metal Complexes** *J. Am. Chem. Soc.* **1995**, 117, 8933-38 B) Demadis, D. D.; Dattelbaum; Kober, E. M.; Concepcion, J. J.; Paul, J. J.; Meyer, T. J.; White, P. S. **Vibrational and Structural Mapping of  $\text{Os}(\text{bpy})_3^{3+/2+}$  and  $\text{Os}(\text{phen})_3^{3+/2+}$** , *Inorg. Chim. Acta* .**2007**, 360, 1143-1153.
- 29) Sistare, M. F.; Holmberg, R. C.; Thorp, H. H. **Electrochemical Studies of Polynucleotide Binding and Oxidation by Metal Complexes: Effects of Scan Rate, Concentration, and Sequence** *J. Phys. Chem. B.* **1999** 103 10718-10728
- 30) a) Rudolph, M., Reddy, D. P., Feldberg, S. W. **A Simulator for Cyclic Voltammetric Response** *Anal. Chem.* **1994** 66, 589A-600A b) Bard, A. J.; Faulkner, L. R. **Electrochemical Methods: Fundamentals and Applications**; John Wiley and Sons, Inc., Hoboken, NJ **2004**
- 31) Johnston, D. H., Glasgow, K. C., Thorp, H. H. **Electrochemical Measurement of the Solvent Accessibility of Nucleobases Using Electron Transfer between DNA and Metal Complexes** *J. Am. Chem. Soc.* **1995** 117, 8933-38
- 32) Nakano, M.; Nakano, N. I.; Higuchi, T. *J. Phys. Chem.* **1967** 71 3954-59
- 33) Ionescu, A.; Grand, D.; Sicard-Roselli, C.; Houee-Levin, C. **Micellular Effect on Tyrosine: One Electron by Azide Radicals.** *Radiation Physics and Chemistry* **2005**, 72, 497-506
- 34) Murphy, C. F.; Gagliardi, C. J.; Thorp, H. H.; Meyer, T. J. **Buffer-Assisted Amino Acid Oxidation at a Carbon Electrode** *J. Am. Chem. Soc.* **2009**, manuscript in prep.
- 35) Albery, W. J.; Davies, M. H. **Mechanistic Conclusions from the Curvature of solvent Isotope Effects.** *J. Chem. Soc., Faraday Trans. 1* **1972**, 68, 167.

- 36) Schowen, K. B.; Limbach, H. H.; Denisov, G. S.; Schowen, R. L. **Hydrogen Bonds and Proton Transfer in General Catalytic Transition State Stabilization in Enzyme Catalysis** *Biochim. Biophys. Acta* **2000**, *43*, 1458
- 37) Decornez, H.; Hammes-Schiffer, S. **Model proton-coupled electron transfer reactions in solution: Predictions of rates, mechanisms, and kinetic isotope effects** *J. Phys. Chem. A*. **104** **2000**, 9370-9384
- 38) Guilini, C.; Traaseth, N. J.; Davies, K. J. **Tyrosine oxidation products: analysis and biological relevance** *A. Amino Acids*, 2003 227-232
- 39) Lind, J.; Shen, X.; Eriksen, T. E.; Merenyi, G. **The one-electron reduction potential of 4-substituted phenoxyl radicals in water** *J. Am. Chem. Soc.* **1990**, *112*, 479-482
- 40) Fuöss, R. M. Ionic Association. III. **The Equilibrium between Ion Pairs and Free Ions** *J. Am. Chem. Soc.* **1958**, *80*, 5059-5061.
- 41) Grabowski, S. J. **Hydrogen Bond Strength-Measures based on Geometric and Topological Parameters.** *J. Phys. Org. Chem.* **2004**, *17*, 18-31
- 42) Steiner, T. **The Hydrogen Bond in the Solid State** *Angew Chem. Int. Ed.* **2002**, *41*, 48-76
- 43) Yates, K. S. **Application of Marcus theory to photochemical proton transfer reactions. II. Modifications based on intersecting state models** *J. Phys. Org.* **2002**, *2* 300-322
- 44) Hynes, J. T. **The Protean Proton in Water** *Nature* **1999**, *397*, 565.
- 45) Ando, K.; Hynes, J. T. **Acid Ionization of HF in Water: An Electronic Structure and Monte Carlo Study** *J. Phys. Chem. A* **1999**, *103*, 10398.
- 46) Ando, K.; Hynes, J. T. **Acid Base Proton Transfer and Ion Pair Formation in Solution** *Adv. Chem. Phys.* **1999**, *119*, 381-430
- 47) Geissler, P. L. P. L.; Dellago, C.; Chandler, D.; Hutter, J.; Parrinello, M. **Autoionization in Liquid Water.** *Science* **2001**, *291*, 2121.
- 48) Borgis, D.; Hynes, J. T. **A Curve Crossing Approach to Chemical Reactions in Solution.** *J. Phys. Chem.* **1996**, *100*, 1118.
- 49) Cukier, R. I.; Zhu, J. **Simulation of Proton Transfer Reaction Rates: The Role of Solvent Polarization.** *J. Phys. Chem. B* **1997**, *101*, 7180.
- 50) Warshel, A. **Molecular Dynamics Simulations of Biological Reactions** *Acc. Chem. Res.* **2002**, *35*, 385.

- 51) Krishtalik, L. I. **The Mechanism of Proton Transfer, An Outline** *Biochim. Biophys. Acta* **2000**, 1458, 6.
- 52) Andreiux, C. P.; Gamby, J.; Hapiot, P.; Saveant, J.-M. **Evidence for Inverted Region Behavior in Proton Transfer to Carbanions** *J. Am. Chem. Soc.* **2003**, 125, 101119-101124
- 53) Peters, K. S. **A Theory-Experiment Conundrum for Proton Transfer** *Acc. Chem. Res.* **2008**
- 54) Heeb, L.; Peters, K. S. **Further Evidence of an Inverted Region Proton Transfer within the Benzophenone/Substituted Aniline Contact Radical Ion Pairs; Importance of Vibrational Reorganizational Energy.** *J. Phys. Chem. A.* **2006**, 110, 6408-6414
- 55) Hammes-Schiffer, S.; Soudackov, A. V. **Proton-Coupled Electron Transfer in Solution, Proteins, and Electrochemistry.** *J. Phys. Chem. B.* **2008**, 112, 14108-14123
- 56) Ishikita, H.; Soudackov, A. V.; Hammes-Schiffer, S. **Buffer-Assisted Proton Coupled Electron Transfer in a model Rhenium-Tyrosine System** *J. Am. Chem. Soc.* **2007**, 11152
- 57) Hammes-Schiffer, S.; Hatcher, E.; Ishikita, H.; Skone, J. H.; Soudackov, A. V. **Theoretical Studies of Proton Coupled Electron Transfer: Models and Concepts Relevant to Bioenergetics.** *Coord. Chem. Revs.* **2008**, 252, 384-394.
- 58) Carra, C.; Iordanova, N.; Hammes-Schiffer, S. **Proton Coupled Electron Transfer in a Model of Tyrosine in Photosystem II.** *J. Am. Chem. Soc.* **2003**, 125, 10429-10436
- 59) Chen, P. Y.; Meyer, T. J. *Chem. Rev.* 1998, 98, 1439. Bixon, M.; Jortner, J. **In Electron Transfer-From Isolated Molecules to Biomolecules**; Jortner, J., Bixon, M., Eds.; Wiley-Interscience: New York, 1999.
- 60) Marcus, R. A. **Chemical and Electrochemical Electron-Transfer Theory.** *Annu. Rev. Phys. Chem.* **1966**, 15, 155.
- 61) Sutin, N. *Prog. Inorg. Chem.* 1983, 30, 441.

**Chapter 4**  
**pH Dependent or Base Assisted Tyrosine Oxidation?**

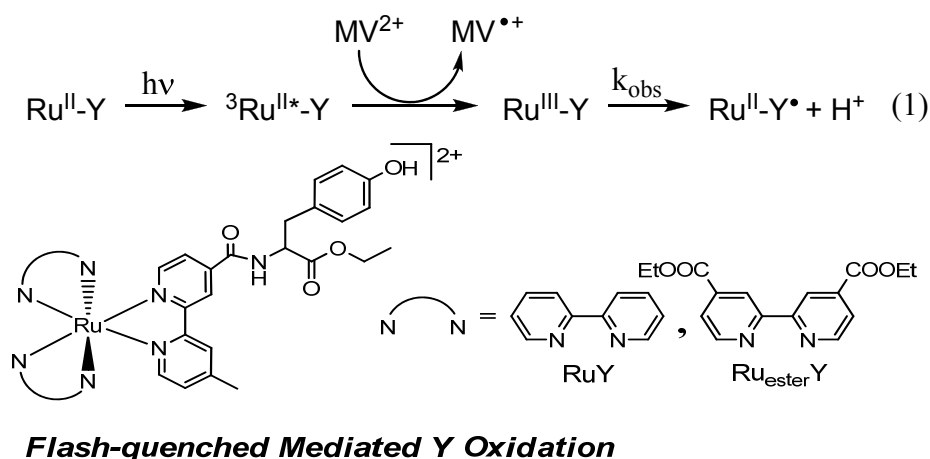
Reproduced with permission of the American Chemical Society  
Christine F. Murphy, M. Kyle Brennaman, H. Holden Thorp, and Thomas J.  
Meyer **pH Dependent or Base-Assisted Tyrosine Oxidation** *J. Am. Chem.*  
*Soc.* **2009** *submitted* © American Chemical Society 2009

#### 4.1 Abstract:

In tyrosine oxidation different pathways have been proposed in which electron transfer is accompanied by proton transfer. In one, proton transfer to the surrounding medium occurs influenced by changes in pH, and driving force. In the second concerted electron-proton transfer has been invoked (EPT) in which the proton is transferred to a H-bonded base. Interpretation based on a pH dependence has been questioned because, at the microscopic level, there is no basis for coupling a local gain or loss of protons in an elementary step to the surrounding ensemble of solvent, protons, buffer, etc. that define the final equilibrium state including the pH. A pH dependence was reported recently for intra-molecular oxidation of a tyrosine derivative linked to Ru<sup>III</sup>. We report here that in the analogous, outer-sphere oxidation of tyrosine by Os(bpy)<sub>3</sub><sup>3+</sup>, Os(bpy)<sub>3</sub><sup>3+</sup> + TyrOH → Os(bpy)<sub>3</sub><sup>2+</sup> + TyrO· + H<sup>+</sup>, a pathway does appear but that is first order in [OH<sup>-</sup>] rather than pH dependent. This pathway arises from a Multiple Site- Electron Proton Transfer (MS-EPT) with OH<sup>-</sup> acting as the proton acceptor base, Os(bpy)<sub>3</sub><sup>3+</sup>, TyrOH---OH<sup>-</sup> → Os(bpy)<sub>3</sub><sup>2+</sup>, TyrO·---H<sub>2</sub>O.

## 4.2 Introduction:

The fate of the hydroxyl proton in tyrosine oxidation is highly debated.<sup>1-6</sup> Pathways have been proposed in which electron transfer is accompanied by proton transfer to the surrounding medium influenced by changes in pH and driving force.<sup>1,2</sup> Coupled electron-proton transfer (EPT) has also been suggested in which the electron and proton are transferred simultaneously to separate electron and proton acceptors, the latter through a pre-formed H-bond to an acceptor base. This pathway is supported by theoretical calculations.<sup>5</sup>



Intramolecular oxidation of a Ru-bpy tyrosine derivative, Eq 1 with  $\text{MV}^{2+}$  methylviologen dication, is dominated by a base-assisted EPT pathway at high buffer concentrations but at low buffer concentrations, where the buffer independent pathway is negligible,  $< 0.5$  mM, a pH dependence remains, Figure 1.<sup>5</sup> The reported pH dependence was attributed to the pH dependence of the driving force for intramolecular  $\text{Y} \rightarrow \text{Ru}^{\text{III}}$  electron transfer. This explanation is questionable because, at the microscopic level, there is no basis for coupling a local gain or loss of protons in an elementary step to the surrounding ensemble of solvent, protons, buffer, etc. that define the final equilibrium state including the pH.<sup>5,8,9</sup>

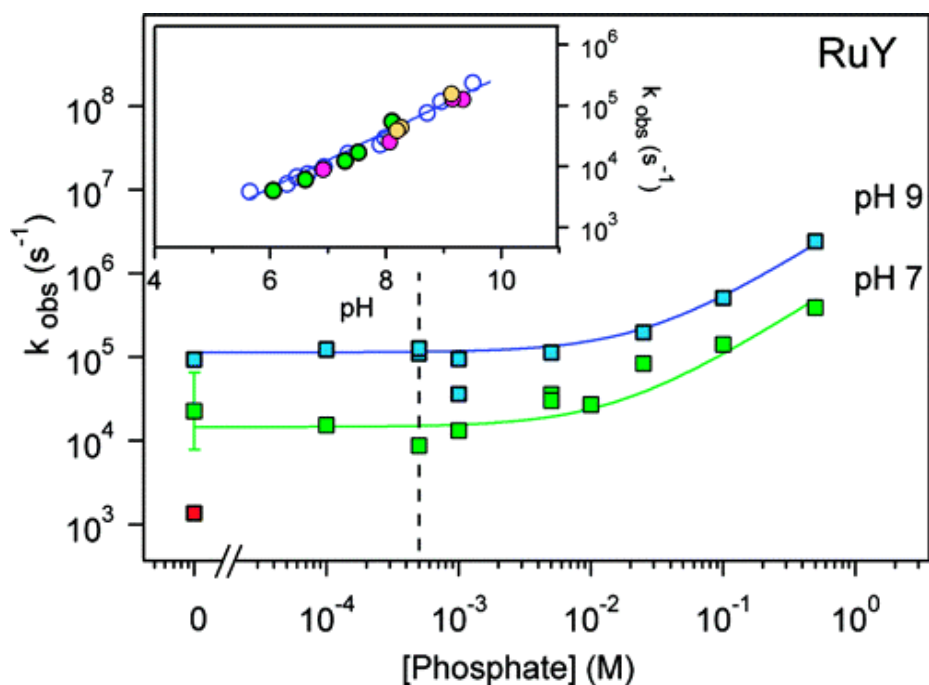
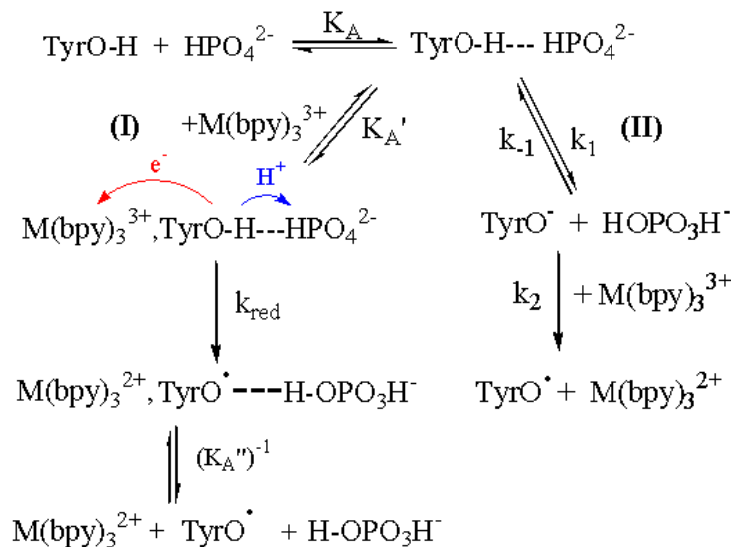


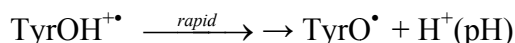
Figure 1: The pH dependence for oxidation of the tyrosine derivative in Eq 1 for 30  $\mu\text{M}$  RuY in the presence of 5-200 mM methyl viologen dichloride or 15 mM  $\text{Co}(\text{NH}_3)_5\text{Cl}^{2+}$  in 0.0 M – 0.5 M phosphate buffer at 298 K.<sup>7</sup> (Reproduced from ref 2 © American Chemical Society, 2007)

We reported that oxidation of unbound tyrosine (TyrOH) by metal complex oxidants, such as  $\text{Os}(\text{bpy})_3^{3+}$  (bpy is 2,2'-bipyridine) is catalyzed by the basic form of added buffers-  $\text{HPO}_4^{2-}$ , histidine, acetate, succinate, and Tris- by the mechanism in Scheme 1. Base catalyzed oxidation occurs by parallel pathways: 1) Multiple Site-Electron Proton Transfer (MS-EPT) and 2) proton transfer to the H-bonded base followed by TyrO<sup>-</sup> oxidation by electron transfer to the oxidant (PT-ET). Both are illustrated in Scheme 1.

### Scheme 1



There are additional pathways for tyrosine oxidation by  $\text{Os}(\text{bpy})_3^{3+}$  and related metal complex oxidants. One is outer sphere oxidation to give  $\text{TyrOH}^{+\bullet}$  which is followed by proton transfer to the surrounding medium at the prevailing pH (ET-PT), Eq 2. This is an outer sphere analog of the intramolecular reaction in Eq 1. It is relatively slow with  $k_{\text{ET}}(23 \pm 2 \text{ }^\circ\text{C}; 0.8 \text{ M NaCl}) = 1.7 \pm 0.4 \times 10^2 \text{ M}^{-1}\text{s}^{-1}$  because  $\Delta G^{\circ'} = +0.54 \text{ eV}$  for the initial electron transfer step. At pH values above  $\text{pK}_a = 10.1$  for tyrosine, tyrosyl anion undergoes rapid oxidation,  $\text{TyrO}^- + \text{Os}(\text{bpy})_3^{3+} \rightarrow \text{TyrO}^\bullet + \text{Os}(\text{bpy})_3^{2+}$ , with  $k = 1.0 \pm 0.5 \times 10^7 \text{ M}^{-1}\text{s}^{-1}$  under the same conditions with  $\Delta G^{\circ'} = -0.09 \text{ eV}$ .



### 4.3 Methods and Materials:

4.3.1 General: Deionized water was purified by passing in-house distilled water through a MilliQ deionizing system (18 $\Omega$ ) and was used to prepare all aqueous solutions. All buffers and tyrosine were purchased from Sigma-Aldrich.  $\text{Os}(\text{bpy})_3\text{Cl}_2$  was prepared by a literature procedure and

purified by recrystallization.<sup>10</sup> The purity of the sample was verified by UV-visible and <sup>1</sup>H NMR measurements.

Os<sup>III</sup>(bpy)<sub>3</sub><sup>3+</sup> was prepared *in situ* by bubbling Cl<sub>2</sub> gas through an aqueous Os(bpy)<sub>3</sub><sup>2+</sup> solution. Oxidation led to a color change from red to dark green. Before use solutions were purged with argon gas to ensure removal of excess Cl<sub>2</sub>. UV-visible measurements showed that Os(bpy)<sub>3</sub><sup>3+</sup> decomposition was negligible on the time scale for the experiments described below.

Ionic strength was held constant by addition of 0.8 M NaCl. This allowed us to vary the buffer concentration without changing the ionic strength of the solution. The temperature was 23±2°C.

Kinetic measurements were repeated in triplicate and rate constants are reported based on the average rate constant for each trial. The error is reported as the standard deviation of all trials. The slope and intercept are reported from plots of average values and the error is reported as the standard deviation of the slope and intercept for each trial.

Aqueous buffer solutions were prepared from 0.5 M or 0.005 M stock solutions, which were then diluted to the appropriate buffer concentration with MilliQ water. Buffer solutions below 0.005 M were prepared as a stock solution without further dilution. The concentration of buffer components was calculated by using the Henderson-Hasselbach equation taking standard pK<sub>a</sub> values for each buffer in aqueous solution. With the help of a digital pH meter (Accumet AB15 plus), the pH of buffered solutions was adjusted post-dilution by adding concentrated HCl or NaOH. A final dilution with MilliQ water was performed, if necessary, to achieve the desired base concentration. The pH of solutions with no added buffer was adjusted in the same way as buffered solutions.

4.3.2 Kinetics. Spectrophotometric Monitoring: In solutions dilute in base, < 0.5mM, oxidation of TyrOH by Os(bpy)<sub>3</sub><sup>3+</sup> is too slow for electrochemical monitoring . Kinetics of tyrosine oxidation by Os(bpy)<sub>3</sub><sup>3+</sup>, prepared as described above, were monitored by UV-visible measurements by using a Cary 300 Bio UV-Visible Spectrophotometer. Appearance of Os(bpy)<sub>3</sub><sup>2+</sup> was monitored at the visible absorption maximum for Os(bpy)<sub>3</sub><sup>2+</sup> at λ<sub>max</sub> = 490 nm (ε = 12,900 M<sup>-1</sup>cm<sup>-1</sup>) which is the only significant absorber at this wave length. Os(bpy)<sub>3</sub><sup>3+</sup> was stable over the timescales used in both mixing and electrochemical experiments.

Absorbance-time traces were monitored and fit to the first order expression in eq 3 under pseudo-first order conditions in TyrOH (≥ 1.0x10<sup>-4</sup> M) relative to Os(bpy)<sub>3</sub><sup>3+</sup> (1.0x10<sup>-5</sup> M). In eq 3, A<sub>0</sub>, and A<sub>t</sub> are the initial absorbance and absorbance at time = t, and A<sub>∞</sub> the final absorbance. The rate constant for electron transfer was calculated from the slope and k = k<sub>obs</sub>/[TyrOH]. A kinetic plot is shown in Figure 2.

$$\ln \left[ \frac{(A_{\infty} - A_t)}{(A_{\infty} - A_0)} \right] = k_{\text{obs}} t \quad (3)$$

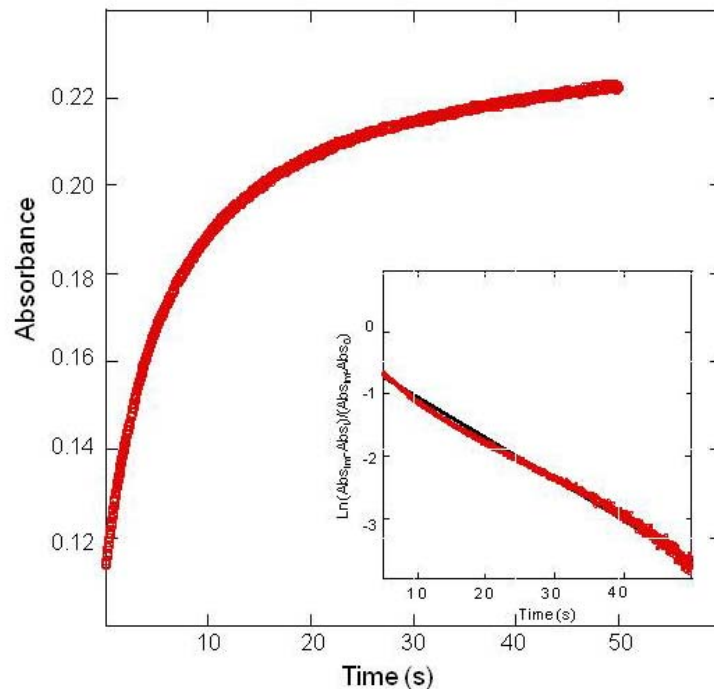


Figure 2: Absorbance-time plot for oxidation of  $1.0 \times 10^{-4}$  M tyrosine by  $1.0 \times 10^{-5}$  M  $\text{Os}(\text{bpy})_3^{3+}$  at pH 7.0 in  $1.0 \times 10^{-5}$  M phosphate buffer in 0.8 M NaCl at  $23 \pm 2$  C. The inset shows a first order plot of  $\ln[A_{\infty-t}/A_{\infty}-A_0]$  vs time with  $k_{\text{obs}}/[\text{TyrOH}] = 1.8 \times 10^2 \text{ M}^{-1} \text{ s}^{-1}$ .

Variations with pH, and  $[\text{OH}^-]$ , were investigated under the same conditions but with dilute phosphate buffer added to maintain pH. In an initial series of experiments, total buffer concentration was held fixed at  $1.0 \times 10^{-5}$  M with pH varied in the range 3.0 ( $\text{H}_3\text{PO}_4/\text{H}_2\text{PO}_4^-$ ), 5.0 ( $\text{H}_2\text{PO}_4^-/\text{HPO}_4^{2-}$ ), 7.0 ( $\text{H}_2\text{PO}_4^-/\text{HPO}_4^{2-}$ ), and 9.0 ( $\text{HPO}_4^{2-}/\text{PO}_4^{3-}$ ). Rate constants obtained as a function of pH were:  $k_{\text{obs}}(23 \pm 2 \text{ } ^\circ\text{C}) = 1.7(\pm 0.9) \times 10^2$  (pH = 3.0)  $1.6(\pm 0.3) \times 10^2$  (pH = 5.0),  $1.8 \pm 0.5 \times 10^2$  (pH = 7.0), and  $3.2 \pm 0.9 \times 10^2$  (pH = 9.0)  $\text{M}^{-1} \text{ s}^{-1}$ .

In a second series of experiments, variations with  $[\text{HPO}_4^{2-}]$  were investigated with the pH fixed at 7.0 and 9.0 by varying total buffer concentration,  $\text{H}_2\text{PO}_4^- + \text{HPO}_4^{2-}$  with  $[\text{TyrOH}] = 1.0 \times 10^{-4}$  M and  $[\text{Os}^{\text{III}}(\text{bpy})_3^{3+}] = 5.0 \times 10^{-6}$  M. Under these conditions PCET reactivity in Scheme 1 is dominated by the MS-EPT pathway.<sup>3</sup> From a plot of  $k_{\text{obs}}$  vs  $[\text{HPO}_4^{2-}]$  at pH = 7.0, intercept =

$1.8 \pm 0.2 \times 10^2 \text{ M}^{-1} \text{ s}^{-1}$  at  $[\text{HPO}_4^{2-}] = 0$  and slope =  $1.8 \pm 0.1 \times 10^5 \text{ M}^{-2} \text{ s}^{-1}$ . For the pH 9.0 data, intercept =  $3.1 \pm 0.3 \times 10^2 \text{ M}^{-1} \text{ s}^{-1}$  and slope =  $5.3 \pm 0.2 \times 10 \text{ M}^{-2} \text{ s}^{-1}$ .

4.3.3 Second Order Unequal Concentration Kinetics. Direct Reaction with  $\text{OH}^-$ : The dependence of  $\text{OH}^-$  as an EPT acceptor base in the oxidation of TyrOH by  $\text{Os}(\text{bpy})_3^{3+}$  was investigated at pH = 9.0, 9.2, and 9.4 in the absence of buffer at 490 nm with  $[\text{TyrOH}] = 1.0 \times 10^{-4} \text{ M}$  and  $[\text{Os}(\text{bpy})_3^{3+}] = 5.0 \times 10^{-6} \text{ M}$ . In these experiments  $[\text{OH}^-]$  was varied from  $1.0 \times 10^{-5}$ – $3.2 \times 10^{-5} \text{ M}$  in 0.8M NaCl. Absorbance-time traces were treated by second-order unequal concentration kinetics, eq 4, to obtain  $k_{\text{OH}^-}$  with  $b = [\text{OH}^-]$  at  $t = 0$ ,  $a = [\text{Os}(\text{bpy})_3^{3+}]$  at  $t = 0$ , and  $k_{\text{obs}} = k_{\text{OH}^-} [\text{TyrOH}]$ .

$$\text{Ln} \left[ \frac{\left( \left( \frac{b}{a} - 1 \right) (A_\infty - A_0) \right)}{(A_\infty - A_t)} + 1 \right] = (b - a) k_{\text{obs}} t \quad (4)$$

The concentration range was narrowly circumscribed to avoid complications by direct oxidation of tyrosyl anion, see above.  $\text{TyrO}^-$ , which is rapid. The concentration of anion at the beginning of the experiment was calculated from  $\text{pK}_a(\text{TyrOH}) = 10.1$  by using eq 5 and the concentration of Os(III) available for the slower EPT reaction with  $\text{OH}^-$  by  $[\text{Os(III)}] = [\text{Os(III)}]_{\text{T}} - [\text{TyrO}^-]$ .  $[\text{Os(III)}]_{\text{T}}$  and  $[\text{TyrOH}]_{\text{T}}$  are the total Os(III) and TyrOH concentrations and  $K_w (= 10^{-14})$  the water ionization constant. At  $[\text{TyrOH}]_{\text{T}} = 1.0 \times 10^{-4} \text{ M}$ ,  $x = 0.14 [\text{OH}^-] = 1.4 \times 10^{-6} \text{ M}$ .

$$x = [\text{TyrO}^-] = \frac{\left( \frac{K_a}{K_w} \right) [\text{TyrOH}] [\text{OH}]_{\text{T}}}{1 + K_a [\text{TyrOH}]} \quad (5)$$

4.3.4 Kinetics. Cyclic Voltammetry: Cyclic voltammetric measurements were performed by using a BAS100B/W series potentiostat in a three electrode cell configuration described

previously.<sup>11-15</sup> The working electrode was glass coated indium tin oxide (ITO) with a reaction area of 0.32 cm<sup>2</sup> purchased from Delta Technologies (Stillwater, MN). The reference electrode was a teflon coated Ag/AgCl microelectrode purchased from Cypress Systems, Inc (Lawrence, KS). The auxiliary electrode was platinum wire, purchased from Sigma Aldrich (St. Louis, MO), wrapped around the base of the teflon on the reference electrode. ITO electrodes were treated before use by sonication in MilliQ water, then isopropanol each for 15 minutes, followed by two washes with MilliQ water for 15 minutes each. They were laid flat and allowed to dry overnight. Each experiment was performed on a solution volume of 50  $\mu$ L. To collect a cyclic voltammogram (CV), the potential was swept in a positively from 0-1.3 V. The ITO electrode was conditioned for 6 consecutive scans in phosphate buffer solution before the first measurement. A final background CV was collected. A CV of buffer with metal complex was then recorded, and ,finally, a scan of buffer and 20  $\mu$ M complex with 100  $\mu$ M tyrosine (reductant). After a scan of buffer with oxidant and reductant was taken, the ITO electrode was discarded and a new electrode was used for the next sample. CV's were background corrected by subtracting scans with buffer alone from scans with complex and complex with reductant. Cyclic voltammetry measurements were conducted in aqueous 0.8 M NaCl solutions at 23 $\pm$ 2 $^{\circ}$ C.

Eqs 6,7 were used in the digital simulations of Scheme 1 as described in the previous paper.<sup>3a</sup> Limiting conditions used to isolate either the MS-EPT or PT-ET pathways kinetically are also discussed there. For the MS-EPT pathway H<sub>2</sub>PO<sub>4</sub><sup>-</sup>/HPO<sub>4</sub><sup>2-</sup> buffers with the buffer acid to base ratio > 10:1 were used. Under these conditions,  $k_{\text{obs}} = k_{\text{red}}K_A K_A' [\text{TyrOH}]$ , Scheme 1. The same procedure was followed for the additional EPT bases investigated.

The rate law derived for Scheme 1 is shown in eq 6a with [TyrOH]<sub>T</sub> the total concentration of TyrOH distributed between TyrOH and its adduct with the buffer base. With

high, pseudo-first order conditions in TyrOH and buffer the rate law becomes eq 6b with  $k_{\text{obs}}$  given by eq 7 in the limit:  $K_A[\text{HPO}_4^{2-}] \ll 1$ ,  $[\text{TyrOH}]_T \sim [\text{TyrOH}]$ .

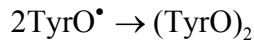
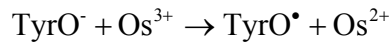
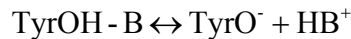
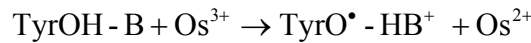
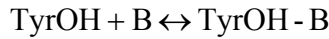
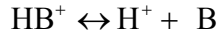
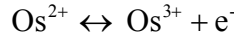
$$-\frac{d[\text{Os}^{3+}]}{dt} = \left[ \frac{K_A [\text{TyrOH}]_T [\text{HPO}_4^{2-}]}{1 + K_A [\text{HPO}_4^{2-}]} \right] \left( K_A' k_{\text{red}} + \frac{k_1 k_2}{k_{-1} [\text{H}_2\text{PO}_4^-] + k_2 [\text{Os}^{3+}]} \right) [\text{Os}^{3+}] \quad (6a)$$

$$\frac{d[\text{Os}^{2+}]}{dt} = k_{\text{obs}} [\text{Os}^{3+}] \quad (6b)$$

$$\frac{k_{\text{obs}}}{[\text{TyrOH}]} = \left( K_A K_A' k_{\text{red}} + \frac{K_A k_1 k_2}{k_{-1} [\text{H}_2\text{PO}_4^-] + k_2 [\text{Os}^{3+}]} \right) [\text{HPO}_4^{2-}] \quad (7)$$

The electrochemical mechanism used in the simulations based on Scheme 1 is given in Scheme 2.

### Scheme 2

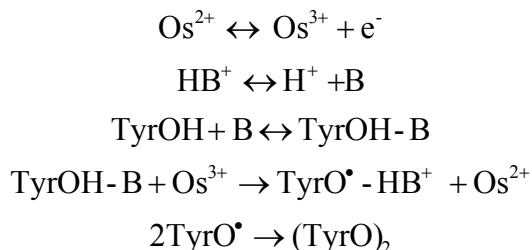


At relatively low buffer concentrations with  $[\text{H}_2\text{PO}_4^-]/[\text{HPO}_4^{2-}] > 10$ , the MS-EPT pathway dominates and with  $K_A[\text{HPO}_4^{2-}] \ll 1$ , adduct formation is negligible which gives eq 8 for  $k_{\text{obs}}$  with  $[\text{TyrOH}]_T \sim [\text{TyrOH}]$ .

$$\frac{k_{\text{obs}}}{[\text{TyrOH}]} = k_{\text{red}} K_A K_A' [\text{HPO}_4^{2-}] \quad (8)$$

Under these conditions the MS-EPT pathway can be digitally simulated by Scheme 3.

**Scheme 3**



**4.3.5 Digital Simulation:** Digital simulations were performed by using the DigiSim software package purchased from BioAnalytical Systems (West Lafayette, IN). The DigiSim software uses the Butler-Volmer equation to correlate current and potential information to evaluate the homogeneous electron transfer rate constant between metal complex oxidant  $\text{Os}^{\text{III}}(\text{bpy})_3^{3+}$  and TyrOH.<sup>13</sup> In the simulations diffusion coefficients for  $\text{Os}(\text{bpy})_3^{3+/2+}$  ( $6.0 \times 10^{-6} \text{ cm}^2/\text{s}$ )<sup>11-12</sup> and tyrosine ( $3.0 \times 10^{-5} \text{ cm}^2/\text{s}$ )<sup>3</sup> were used. The reduction potential for the metal complex ( $E^0 = 0.85 \text{ V}$  vs NHE in  $0.05 \text{ M H}_2\text{PO}_4^- + \text{HPO}_4^{2-} - 0.8 \text{ M NaCl}$ ) and the heterogeneous electron transfer rate constant ( $k_s = 0.01 \text{ cm/s}$ ) at  $23 \pm 2^\circ\text{C}$  were obtained by fitting cyclic voltammograms of the metal complex alone in solution. The mechanisms in schemes 2-3 were used to simulate the electrochemical data over the entire pH range investigated.

**4.4. Results and Discussion**

**4.4.1 pH Dependence in the Oxidation of TyrOH by  $\text{Os}(\text{bpy})_3^{3+}$ :** Oxidation of TyrOH by  $\text{Os}(\text{bpy})_3^{3+}$  in dilute ( $1.0 \times 10^{-5} \text{ M}$ )  $\text{H}_2\text{PO}_4^-/\text{HPO}_4^{2-} - \text{H}_3\text{PO}_4/\text{H}_2\text{PO}_4^-$  buffers in  $0.8 \text{ M NaCl}$  at pH 3.0, 5.0, and 7.0 at  $23 \pm 2^\circ\text{C}$  reveals an apparent pH dependence, Figure 3. Under these conditions the rate law was,  $-\text{d}[\text{Os}(\text{bpy})_3^{3+}]/\text{dt} = k_{\text{obs}}[\text{Os}(\text{bpy})_3^{3+}][\text{TyrOH}]$ , with  $k_{\text{obs}}(23 \pm 2^\circ\text{C}) = 1.7(\pm 0.9) \times 10^2$  (pH = 3.0)  $1.6(\pm 0.3) \times 10^2$  (pH = 5.0),  $1.8 \pm 0.5 \times 10^2$  (pH = 7.0), and  $3.2 \pm 0.9 \times 10^2$  (pH = 9.0)  $\text{M}^{-1}\text{s}^{-1}$ .

The rate constants in Figure 3 report the average of multiple trials (3 or more) with the error reported as the standard deviations.

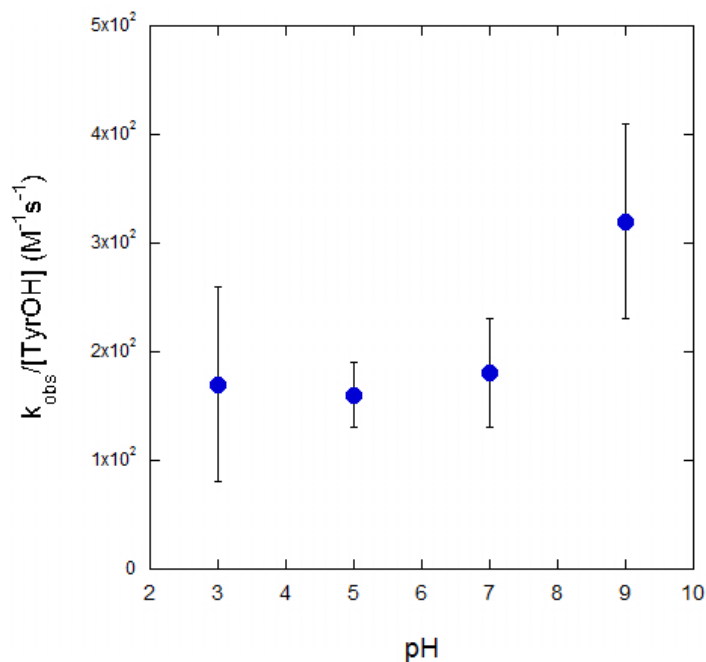


Figure 3: Plot of  $k_{\text{obs}}/[\text{TyrOH}]$  vs pH in the oxidation of tyrosine by  $\text{Os}(\text{bpy})_3^{3+}$  at  $23 \pm 2^\circ\text{C}$  in 0.8 M NaCl containing  $1.0 \times 10^{-5}$  M phosphate buffer ( $\text{H}_3\text{PO}_4/\text{H}_2\text{PO}_4^-/\text{H}_2\text{PO}_4^-/\text{HPO}_4^{2-}$ ).

The origin of the apparent pH effect was investigated in more detail by application of the cyclic voltammetric technique over a more extended range of buffer concentrations. With added  $\text{H}_2\text{PO}_4^-/\text{HPO}_4^{2-}$  buffer, oxidation of TyrOH is accelerated even at fixed pH. As shown by the plots of  $k_{\text{obs}}/[\text{TyrOH}]$  vs  $[\text{HPO}_4^{2-}]$  at pH = 7 and 9 in Figure 4,  $k_{\text{obs}}/[\text{TyrOH}]$  increases linearly with  $[\text{HPO}_4^{2-}]$  under these conditions with the MS-EPT pathway dominating. These experiments were carried out under pseudo first order conditions in both  $[\text{TyrOH}]$  ( $1.0 \times 10^{-4}$  M) and  $[\text{HPO}_4^{2-}]$  ( $3.0 \times 10^{-3}$  M -  $1.0 \times 10^{-4}$  M).

The slopes of the plots of  $k_{\text{obs}}$  vs.  $[\text{HPO}_4^{2-}]$  at pH 7 and 9 in Figure 4 are the same within experimental error,  $5.0 \pm 0.5 \times 10^5 \text{ M}^{-2} \text{ s}^{-1}$ . The intercepts at  $[\text{HPO}_4^{2-}] = 0$  are offset by  $\Delta k = 1.3 \times 10^2 \text{ M}^{-1} \text{ s}^{-1}$  with  $k_{\text{obs}}$  higher at pH = 9.

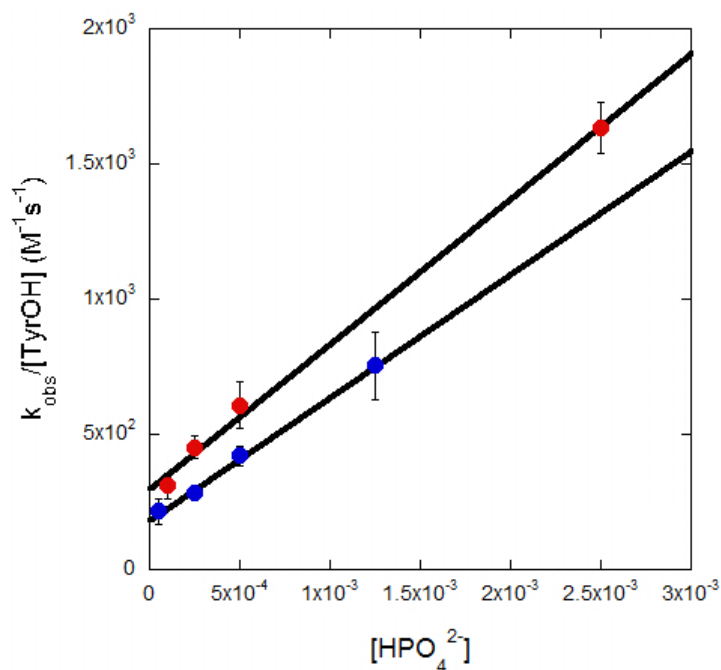


Figure 4: Plots of  $k_{\text{obs}}/[\text{TyrOH}]$  vs  $[\text{HPO}_4^{2-}]$  for oxidation of tyrosine by  $\text{Os}(\text{bpy})_3^{3+}$  in phosphate buffer at pH 7.0 (red;  $[\text{H}_2\text{PO}_4^-]/[\text{HPO}_4^{2-}] = 3/2$ ) and 9.0 (blue;  $[\text{H}_2\text{PO}_4^-]/[\text{HPO}_4^{2-}] = 1/60$ ) in 0.8M NaCl at  $23 \pm 2^\circ\text{C}$ . The total buffer concentration was varied between  $1.0 \times 10^{-4}$ - $3.0 \times 10^{-3}$  M.

**4.4.2 Hydroxide as an EPT Base:** To explain the difference in intercepts, we explored a possible role for hydroxide as EPT acceptor base in unbuffered solutions of 0.8 M NaCl. In these experiments tyrosine was in pseudo-first order excess ( $1.0 \times 10^{-4}$  M),  $[\text{OH}^-]$  was varied from  $1.0 \times 10^{-5}$  to  $3.2 \times 10^{-5}$  M and  $[\text{Os}(\text{bpy})_3^{3+}]$  was  $5.0 \times 10^{-6}$  M. The concentration of  $\text{OH}^-$  was limited to dilute conditions to avoid domination by direct oxidation of  $\text{TyrO}^-$ , eq 5. Reactions were monitored spectrophotometrically and found to be consistent with the rate law in eq 9. A fit to the second order, unequal concentration expression in eq 4, which gives  $k_{\text{obs}}$ , is shown in Figure 5. Based on the results of twelve separate experiments,  $k_{\text{OH}^-} = 1.5 \pm 0.9 \times 10^7 \text{ M}^{-2} \text{ s}^{-1}$ .

$$-d[\text{Os}(\text{bpy})_3^{3+}]/dt = k_{\text{OH}^-}[\text{OH}^-][\text{Os}(\text{bpy})_3^{3+}][\text{TyrOH}] = k_{\text{obs}}[\text{Os}^{\text{III}}][\text{TyrOH}] \quad (9a)$$

$$k_{\text{obs}} = k_{\text{OH}^-}[\text{OH}^-] \quad (9b)$$

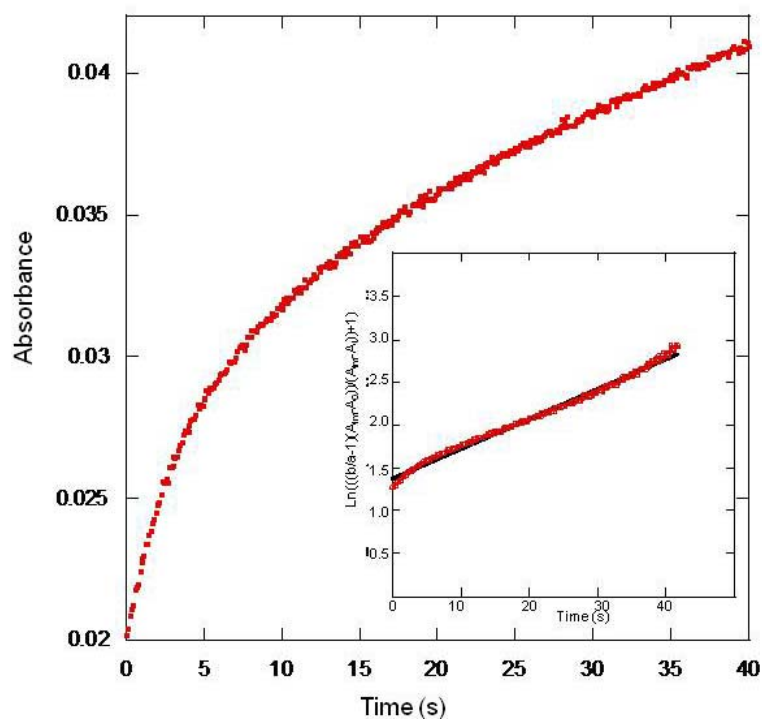


Figure 5: Absorbance-time traces for oxidation of tyrosine by  $\text{Os}(\text{bpy})_3^{3+}$  in 0.8M NaCl at  $23 \pm 2^\circ\text{C}$  with  $[\text{TyrOH}] = 1.0 \times 10^{-4}$  M. The inset shows a fit of the data to the second order unequal concentration kinetic expression in eq 4 which gave  $k_{\text{obs}}/[\text{TyrOH}] = 1.5 \times 10^7 \text{ M}^{-2}\text{s}^{-1}$ .

These data with those from Figure 4 are consistent with a three term rate law for TyrOH oxidation from pH = 7-9 with added  $\text{HPO}_4^{2-}$ , eq 10.

$$-d[\text{Os}(\text{bpy})_3^{3+}]/dt = \{k_0 + k_{\text{OH}^-}[\text{OH}^-] + k_{\text{B}}[\text{HPO}_4^{2-}]\}[\text{Os}(\text{bpy})_3^{3+}][\text{TyrOH}] = k_{\text{obs}}[\text{Os}^{\text{III}}][\text{TyrOH}] \quad (10a)$$

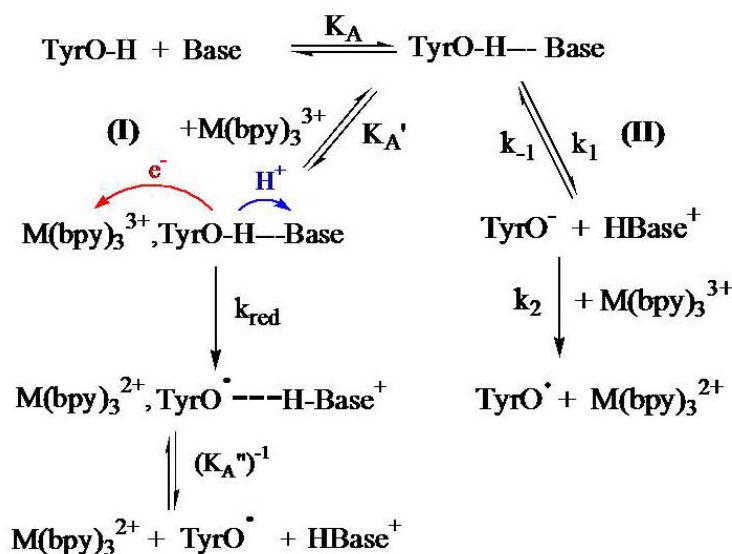
$$k_{\text{obs}} = k_0 + k_{\text{B}}[\text{HPO}_4^{2-}] + k_{\text{OH}^-}[\text{OH}^-] \quad (10b)$$

In this expression the  $k_0$  term arises from outer sphere oxidation, eq 2 and the  $k_{\text{B}}$  term from MS-EPT oxidation with  $\text{HPO}_4^{2-}$  (= B) as the proton acceptor base. We interpret the  $k_{\text{OH}^-}$  term as arising from an additional MS-EPT pathway with  $\text{OH}^-$  acting as the EPT acceptor base.

Intervention of this pathway explains the offset in intercepts between the buffer base plots in Fig. 4 with  $\Delta k/[TyrOH] \sim k_{OH^-}([OH^-]_2 - [OH^-]_1) = 1.5 \times 10^2 M^{-1}s^{-1}$  compared to  $1.3 \times 10^2 M^{-1}s^{-1}$  from the plots in Figure 4.

4.4.3 Additional EPT Bases; As described in the earlier paper,<sup>3a</sup> tyrosine MS-EPT oxidation has been extended to a series of bases: Tris,  $HPO_4^{2-}$ , histidine, succinate, and acetate, by cyclic voltammetry.<sup>3,9</sup> A generalized version of Scheme 1 with acceptor base B, is shown in Scheme 4. Based on that scheme with  $[HB^+]/[HB] > 10$  and total buffer concentration low, the base-catalyzed rate constant,  $k_B$ , is given by,  $k_{obs} = k_B = k_{EPT}K_A K_A'$ . As for  $HPO_4^{2-}$  as base  $k_{EPT}$  is the rate constant for the EPT step. The constants  $K_A$  and  $K_A'$  are association constants for formation of the initial H-bonded adduct ( $K_A$ ) and of the adduct with  $Os(bpy)_3^{3+}$  ( $K_A'$ ).

Scheme 4



Under these conditions the kinetically observed rate law, analogous to eq 8, becomes eq 11. In Figure 6 are shown plots of  $k_{obs}/[TyrOH]$  vs  $[B]$  for the series of bases studied ranging from acetate ( $pK_a=4.7$ ) - tris ( $pK_a=8.1$ ).

$$\frac{k_{\text{obs}}}{[\text{TyrOH}]} = k_{\text{red}} K_A K_A' [\text{B}] \quad (11)$$

These data demonstrate the generality of the MS-EPT phenomenon in the oxidation of tyrosine for five EPT acceptor bases ranging from acetate ( $\text{pK}_a = 4.7$ ) to Tris ( $\text{pK}_a = 8.1$ ). Each of the data points in Figure 6 is the average of 3-6 separate experimental determinations and the standard deviation is reported as the error.

The slopes of the plots give  $k_{\text{EPT}} K_A K_A'$ , **the MS-EPT reactivity factor**. It is the product of the EPT rate constant and association constants  $K_A K_A'$ . From the data in Figure 6,  $k_{\text{EPT}} K_A K_A'$  varies from  $6.5 \times 10^4 \text{ M}^{-2} \text{ s}^{-1}$  (acetate) to  $1.1 \times 10^6 \text{ M}^{-2} \text{ s}^{-1}$  (Tris), with slopes and intercepts reported in table 1. The trends in  $k_{\text{EPT}} K_A K_A'$  are consistent with earlier observations, namely that  $k_{\text{EPT}}$  increases with the base strength of the acceptor due to the increase in EPT driving force.<sup>15</sup>

Table 1 Slope and intercept values from plot of  $k_{\text{obs}}/[\text{TyrOH}]$  vs  $[\text{Base}]$ .

Base	Slope ( $\text{M}^{-2} \text{s}^{-1}$ )	Intercept ( $\text{M}^{-1} \text{s}^{-1}$ )
Acetate	$6.5 \times 10^4$	167
Succinate	$1.1 \times 10^5$	168
Histidine	$2.0 \times 10^5$	170
Phosphate	$6.7 \times 10^5$	175
Tris	$1.1 \times 10^6$	198

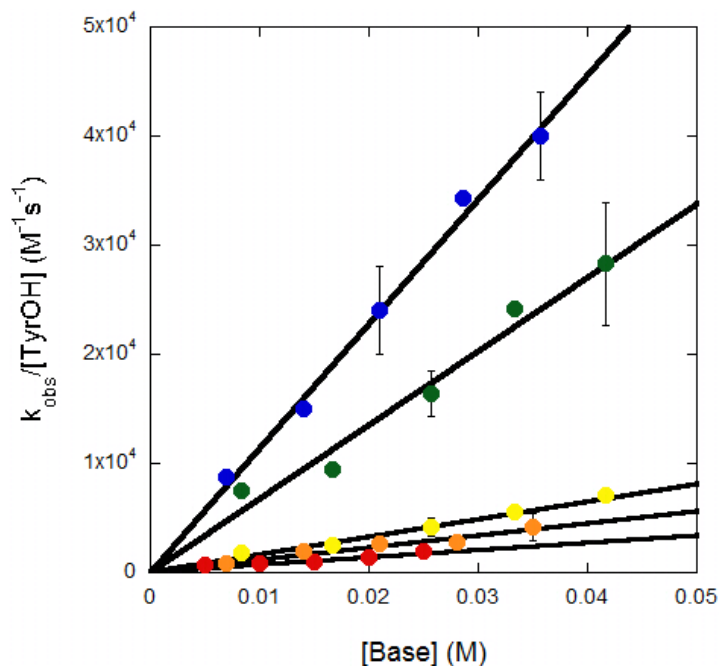


Figure 6. Plots of  $k_{\text{obs}}/[\text{TyrOH}]$  vs  $[\text{base}]$  for the base forms of added buffers from acetate to  $\text{OH}^-$  in 0.8 M NaCl at  $23 \pm 2$  °C according to eq 10. The slopes of the lines give  $k_{\text{B}} = k_{\text{EPT}}K_{\text{A}}K_{\text{A}'}$ , the **MS-EPT reactivity factor**.

4.4.4 A General Role for  $\text{OH}^-$ : As found for  $\text{HPO}_4^{2-}$  as acceptor base in Figure 4, extrapolation of plots of  $k_{\text{obs}}$  vs  $[\text{B}]$  to  $[\text{B}] = 0$  provides additional evidence for  $\text{OH}^-$  as a competitive EPT acceptor base and the general rate law in eq 12 which is analogous to eq 10. In the limit that  $[\text{B}] = 0$ ,  $k_{\text{obs}}$  is given by eq 13.

$$-\text{d}[\text{Os}(\text{bpy})_3^{3+}]/\text{dt} = \{k_0 + k_{\text{OH}^-}[\text{OH}^-] + k_{\text{B}}[\text{B}]\}[\text{Os}(\text{bpy})_3^{3+}][\text{TyrOH}]$$

$$k_{\text{obs}}[\text{Os}^{\text{III}}][\text{TyrOH}] \quad (12\text{a})$$

$$k_{\text{obs}} = k_0 + k_{\text{B}}[\text{B}] + k_{\text{OH}^-}[\text{OH}^-] \quad (12\text{b})$$

$$k_{\text{obs}} = k_0 + k_{\text{OH}^-}[\text{OH}^-] \quad (13)$$

Consistent with eq 13, a plot of the intercepts in Figure 6 ( $= k_0 + k_{\text{OH}^-}[\text{OH}^-]$ ) vs  $[\text{OH}^-]$  is shown in Figure 7. Also shown are data from a separate series of experiments with  $\text{HPO}_4^{2-}$  as base at pH = 6.0, 7.0, 7.5, 8.0, and 9.0. The inset in Figure 7 shows points below  $3.0 \times 10^{-7}$

M OH<sup>-</sup>. From the slope and intercept of the line,  $k_o = 1.7 \times 10^2 \text{M}^{-1} \text{s}^{-1}$  and  $k_{\text{OH}^-} = 1.3 \times 10^7 \text{M}^{-2} \text{s}^{-1}$  in good agreement with the values obtained by independent measurement,  $1.7 \times 10^2 \text{M}^{-1} \text{s}^{-1}$  and  $1.5 \times 10^7 \text{M}^{-2} \text{s}^{-1}$ .

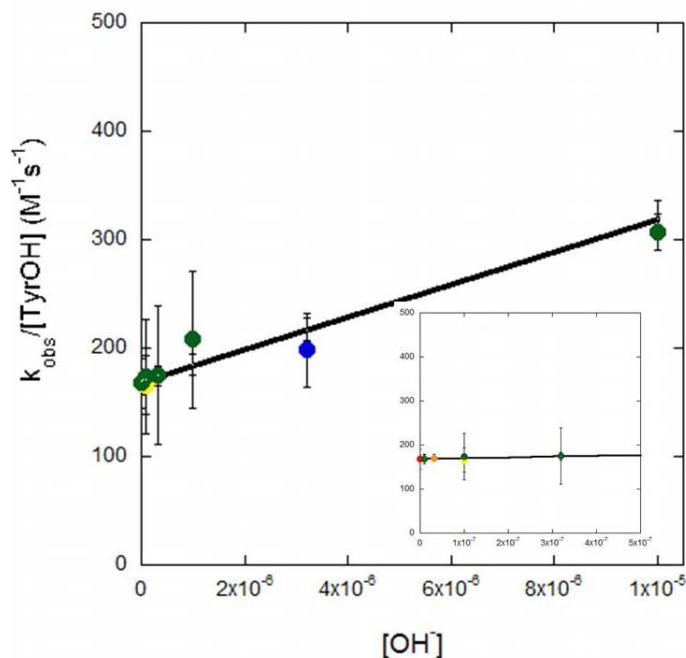


Figure 7: Plot of the intercepts from Figure 6 ( $k_o + k_{\text{OH}^-}[\text{OH}^-]$ , eq 13) vs.  $[\text{OH}^-]$  (acetate (red) succinate (orange), histidine (yellow), tris (blue) and from plots of  $k_{\text{obs}}/[\text{TyrOH}]$  vs.  $[\text{HPO}_4^{2-}]$  at pH = 6.0, 7.0, 7.5, 8.0, and 9.0 (green).

The data in Figure 7 are shown plotted vs pH rather than vs  $[\text{OH}^-]$  in Figure 8. For the diffusional reaction, the linear dependence on  $[\text{OH}^-]$  rather pH supports the origin of the apparent “pH effect” in tyrosine oxidation to a kinetic effect rather than a thermodynamic effect. In this interpretation the role of  $\text{OH}^-$  is as a very special EPT base, see below, rather than through its influence on  $\Delta G$ .

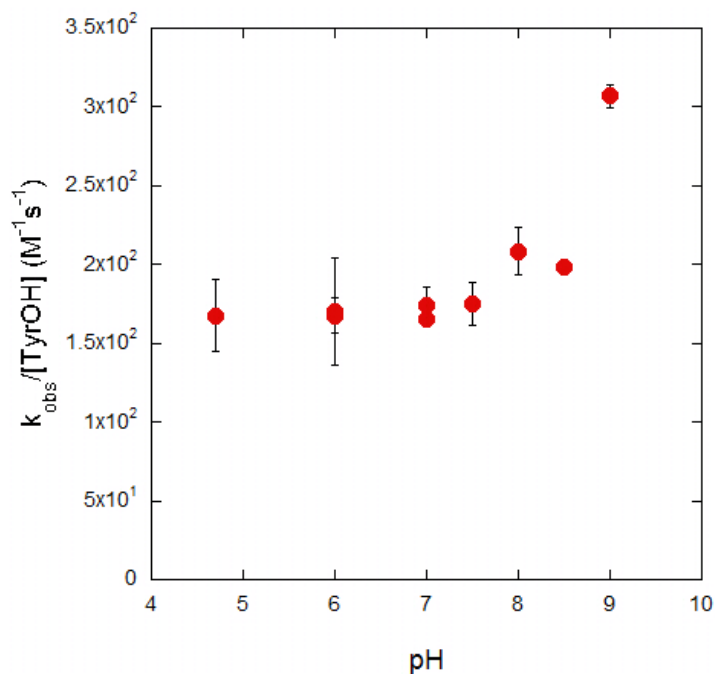
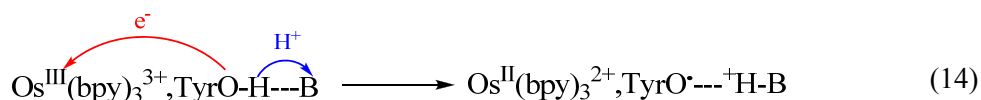


Figure 8: As in Figure 7 but with  $k_{\text{obs}}/[\text{TyrOH}]$  plotted against pH rather than  $[\text{OH}^-]$ .

#### 4.5 Conclusions

Our results on a diffusional analog of intramolecular tyrosine oxidation in eq 1 also reveal a pH dependence but with a different microscopic origin from the one proposed for the intramolecular reaction. Our results can be explained by invoking a role for  $\text{OH}^-$  as a proton acceptor in a coupled electron-transfer pathway in which the metal complex oxidant,  $\text{Os}(\text{bpy})_3^{3+}$  acts as the electron acceptor, eq 14.



In this interpretation  $\text{OH}^-$  is one of a family of aqueous bases that function as proton acceptor bases both in proton transfer and in coupled electron-proton transfer. Comparison of the EPT reactivity factors,  $k_{\text{EPT}}K_{\text{A}}K_{\text{A}}'$ , among the EPT bases in Table 1 shows that is the most effective base in the series, by a factor of  $10^4$  compared to the weakest base acetate. As shown

earlier, an important factor in such comparisons is the influence of the difference in  $pK_a$  between TyrOH and the acceptor base with  $pK_a = 4.7$  for  $Oac^-$  and 15.5 for  $OH^-$  on the driving force for concerted electron-proton transfer. Our results also point to complexities in interpreting apparent “pH” effects in complex mixtures containing more than one acceptor base with contributions from multiple bases and  $OH^-$  potentially playing a role even in solutions as dilute in  $OH^-$  as pH 7.

#### 4.6 References:

- 1) Sjödin, M.; Styring, S.; Wolpher, H.; Xu, Y.; Sun, L.; Hammarström **Switching the Redox Mechanism: Models for Proton Coupled Electron Transfer for Tyrosine and Tryptophan** *J. Am. Chem. Soc.* **2005**, *127*, 3855-3863.
- 2) Irebo, T.; Reece, S. Y.; Sjödin, M.; Nocera, D. G.; Hammarström, L. **Proton Coupled Electron Transfer of Tyrosine Oxidation: Buffer Dependence and Parallel Mechanisms.** *J. Am. Chem. Soc.* **2007**, *129*, 15462-15464.
- 3) A) Fecenko, C. J.; Meyer, T. J.; Thorp, H. H. **Electrocatalytic Oxidation of Tyrosine through Parallel Rate-Determining Proton Transfer and MS-EPT.** *J. Am. Chem. Soc.* **2006**, *128*, 11020-11021. B) Murphy, C. F.; Thorp, H. H.; Meyer, T. J. **Coupled Electron Proton Transfer Pathways in Tyrosine Oxidation.** *J. Am. Chem. Soc.* **2009** manuscript in prep.
- 4) Costentin, C.; Robert, M.; Saveant, J. M. **Concerted Proton Coupled Electron Transfer Reactions in Water. Are the Driving Force and the Rate Constant Depending on pH when Water Acts as a Proton Donor or Acceptor.** *J. Am. Chem. Soc.* **2007**, *129*, 5870-5879.
- 5) Ishikita, H.; Soudackov, A. V.; Hammes-Schiffer, S. **Buffer Assisted Proton Coupled Electron Transfer in a Model Rhenium-Tyrosine Complex** *J. Am. Chem. Soc.* **2007**, *129*, 11146-11152.
- 6) Costentin, C.; Louault, C.; Robert, M.; Saveant, J.-M. **Evidence of Concerted Proton Electron Transfer in the Electrochemical Oxidation of Phenols with Water as a Proton Acceptor.** *J. Am. Chem. Soc.* **2008**, *130*, 15817-15819.
- 7) Figure 1 and Equation 1 adapted with permission from Hammarström et al *J. Am. Chem. Soc.* **2007**, *129*, 15462-64.
- 8) Krishtalik, L. I. **Activation Energy of photosynthetic oxygen evolution: An Attempt at Theoretical Analysis.** *Bioelectrochem. Bioenerg.* **1990**, *23*, 249.
- 9) Huynh, M. H. V.; Meyer, T. J. **Proton Coupled Electron Transfer.** *Chem. Rev.* **2007**, *107*, 5004-5064. Fecenko, C. J.; Thorp, H. H.; Meyer, T. J. **The Role of Free Energy in Coupled Multi-Site EPT.** *J. Am. Chem. Soc.* **2007**, *129*, 15098-15099.
- 10) Demadis, D. D.; Dattelbaum; Kober, E. M.; Concepcion, J. J.; Paul, J. J.; Meyer, T. J.; White, P. S. **Vibrational and Structural Mapping of Os(bpy)<sub>3</sub><sup>3+/2+</sup> and Os(phen)<sub>3</sub><sup>3+/2+</sup>,** *Inorg. Chim. Acta.* **2007**, *360*, 1143-1153.

- 11) Johnston, D. H.; Glasgow, K. C.; Thorp, H. H. **Electrochemical Measurement of the Solvent Accessibility of the Nucleobases Using Electron Transfer between DNA and Metal Complexes** *J. Am. Chem. Soc.* **1995**, *117*, 8933-38
- 12) Sistare, M. F.; Holmberg, R. C.; Thorp, H. H. **Electrochemical Studies of Polynucleotide Binding and Oxidation by Metal Complexes: Effects of Scan Rate, Concentration, and Sequence** *J. Phys. Chem. B.* **1999** *103* 10718-10728
- 13) Willit, J. L., Bowden, E. F., **Adsorption and redox thermodynamics of strongly adsorbed cytochrome c on tin oxide electrodes** *J. Phys. Chem.* **1990** *94*, 8241-824
- 14) Rudolph, M., Reddy, D. P., Feldberg, S. W. *Anal. Chem.* **1994** *66*, 589A-600A
- 15) Fecenko, C. F.; Thorp, H. H.; Meyer, T. J. **The Role of Free Energy Change in Coupled Electron Proton Transfer**, *J. Am. Chem. Soc.* **2007**, *129*, 15098-15099
- 16) Luz, Z.; Meiboom, S. **Rate and Mechanism of Proton Exchange in Phosphate Buffer** *J. Am. Chem. Soc.* **1964** *86*, 4766-4768.

## Chapter 5

### **Coupled Electron Proton Transfer (EPT) in Guanine Oxidation**

Reproduced in part with permission from the National Academy of Science

Christine F. Murphy, Dana R. Holcomb, Stephanie C. Weatherly, Thomas J. Meyer\*, H. Holden Thorp\* **Coupled Electron Proton Transfer (EPT) in Guanine Oxidation** *Proc. Natl. Acad. Sci. U.S.A.* **2009**, *manuscript in prep.* © PNAS 2009

## 5.1 Abstract

Oxidation of guanine by the metal complex oxidant  $\text{Ru}(\text{bpy})_3^{3+}$  (bpy is 2,2'-bipyridine), generated chemically, or electrochemically, has been investigated in deoxyguanosine 5'-monophosphate (dGMP), single-stranded (ssDNA), and double-stranded (dsDNA) DNA. Oxidation of dGMP with added  $\text{H}_2\text{PO}_4^-/\text{HPO}_4^{2-}$  buffer over an extended range of buffer concentrations and ratios has provided evidence for three pathways for guanine oxidation as found earlier for tyrosine oxidation; electron transfer followed by proton transfer (ET-PT), concerted electron proton transfer (EPT) with  $\text{HPO}_4^{2-}$  acting as acceptor base, and proton transfer followed by electron transfer (PT-ET). The latter two pathways occur following prior H-bond association of guanine with a proton acceptor base. In media buffered by  $\text{H}_2\text{PO}_4^-/\text{HPO}_4^{2-}$ , cytosine as deoxycytosine 5'-monophosphate (dCMP) competes as the EPT base in the oxidation of dGMP or ssDNA as does cytosine in the oxidation of guanine in 1:1 MeCN- $\text{H}_2\text{O}$ . There is no  $\text{HPO}_4^{2-}$  dependence in the oxidation of dsDNA or of ssDNA with an added 7-mer base complement. All of these observations are consistent with cytosine acting as EPT acceptor base. Rate constant comparisons reveal a rate enhancement of  $\sim 10^4$  for EPT oxidation of dGMP with  $\text{HPO}_4^{2-}$  as EPT base compared to outer sphere oxidation and of  $\sim 10^3$  for EPT with cytosine as acceptor base compared to acetate both of which have comparable EPT driving forces. Rate comparisons show that guanine oxidation with cytosine as proton acceptor base is comparable for guanine-cytosine pairs as separate nucleobases or in DNA. Although guanine-cytosine EPT enhances oxidative reactivity of guanine in DNA, transfer of the proton has a small effect on long-range hole transfer in DNA because of the similar  $\text{pK}_a$ 's of guanine<sup>+</sup> and cytosine.

## 5.2 Introduction

Oxidative stress in biological systems is caused by a cellular imbalance between reactive intermediates and repair mechanisms for cellular damage.<sup>1-7</sup> Of the DNA nucleobases, guanine has the lowest one-electron redox potential ( $E^0(\text{G-H}^{+/0}) = 1.58\text{V}$ ).<sup>6</sup> As the thermodynamic trap for DNA oxidation it has been the focus of investigations of oxidative damage in DNA.

Under physiological conditions, oxidation is accompanied by loss of two electrons and one proton but the mechanism is unclear.<sup>9-14</sup> Oxidation of deoxyguanosine decreases  $pK_a$  for the N1 proton from 9.3 in guanine (G-H) to 3.9 in guanine<sup>+•</sup> (G-H<sup>+</sup>) and the  $1e^-$  potential for the guanine<sup>-•</sup> (G<sup>-•</sup>) couple decreases from 1.58V vs NHE to 1.27V vs NHE.<sup>7</sup> These observations suggest a possible role for proton coupled electron transfer (PCET) in guanine oxidation. They also suggest the potential benefit of mechanisms in which electron transfer occurs before proton transfer (ET-PT) or in which both transfer in a concerted manner, electron-proton transfer (EPT). EPT can have a significant advantage in avoiding high-energy intermediates.<sup>21-23</sup>

The role of proton transfer from oxidized guanine to complementary base cytosine (C) in DNA oxidation has been discussed by Steenken.<sup>6-8</sup> As he noted, the  $pK_a$  value for protonation of deoxycytidine of 4.3 is comparable to that for the G-H<sup>+</sup> radical cation. Although  $pK_a$  values in the interior of DNA are not available this suggests that deprotonation of guanosine radical cation may not be complete with both G-H<sup>+</sup>---C and G<sup>•</sup>---<sup>+</sup>H-C existing at equilibrium. Gas phase DFT calculations point to the occurrence of coupled electron-transfer (EPT) in the H-bonded  $\pi\pi^*$  guanine<sup>+•</sup>-cytosine<sup>-•</sup> singlet charge-transfer excited

state.<sup>15-18</sup> Direct evidence for guanine oxidation in DNA accompanied by proton transfer to cytosine has been obtained by transient FTIR measurements.<sup>18</sup>

Of particular relevance to guanine oxidation in biology is a possible kinetic role for cytosine which engages in a three point H-bond interaction with guanine in nucleic acids. There is evidence for a role for proton coupled electron transfer (PCET), not just in proton transfer to cytosine, but also in long range hole transfer in DNA. Giese and Wessely demonstrated a role for cytosine, or the absence of cytosine, on hole transfer through an abasic DNA.<sup>15</sup> In a later study they showed that substitution of methylguanosine-5 for guanosine did not inhibit long range hole transport.<sup>16</sup> Similarly, Ghosh and Schuster showed that substitution of cytosine by 5-fluoro-2'-deoxycytidine, with  $\Delta pK_a = 0.15$ , also did not inhibit hole transfer.<sup>17, 24-31</sup>

We report here the results of a kinetics study designed to reveal the possible role of EPT and its base complement cytosine in the oxidation of guanine in a variety of environments; deoxyguanosine 5'-monophosphate (dGMP) nucleotide, single stranded DNA (ssDNA), and double stranded DNA (dsDNA). The oxidant in these studies was  $Ru(bpy)_3^{3+}$  (bpy = 2,2'-bipyridine) generated by electrochemical,<sup>47</sup> and chemical oxidation. We had reported a pH dependence in guanine oxidation in earlier work and develop that theme further to demonstrate its origin in the base buffer component acting as a proton acceptor base in coupled electron-proton transfer.<sup>31-34</sup>

## 5.3 Materials and Methods

5.3.1 DNA: All nucleotides and nucleobases were purchased from Sigma-Aldrich. All synthetic oligonucleotides were obtained from the Lineberger Nucleic Acids Core Facility at

UNC. Nucleotides, nucleobases and oligonucleotides were prepared using MilliQ water unless otherwise noted. The DNA sequences used for ssDNA studies were the 15-mer sequence 5'-AAA-TAT-AGT-ATA-AAA-3' used previously in our laboratory<sup>10</sup>. For the dsDNA studies, the 15-mer ssDNA sequence 5'-AAA-TAT-AGT-ATA-AAA-3' and its 15-mer complement 5'-TTT-TAT-ACT-ATA-TTT-3' were annealed at 90°C for 5 min and allowed to cool to room temperature. The non-electroactive complement was used in excess to ensure all ssDNA was bound to the complement. Hybridization of the two strands was confirmed via native gel electrophoresis. For the ssDNA in the presence of the 7-mer complement 5'-ATA-CTA-T-3', the 7-mer and 15-mer ssDNA (5'-AAA-TAT-AGT-ATA-AAA-3') were co-incubated at 90°C for 5 min and slow cooled to room temperature. A 2 mM excess of the 7-mer complementary strand was added to the solution to ensure that no ssDNA with an electroactive guanine would remain exposed, although hybridization for these studies was not confirmed.

5.3.2 General: Distilled water was further purified by using a Milli-Q Ultrapure (18  $\Omega$ ) water purification system (Millipore). The [Ru(bpy)<sub>3</sub>]Cl<sub>2</sub> complex was purchased from Sigma Aldrich and recrystallized in acetonitrile. The concentration and purity of the sample was verified by a Cary 300 Bio UV-Visible Spectrophotometer ( $\lambda_{\text{max}}$  at 452 nm,  $\epsilon_{452} = 17,900 \text{ M}^{-1} \text{ cm}^{-1}$ ). Stock solutions of sodium phosphate buffer (1:1 H<sub>2</sub>PO<sub>4</sub><sup>-</sup>/ HPO<sub>4</sub><sup>2-</sup>; pK<sub>a</sub> 7.2) and acetic acid/sodium acetate buffer (pK<sub>a</sub> 4.7) were prepared by using Milli-Q water. All other reagents were ACS grade and used without additional purification.

5.3.3 Isotope Effects: To determine the isotope effects of guanine oxidation, the metal complex, guanine, and buffers were prepared in deuterium oxide (99.9 atom %) purchased from Sigma-Aldrich. Buffer components and dGMP were dissolved in D<sub>2</sub>O, and

deprotonated by adding NaOD to pH 10.6. The solutions were re-acidified to pD ~ 7.4 by adding DCl and D<sub>2</sub>O was removed by distillation. DNA oligonucleotides were dissolved in D<sub>2</sub>O and allowed to equilibrate in D<sub>2</sub>O at 42°C for up to 24 hours to ensure proton/deuteron exchange. NMR was used to confirm deuteration.

5.3.4 Electrodes: The working electrode was an indium tin oxide (ITO)-coated glass electrode with a reaction area of 0.32 cm<sup>2</sup>, purchased from Delta Technologies (Stillwater, MN). The reference electrode was a Teflon-coated Ag/AgCl micro-electrode purchased from Cypress Systems, Inc (Lawrence, KS). The auxiliary electrode was platinum wire purchased from Sigma-Aldrich (St. Louis, MO). ITO electrodes were treated before use by sonication in MilliQ water for 15 min, isopropanol for 15 min, followed by two washes with MilliQ water for 15 min each. ITO electrodes were laid flat and allowed to dry overnight.

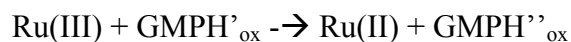
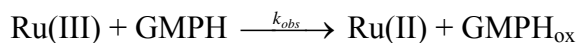
5.3.5 Electrochemistry: Electrochemical experiments were performed by using a BAS100B/W series potentiostat, in a three-electrode cell described previously.<sup>35</sup> The potential was swept in a positive direction from 0-1.3 V. The ITO electrode was conditioned for six consecutive scans in phosphate buffer solution, and a final background scan was taken. A scan of buffer plus 20 μM metal complex was scanned next, and then a final scan with buffer and 20 μM metal complex and 100 μM reductant (dGMP, ssDNA, or dsDNA) in a total experimental volume of 50 μL. The ITO electrode was then discarded and a new electrode was used for the next sample. Cyclic voltammograms (CV) were background-corrected by subtracting buffer scans from the CVs of metal and metal + reductant. Rate constants for CVs were determined by methods outlined previously for tyrosine oxidation in the presence of added proton acceptors by using the digital simulation software Digisim,

purchased through Bioanalytical Systems (West Lafayette, IN).<sup>32</sup> The average value is reported for each rate constant and standard error is reported.

Digital simulations were performed by using the DigiSim software package purchased from BioAnalytical Systems (West Layfayette, IN). Diffusion constants used in electrochemical simulations were as follows:  $6.0 \times 10^{-6} \text{ cm}^2/\text{s}$  for  $\text{Ru}(\text{bpy})_3^{3+}$ ,<sup>1</sup>  $6.0 \times 10^{-6} \text{ cm}^2/\text{s}$  for dGMP,<sup>2</sup> and  $2.0 \times 10^{-7} \text{ cm}^2/\text{s}$  for DNA.<sup>3</sup> The reduction potential of the metal complex ( $E^{\circ} = 1.26 \text{ V vs NHE}$  for  $\text{Ru}(\text{bpy})_3^{2+/3+}$  in 50 mM phosphate. and the heterogeneous electron transfer rate constant ( $k_s = 0.01 \text{ cm/s}$ ) were obtained by fitting cyclic voltammograms (CVs) of the metal complex alone in solution.

The MS-EPT pathway was isolated under conditions where the acid concentration was in a 10:1 excess to the proton acceptor concentration in a phosphate buffer solution. Guanine undergoes a two-electron oxidation to form a neutral product. Both electron transfers are present in electrochemical models. The second electron transfer is not rate determining and is not pH dependent. The MS-EPT pathway could be simulated using the following mechanism. Analysis of the data by this mechanism provided values for  $K_A$  and  $K_A'k_{\text{red}}$ . The onset of a second region of saturation kinetics under conditions of high concentrations of tyrosine and base allowed for isolation of rate constants for  $K_A'$  and  $k_{\text{red}}$ .

#### Scheme 2

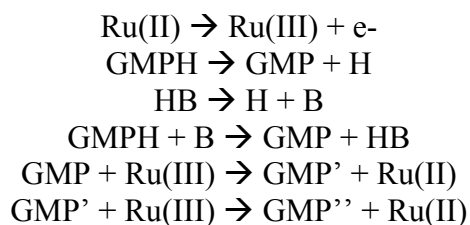


$$\text{rate} = k_{\text{obs}} [\text{GMPH}]$$

Free energy investigations through variation of buffer base were performed in 0.5M buffer at  $23 \pm 2^\circ\text{C}$  over a 0.3eV range using acetate (4.7), succinate dianion (5.6), histidine (6.6),  $\text{HPO}_4^{2-}$  (7.2), and tris (8.1) with oxidants  $\text{Fe}(\text{bpy})_3^{3+}$  (1.05V vs NHE),  $\text{Ru}(\text{dmb})_3^{3+}$  (1.07V vs NHE),  $\text{Ru}(\text{bpy})(\text{dmb})_2^{3+}$  (1.1V vs NHE), and  $\text{Ru}(\text{bpy})_3^{3+}$  (1.3V vs NHE). Cyclic voltammograms were simulated using the mechanism outlined in scheme 2 for  $\text{Ru}(\text{bpy})_3^{3+}$ . The studies were performed under saturation conditions in buffer, though resolution of  $K_A$   $k_{\text{red}}$  was not performed.

The mechanism used for the deprotonation pathway is shown below. The deprotonation pathway was selected for proton acceptor concentrations that exceeded a 10:1 excess to the acid concentration. The kinetic constants obtained from these fits were  $K_A$ ,  $k_1$ ,  $k_{-1}$ , and  $k_2$ . The CVs were fit by Digisim using the deprotonation mechanism reported Scheme3, where the proton acceptor is (B).

Scheme 3



5.3.6 Mixing Studies: Mixing experiments were used to monitor the oxidation of guanine by  $\text{Ru}(\text{bpy})_3^{3+}$ . Stock solutions of  $\text{Ru}(\text{bpy})_3^{3+}$  were prepared by bubbling  $\text{Cl}_2$  gas through a  $[\text{Ru}(\text{bpy})_3]\text{Cl}_2$  solution in water. Before use in kinetics experiments, the reaction cell was purged with argon gas to ensure removal of excess  $\text{Cl}_2$ . Decomposition of  $\text{Ru}(\text{bpy})_3^{3+}$  was monitored by absorption-time measurements at  $\lambda_{\text{max}} = 452 \text{ nm}$  for  $\text{Ru}(\text{bpy})_3^{2+}$  and found to be sufficiently slow on the time scale of

the experiments to not be an interference. In rate measurements of oxidation of dGMP, varying concentrations of dGMP ( $1.0 \times 10^{-3}$ - $3.0 \times 10^{-4}$  M) were mixed with a varying concentration of  $\text{Ru}(\text{bpy})_3^{3+}$  ( $1.0$ - $5.0 \times 10^{-5}$  M) and the time of conversion from Ru(III) to Ru(II) was monitored spectrophotometrically at 452 nm and the data was analyzed using eq 6. The rate constant,  $k_{\text{obs}}$ , was determined under pseudo-first order conditions in dGMP. The  $k_{\text{obs}}$  value was obtained as the slope of a plot of  $k_{\text{obs}}$  vs [dGMP].

$$\text{Ln} \left( \frac{\text{Abs}_{\infty} - \text{Abs}_t}{\text{Abs}_{\infty} - \text{Abs}_0} \right) = k_{\text{obs}} t \quad (6)$$

The same procedure was applied to the oxidation of guanine by  $\text{Ru}(\text{bpy})_3^{3+}$  in the presence of cytosine in 1:1 v:v  $\text{CH}_3\text{CN}:\text{H}_2\text{O}$  and the data was analyzed using eq 6. The concentration of cytosine was varied between  $0.1$ - $1.0 \times 10^{-3}$  M. in the presence of  $0.1$ - $1.0 \times 10^{-3}$  M guanine and  $1.0 \times 10^{-5}$  M  $\text{Ru}(\text{bpy})_3^{3+}$  and reaction progress monitored at 452 nm (Figure 1).

The EPT rate constant ( $K_A K_A' k_{\text{red}}$ ) was obtained from plots of  $k_{\text{obs}}/[\text{dGMP}]$  vs [dCMP].

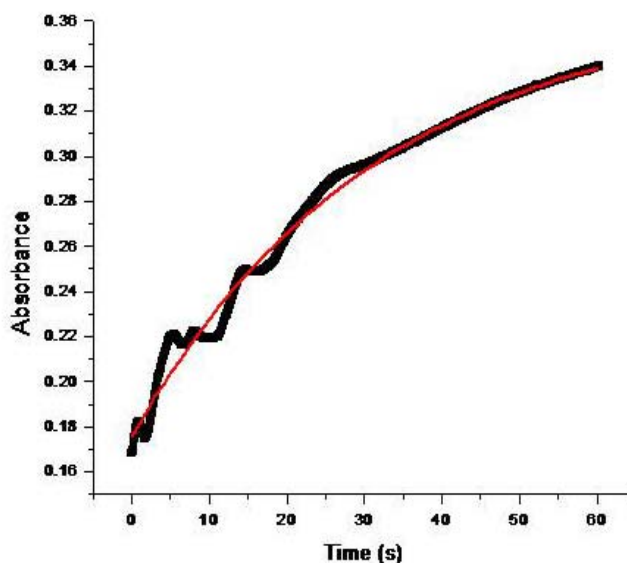
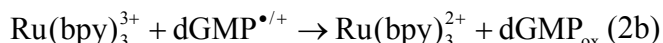
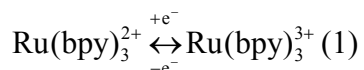


Figure 1 Absorbance over time plot for the reaction of  $1.0 \times 10^{-3}$  M guanine with  $2.0 \times 10^{-4}$  M cytosine in 1:1 v:v  $\text{CH}_3\text{CN}:\text{H}_2\text{O}$

### 3.5 Results and Discussion

#### 3.5.1 Oxidation of dGMP

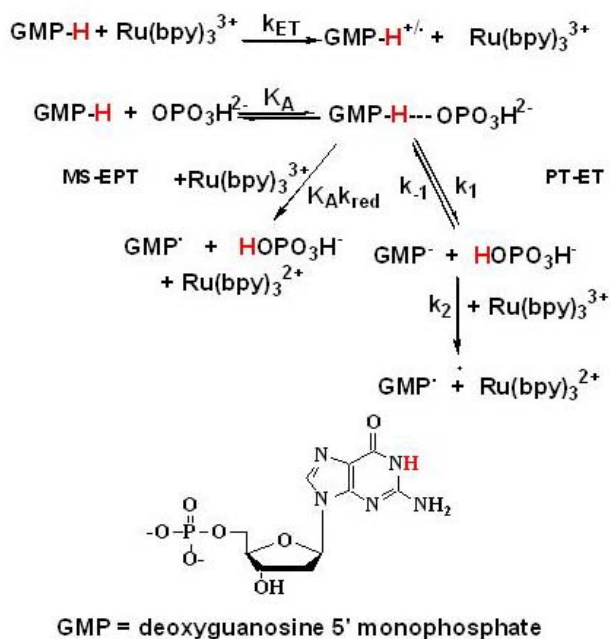
Experimental Evidence for Coupled Electron-Proton Transfer.  $\text{Ru}(\text{bpy})_3^{2+}$  undergoes a reversible 1 electron oxidation to form  $\text{Ru}(\text{bpy})_3^{3+}$  (Eq 1). Oxidation of dGMP by  $\text{Ru}(\text{bpy})_3^{3+}$  at pH 2.8 in sodium phosphate/sodium citrate buffer at  $23 \pm 2^\circ\text{C}$  occurs with  $k_{\text{obs}} = 2.6 \times 10^2 \text{ M}^{-1} \text{ s}^{-1}$  as monitored spectrophotometrically by stopped flow.<sup>33,34</sup> Assuming the  $2e^-$  oxidation stoichiometry found earlier for electrocatalytic guanine oxidation,<sup>31,33-37</sup> gives  $k = 2.6 \times 10^2 \text{ M}^{-1} \text{ s}^{-1}$  for initial outer sphere electron transfer oxidation of dGMP followed by further rapid oxidation and proton loss, eq 2a. Two electron oxidation of guanine gives 8-oxoguanosine as product (Eq 2b).



Addition of  $\text{H}_2\text{PO}_4^-/\text{HPO}_4^{2-}$  buffer catalyzed the reaction. Catalysis was investigated by an electrochemical (cyclic voltammetry) procedure, Experimental, used extensively to investigate DNA oxidation.<sup>16,47</sup> In this procedure the metal complex becomes a redox mediator, undergoing re-oxidation to  $\text{Ru}(\text{bpy})_3^{3+}$  at the electrode following reduction (eq 1), resulting in electrocatalytic oxidation of guanine. Catalytic voltammetric wave forms were analyzed by digital simulation to yield rate constants for guanine oxidation. Voltammograms were recorded over a wide range of dGMP  $0.1\text{-}1.0 \times 10^{-3} \text{ M}$  and  $\text{Ru}(\text{bpy})_3^{3+}$  ( $1.0\text{-}5.0 \times 10^{-5}$ )

concentrations and  $\text{H}_2\text{PO}_4^-/\text{HPO}_4^{2-}$  buffer concentrations (0.01-1.6M buffer) and buffer ratios (15:1 excess of acid-15:1 excess of base).

The magnitude of the electrocatalytic effect varies with added GMP,  $\text{HPO}_4^{2-}$ , and metal complex in a complex way consistent with the rate law in eq 3 derived from the mechanism shown in Scheme 1. It is analogous to a kinetic scheme identified earlier for tyrosine oxidation by  $\text{Ru}(\text{bpy})_3^{3+}$  and related metal complex oxidants.<sup>32,38</sup> In eq 3,  $[\text{dGMP}]_{\text{T}}$  is the total concentration of dGMP. The electrocatalytic studies were carried out at  $23 \pm 2^\circ\text{C}$  in aqueous phosphate solution.



$$-\frac{d[\text{Ru(III)}]}{dt} = \left[ \frac{K_A [\text{HPO}_4^{2-}] [\text{GMP}]_{\text{T}}}{1 + K_A [\text{HPO}_4^{2-}]} \right] \left( K_A' k_{\text{red}} + \frac{k_1 k_2}{k_{-1} [\text{H}_2\text{PO}_4^-] + k_2 [\text{Ru(III)}]} \right) [\text{Ru(III)}] \quad (3a)$$

$$-\frac{d[\text{Ru(III)}]}{dt} = k_{\text{obs}} [\text{GMP}] [\text{Ru(III)}] \quad (3b)$$

$$\frac{k_{\text{obs}}}{[\text{GMP}]} = \left( K_A K_A' k_{\text{red}} + \frac{K_A k_1 k_2}{k_{-1}[\text{H}_2\text{PO}_4^-] + k_2[\text{Ru(III)}]} \right) [\text{HPO}_4^{2-}] \quad (3c)$$

The rate law was tested by varying concentrations of reactants to achieve limiting forms. At relatively high concentrations of the acid form of the buffer with  $[\text{H}_2\text{PO}_4^-]/[\text{HPO}_4^{2-}] > 10$ , the pathway labeled MS-EPT (Multisite-Electron Proton Transfer, see below) dominates and the rate law becomes eq 4. Under these conditions dGMP exists dominantly as a, presumably, H-bonded adduct with buffer base  $\text{HPO}_4^{2-}$ . The predicted saturation kinetics are observed at relatively high  $[\text{HPO}_4^{2-}]$  ( $> 50$  mM) Figure 2, from which  $K_A = 114.3 \pm 0.1 \text{ M}^{-1}$ . A second saturation region is reached in solutions high in both  $[\text{HPO}_4^{2-}]$  and  $[\text{dGMP}]$ , Figure 3, from which  $K_A' = 26.3 \pm 0.2 \text{ M}^{-1}$  and  $k_{\text{red}} = 3.3 \pm 0.4 \times 10^6 \text{ s}^{-1}$  with the latter the rate constant for coupled electron-proton transfer within the association complex between dGMP and the base.

$$\frac{k_{\text{obs}}}{[\text{GMP}]} = K_A K_A' k_{\text{red}} [\text{HPO}_4^{2-}] \quad (4a)$$

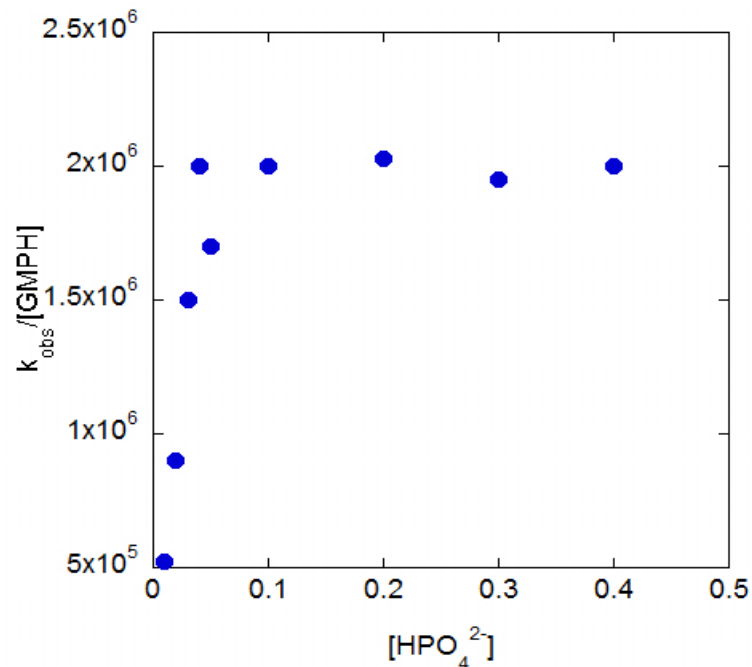


Figure 2: Plot of  $k_{\text{obs}}/[\text{GMPH}]$  vs  $[\text{HPO}_4^{2-}]$  exhibiting saturation kinetics at concentrations of  $\text{HPO}_4^{2-}$ . Cyclic voltammetric studies were performed in  $1.0 \times 10^{-4} \text{M}$  dGMP with  $2.0 \times 10^{-5} \text{M}$   $\text{Ru}(\text{bpy})_3^{3+}$  in varied amounts of phosphate at  $23 \pm 2^\circ\text{C}$ .

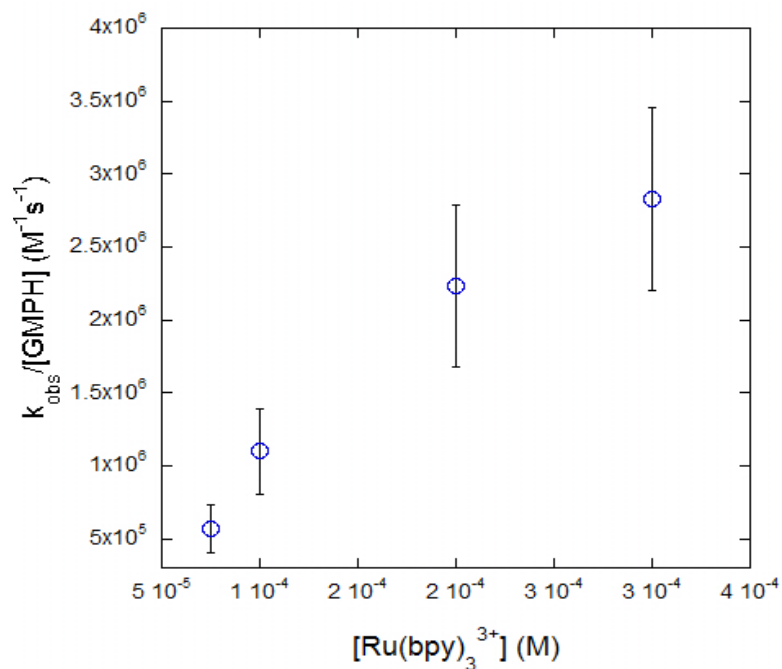


Figure 3: Plot of  $k_{\text{obs}}/[\text{GMPH}]$  vs  $[\text{Ru}(\text{bpy})_3^{3+}]$  exhibiting saturation kinetics at high concentrations of association complex. Experimental data was obtained through cyclic voltammetric studies at  $0.5 \text{M}$  phosphate buffer in  $1.0 \times 10^{-4} \text{M}$  in GMPH at  $23 \pm 2^\circ\text{C}$ .

Similarly, with  $[\text{HPO}_4^{2-}]/[\text{H}_2\text{PO}_4^-] < 10$ , the pathway labeled PT-ET (proton transfer followed by electron transfer) in Scheme 1 dominates. In the limit that  $k_2[\text{Ru}(\text{bpy})_3^{3+}] \gg k_1[\text{H}_2\text{PO}_4^-]$ , the general rate law in eq 3 reduces to eq 4b with  $k_{\text{obs}}$  becoming independent of  $[\text{Ru}(\text{bpy})_3^{3+}]$ , from which  $k_1 = 5.0 \pm 0.3 \times 10^4 \text{ s}^{-1}$  with  $k_1$  the rate constant for proton transfer within the association complex.

$$\frac{k_{\text{obs}}}{[\text{GMP}]} = K_A k_1 [\text{HPO}_4^{2-}] \quad (4b)$$

The rate constant for  $k_2$  was determined by cyclic voltammetric studies on the deprotonated GMP species where  $k_2$  was determined to be  $1.1 \pm 0.2 \times 10^7 \text{ M}^{-1} \text{ s}^{-1}$ . With the value of  $k_2$  available by independent measurement,  $k_1$  was determined by simulation of voltammograms under conditions where  $[\text{HPO}_4^{2-}]$  was held constant and  $[\text{H}_2\text{PO}_4^-]$  was varied between 0.002M-1.48M where  $k_1 = 2.1 \pm 0.8 \times 10^9 \text{ M}^{-1} \text{ s}^{-1}$  was determined from the slope of the line from plots of  $k_{\text{obs}}$  vs  $[\text{H}_2\text{PO}_4^-]^{-1}$ .

In Table 1 are listed rate and equilibrium constants obtained for dGMP oxidation by  $\text{Ru}(\text{bpy})_3^{3+}$ . For purposes of comparison they are compared with values obtained for oxidation of tyrosine by the same oxidant in Table 1.

Substrate	$K_A(M^{-1})$	$k_1(s^{-1})$	$k_{-1}(M^{-1}s^{-1})$	$k_2(M^{-1}s^{-1})$	$K_A'(M^{-1})$	$k_{red}(M^{-1}s^{-1})$
<b>GMP</b>	<b>114±2</b>	<b>5.0±0.3x10<sup>4</sup></b>	<b>2.1±0.8x10<sup>9</sup></b>	<b>1.1±0.2x10<sup>7</sup></b>	<b>26.3±0.2</b>	<b>3.3±0.4x10<sup>6</sup></b>
<b>TyrOH</b>	<b>30±1</b>	<b>3.3±0.1x10<sup>5</sup></b>	<b>7.8±0.4x10<sup>9</sup></b>	<b>1.7±0.3x10<sup>7</sup></b>	<b>22.2±0.1</b>	<b>4.4±0.5x10<sup>7</sup></b>

**Table 1.** Kinetic parameters for EPT oxidation of dGMP and TyrOH by  $Ru(bpy)_3^{3+}$  with  $HPO_4^{2-}$  as base at  $23\pm0.2^\circ C$  with total phosphate = 0.01- 1.6 M for dGMP and TyrOH oxidation and in 0.8 M NaCl for tyrosine. Values reported are the average value determined for each rate constant and the standard deviation is reported as error. Note Scheme 1.

The electrochemical technique was also used to investigate oxidation of dGMP by  $Ru(bpy)_3^{3+}$  in  $D_2O$  and  $H_2O/D_2O$  mixtures under the same conditions. Key  $H_2O/D_2O$  kinetic isotope effect (KIE) results are:  $k_{red}(H_2O)/k_{red}(D_2O) = 2.4\pm0.4$  for the EPT step and  $k_1 = 1.3\pm0.2$ , for proton loss within the association complex. There is an equilibrium isotope effect for the association complex of  $K_A(H_2O)/K_A(D_2O)=1.2\pm0.1$ .

In Figure 4 is shows the magnitude of the isotope effect for dGMP. The magnitude of the KIE is consistent with a EPT pathway and the linearity of the plot with transfer of a single proton in the coupled step.<sup>38</sup>

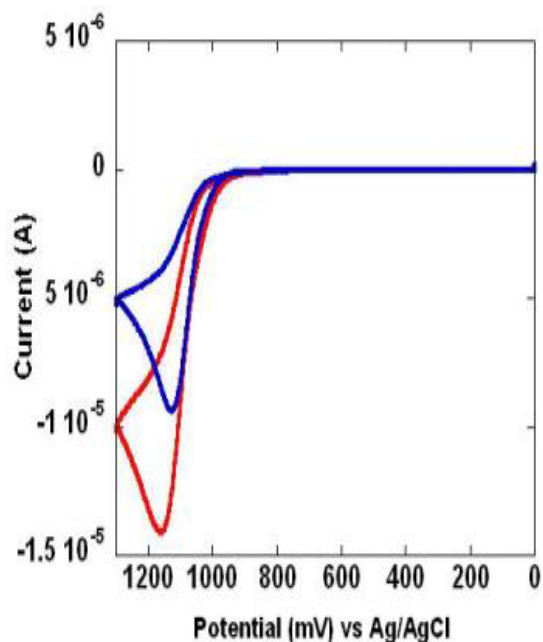
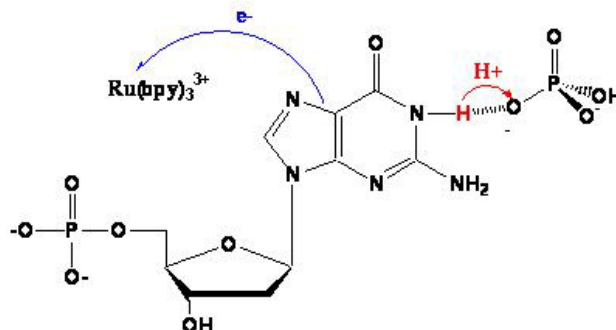


Figure 4: Cyclic voltammograms obtained in protonated (red) and deuterated (blue) solution in 0.5M phosphate buffer at pH 6.0 phosphate buffer. The cyclic voltammogram in H<sub>2</sub>O shows significantly greater current enhancement over the cyclic voltammogram in deuterated solution.

EPT in the Oxidation of dGMP. The results of the kinetic study with added HPO<sub>4</sub><sup>2-</sup>/HPO<sub>4</sub><sup>2-</sup> buffer are consistent with Scheme 1. As noted above, an analogous scheme has been observed in the oxidation of tyrosine by Ru(bpy)<sub>3</sub><sup>3+</sup> and related metal complex oxidants.<sup>32,39</sup> In this scheme there are two pathways for the observed rate enhancement with added buffer base. In both the key to rate enhancement is preliminary formation of a, presumably, H-bonded adduct with added base, G-H---OPO<sub>3</sub>H<sup>2-</sup>, followed by competitive proton loss and rapid oxidation of deprotonated dGMP, eq 4b, or oxidation of the adduct by Ru(bpy)<sub>3</sub><sup>3+</sup>, eq 4a. In the latter pathway coupled electron-proton transfer occurs but with different electron and proton acceptors; Ru(bpy)<sub>3</sub><sup>3+</sup> for the transferred electron, and HPO<sub>4</sub><sup>2-</sup> for the proton. Pathways of this kind have been described as Multiple Site-Electron Proton Transfer (MS-EPT) illustrated in scheme 2.

Scheme 2



Rate comparisons reveal a significant rate advantage of MS-EPT in eq 5 over electron transfer (ET) in eq 2 of  $\sim 10^4$ . Oxidation of the dGMP-HPO<sub>4</sub><sup>2-</sup> association complex by Ru(bpy)<sub>3</sub><sup>3+</sup> by the MS-EPT pathway occurs by  $K_A K_A' k_{\text{red}} = 2.2 \pm 0.5 \times 10^6 \text{ M}^{-2} \text{ s}^{-1}$ , Scheme 1, compared to  $k_{\text{ET}} = 3.6 \pm 0.5 \times 10^2 \text{ M}^{-1} \text{ s}^{-1}$  for outer sphere electron transfer.

MS-EPT is a more complex process microscopically since it involves both electron and proton transfer.<sup>40,41</sup> The origin of the rate enhancement is a more favorable driving force arising from the enhanced acidity of dGMP<sup>+•</sup> ( $\text{p}K_a = 3.9$ ) compared to dGMP ( $\text{p}K_a = 9.3$ ). Neglecting the difference in  $\Delta G^\circ$  values for formation of H-bonded adducts before,  $\text{G-H} + \text{HPO}_4^{2-} \rightarrow \text{G-H} \cdots \text{OPO}_2\text{OH}^{2-}$ , and after the EPT step,  $\text{G}^{\cdot-} \cdots \text{H-OPO}_2\text{OH}^- \rightarrow \text{G}^{\cdot-} + \text{H-OPO}_2\text{OH}^-$ ,  $\Delta G_{\text{EPT}}^\circ = -0.2 \text{ eV}$  compared to  $\Delta G_{\text{ET}}^\circ = 0.32 \text{ eV}$  for outer sphere electron transfer.<sup>7</sup>

For purposes of later rate comparisons, the **EPT reactivity factor**, which is the product of the association constants  $K_A$  and  $K_A'$  in Scheme 1 and the EPT rate constant,  $k_{\text{EPT}}$ , is  $K_A K_A' k_{\text{red}} = 2.2 \pm 0.5 \times 10^6 \text{ M}^{-2} \text{ s}^{-1}$ . It is a kinetically useful quantity for rate comparisons, obtained experimentally under conditions dilute in reactants. The experimental value of  $K_A K_A' k_{\text{red}}$  for dGMP with phosphate buffer was verified independently by stopped flow

measurements.<sup>42</sup> From those measurements  $K_A K_A' k_{red} = 1.5 \pm 0.1 \times 10^6 \text{ M}^{-2} \text{ s}^{-1}$  at  $23 \pm 2^\circ \text{C}$  in 0.8M NaCl.

Although not studied in detail here, there is also evidence for  $\text{OH}^-$  as EPT base as documented in detail for TyrOH elsewhere.<sup>43</sup> Evidence for this pathway comes from rate enhancement for oxidation of dGMP by  $\text{Ru}(\text{bpy})_3^{3+}$ , eq 2, from  $k_{ET} = 2.6 \times 10^2 \text{ M}^{-1} \text{ s}^{-1}$  at  $\text{pH} = 2.8$  to  $k_{ET} = 3.6 \pm 0.5 \times 10^2 \text{ M}^{-1} \text{ s}^{-1}$  in un-buffered solution aqueous solution at  $\text{pH} = 7$  in 0.8M NaCl at  $23 \pm 2^\circ \text{C}$ .

EPT Oxidation of dGMP General Base Catalysis: The oxidation mechanism of dGMP was investigated further through variation of the proton acceptor. The buffer base was varied from acetate  $\text{pK}_a = 4.7$  to tris  $\text{pK}_a = 8.1$ . Catalytic current is responsive to base strength, showing a large increase in peak current as base strength increased from acetate to tris base. Digital simulation of cyclic voltammograms  $1.0 \times 10^{-4} \text{ M}$  dGMP with  $2.0 \times 10^{-5} \text{ M}$   $\text{Ru}(\text{bpy})_3^{3+}$  in 0.5 M buffer (10:1 Base:Acid) showed a  $10^4$  increase in rate from acetate to tris.

The role of free energy change was examined through variation of both the base and the oxidant. Variation of the oxidant over a 0.3eV range resulted in a linear dependence on oxidant strength with a slope of the line of 0.60 in 0.5M phosphate buffered solution at  $23 \pm 2^\circ \text{C}$  (Figure 5a). Variation of base strength over a 0.2eV range resulted in a linear dependence on base strength with a slope of 0.54 using  $\text{Ru}(\text{bpy})_3^{3+}$  as the electron acceptor in 0.5M buffered solution at  $23 \pm 2^\circ \text{C}$  (Figure 5b).  $\Delta G$  was calculated using eq 5. Deviation from the expected Marcus value of 0.5 is expected in electron transfer reactions involving a proton in the rate determining step which is consistent with a concerted transfer through a hydrogen bonded adduct.<sup>44,45</sup>

$$\Delta G = E_{\text{dGMP}}^{0'} - E_{\text{M}^{2+/3+}}^{0'} - 0.059(\text{pK}_{\text{a}_{\text{HB}^+}} - \text{pK}_{\text{a}_{\text{dGMP}^*/+}}) \quad (5)$$

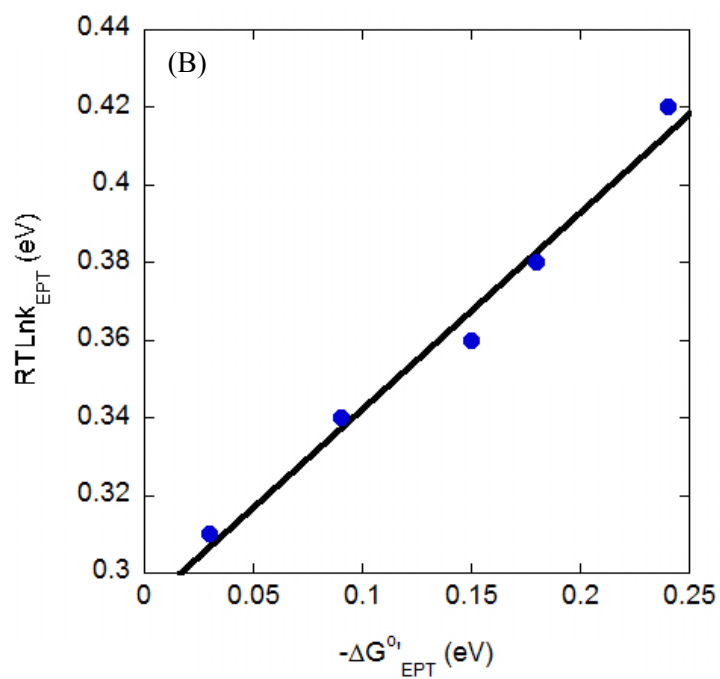
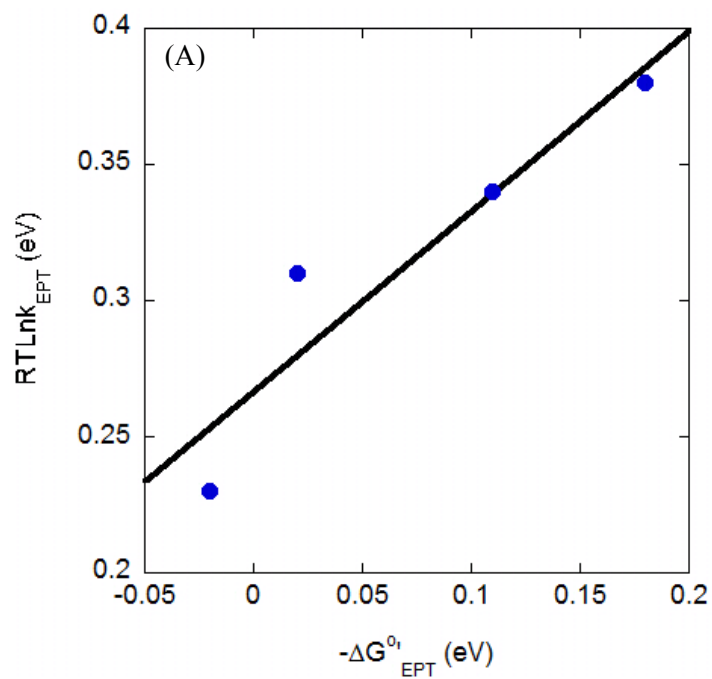


Figure 5: A) Variation of  $RT\ln k_{\text{EPT}}$  through variation of oxidant strength from  $\text{Fe}(\text{bpy})_3^{3+}$  at 1.05V vs NHE to  $\text{Ru}(\text{bpy})_3^{3+}$  at 1.25V vs NHE. The slope of the line is 0.6. B) Variation of  $RT\ln k_{\text{EPT}}$  through variation of base strength from acetate  $\text{pK}_a=4.7$  to tris  $\text{pK}_a=8.1$ . The slope of the line is 0.54. Each investigation used  $1.0 \times 10^{-4}\text{M}$  dGMP with  $2.0 \times 10^{-5}\text{M}$   $\text{M}(\text{bpy})_3^{3+}$  in 0.5M buffer at  $23 \pm 2^\circ\text{C}$ .

The role of free energy was investigated further through variation of both the oxidant and the base simultaneously. The result on  $RT\ln k_{\text{EPT}}$  through variation of both base and oxidant results in a quadratic like dependence (Figure 6). These results are important because they further demonstrate the systematic dependence on  $\Delta G^{0'}$  that exists for EPT despite how the free energy is varied as found initially for tyrosine.<sup>38</sup>

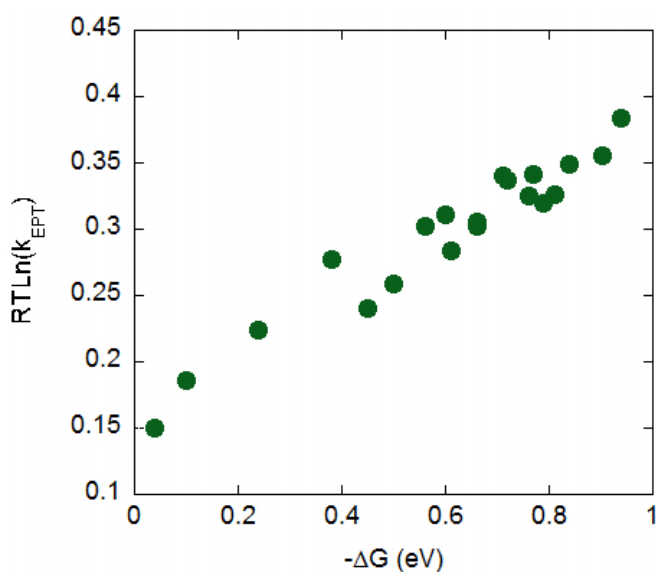


Figure 6: Variation of  $RT\ln(k_{\text{red}})$  vs  $-\Delta G^{0'}$  in eV by varying both  $E^{0'}$  for the oxidant and  $\text{pK}_a$  for the acceptor base.

### 5.5.2 EPT Oxidation of dGMP and Guanine with Added dCMP and Cytosine

Oxidation of dGMP by  $\text{Ru}(\text{bpy})_3^{3+}$  was investigated by cyclic voltammetry in  $\text{H}_2\text{PO}_4^-/\text{HPO}_4^{2-}$  buffer with added dCMP. Due to limited solubility a relatively narrow concentration range in dCMP,  $0.1-1.0 \times 10^{-3}\text{M}$ , was investigated. Voltammetric responses in solutions 0.1

mM in dGMP and 0.02 mM in  $\text{Ru}(\text{bpy})_3^{2+}$  in 100 mM phosphate buffer (pH 7.0) with added dCMP showed significant current enhancements relative to enhancements observed with added phosphate buffer alone, Figure 7. Current enhancements varied linearly with added dCMP over the concentration range  $0.1\text{-}1.0 \times 10^{-3}\text{M}$ .

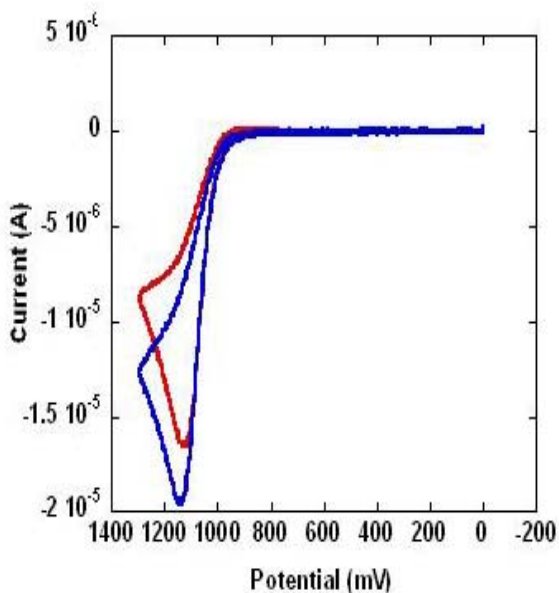


Figure 7: Red Line: Cyclic voltammogram of 0.02mM  $\text{Ru}(\text{bpy})_3^{2+}$  in the presence of 100  $\mu\text{M}$  dGMP (in 100 mM phosphate buffer at pH 7.5). The EPT rate constant for this reaction is  $2.2 \times 10^6 \text{M}^{-1}\text{s}^{-1}$ . Blue Line: Cyclic voltammogram of 20  $\mu\text{M}$   $\text{Ru}(\text{bpy})_3^{2+}$ , in the presence of 100  $\mu\text{M}$  dGMP, 100  $\mu\text{M}$  dCMP (in 100 mM phosphate buffer pH 7.0).

Analysis of voltammograms for enhanced electrocatalytic oxidation of dGMP compared to the  $[\text{HPO}_4^{2-}]/[\text{H}_2\text{PO}_4^-]$  buffer background by digital simulation gave for the EPT reactivity factor,  $k_{\text{red}}K_AK_A' = 5.5 \pm 0.1 \times 10^6 \text{M}^{-2}\text{s}^{-1}$ .

An ambiguity exists in interpreting rate enhancements induced by dCMP since the EPT effect could be due to H-bonding through the nucleobase or phosphate ( $\text{p}K_{\text{a},1} = 2.7$ ). To probe the role of cytosine as EPT base in guanine oxidation we conducted a series of

experiments in 1:1 v:v H<sub>2</sub>O:CH<sub>3</sub>CN mixtures. With this solvent mixture sufficient solubility was achieved to investigate guanine oxidation by Ru(bpy)<sub>3</sub><sup>3+</sup> over an extended concentration range. The reaction was investigated by mixing with spectrophotometric monitoring of the growth of Ru(bpy)<sub>3</sub><sup>2+</sup> at λ<sub>max</sub> = 452 nm. Reaction conditions were pseudo first order in cytosine (0.1-1.0x10<sup>-3</sup>M) with guanine varied from 0.1-0.5x10<sup>-3</sup>M. From the intercept of the plot of k<sub>obs</sub> vs. [cytosine] in Figure 8, K<sub>A</sub>K<sub>A</sub>'k<sub>red</sub> = 7.5±0.9x10<sup>5</sup> M<sup>-2</sup>s<sup>-1</sup> at 23±2°C. This is comparable to but less than the EPT reactivity factor for dCMP in 0.1M phosphate buffer at 23±2°C for which K<sub>A</sub>K<sub>A</sub>'k<sub>red</sub> = 5.5±0.1x10<sup>6</sup> M<sup>-2</sup>s<sup>-1</sup>, Table 1. The higher value may be largely due to electrostatic enhancement in the association complex for dCMP, Ru(bpy)<sub>3</sub><sup>3+</sup>,(dGMP---dCMP)<sup>4-</sup>, and a larger value for K<sub>A</sub>' in Scheme 1 with comparable reactivity for cytosine and dCMP as EPT proton acceptor bases.

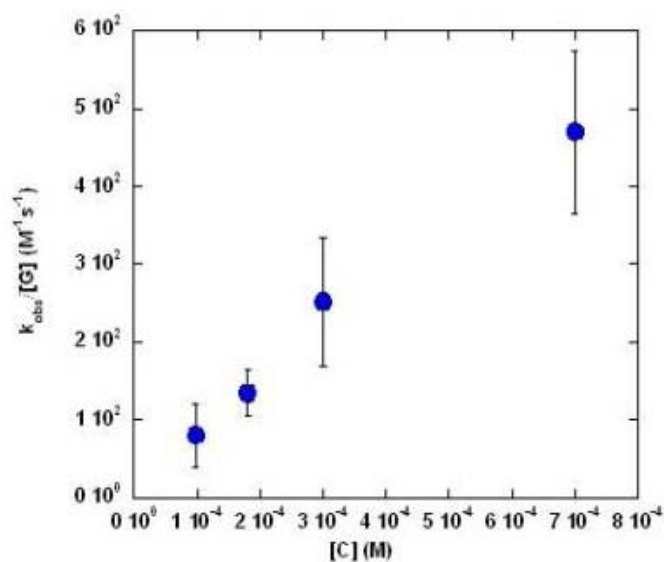


Figure 8: Plot of k<sub>obs</sub> vs [Cytosine]. Studies done spectrochemically monitored Ru(bpy)<sub>3</sub><sup>2+</sup> formation over time. A series of [Cytosine] concentrations (1.0x10<sup>-3</sup>-1.0x10<sup>-4</sup>M) were used and the slope of the line reflects the reactivity factor of K<sub>A</sub>K<sub>A</sub>'k<sub>red</sub> using cytosine as a proton acceptor.

The magnitudes of the  $K_A K_A' k_{\text{red}}$  values for dCMP and cytosine point to a special kinetic enhancement for cytosine as an EPT proton acceptor. This conclusion follows from experiments on dGMP oxidation by  $\text{Ru}(\text{bpy})_3^{3+}$  in acetic acid/acetate ( $\text{HOAc}/\text{Oac}^-$ ) buffer solutions with  $\text{Oac}^-$  as the EPT base. These experiments were carried out as described for the  $\text{HPO}_4^{2-}/\text{H}_2\text{PO}_4^-$  buffer with  $\text{HPO}_4^{2-}$  as base by simulation of cyclic voltammograms but over a relatively limited concentration range with  $[\text{HOAc}]/[\text{Oac}^-] > 10$ . Based on the results of digital simulations,  $K_A K_A' k_{\text{red}} = 2.4 \pm 0.4 \times 10^3 \text{ M}^{-2} \text{ s}^{-1}$  (at  $23 \pm 2^\circ \text{C}$ ). The electrochemical rate constant was verified independently spectrophotometrically.

This is an important comparison. Acetate and dGMP have comparable  $\text{pK}_a$ 's with  $\text{pK}_a(\text{dCMP}) = 4.3$  for cytosine and  $\text{pK}_a(\text{HOAc}) = 4.7$ . Given the comparable  $\text{pK}_a$  values, the driving forces for MS-EPT are comparable for the two oxidations,  $\text{Ru}(\text{bpy})_3^{3+}, \text{G-H} \rightarrow \text{Ru}(\text{bpy})_3^{2+}, \text{G}^{\cdot-} + \text{H-OAc}$  and  $\text{Ru}(\text{bpy})_3^{3+}, \text{G-H} \rightarrow \text{Ru}(\text{bpy})_3^{2+}, \text{G}^{\cdot-} + \text{H-C}$ , with  $\Delta G^\circ \sim -0.04 \text{ eV}$ . Even though driving forces are comparable, EPT is favored for cytosine as proton acceptor base kinetically by  $\sim 10^3$ .

### 5.4.3 Oxidation of ssDNA

In an extension of earlier work by Weatherly et al.,<sup>33,34,42</sup> guanine oxidation in ssDNA and dsDNA was also studied by the catalytic electrochemical technique. Oxidation of guanine in the 15-mer ssDNA 5'-AAA-TAT-AGT-ATA-AAA-3' by  $\text{Ru}(\text{bpy})_3^{3+}$  was investigated with added  $\text{H}_2\text{PO}_4^-/\text{HPO}_4^{2-}$  buffer by using the same conditions as oxidation of dGMP. Catalytic currents increased with increasing concentrations of  $\text{HPO}_4^{2-}$  as in oxidation of dGMP, Figure 9a. Digital simulation of cyclic voltammograms in phosphate buffer resulted in a rate constant of  $K_A K_A' k_{\text{red}} = 9.0 \pm 0.2 \times 10^5 \text{ M}^{-2} \text{ s}^{-1}$ .

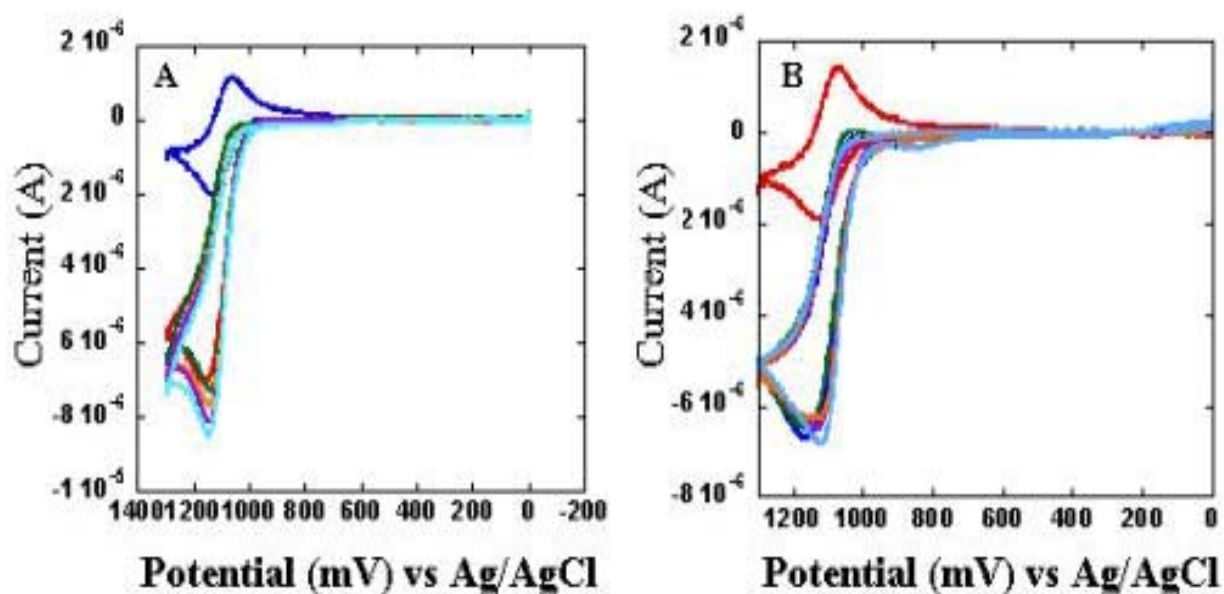


**Figure 9** A) Cyclic voltammograms of  $20 \mu\text{M Ru}(\text{bpy})_3^{2+}$  in the presence of  $100 \mu\text{M ssDNA}$  and increasing concentrations of phosphate buffer (10-50 mM) at pH 7.0. The cyclic voltammograms show an increase in oxidative current as a function of phosphate concentration. B) Cyclic voltammograms of  $20 \mu\text{M Ru}(\text{bpy})_3^{2+}$  in the presence of  $100 \mu\text{M dsDNA}$  and increasing concentrations of phosphate buffer (10-50 mM) at pH 7.0. The cyclic voltammograms show no change in oxidative current as a function of phosphate concentration.

Isotope studies in deuterated solution at  $\text{pD} = 7.4$  resulted in a kinetic isotope effect of  $1.4 \pm 0.1$  for ssDNA with phosphate acting as a proton acceptor for the buffer dependent oxidation of ssDNA. The oxidation mechanism of ssDNA was examined by stopped flow in sodium phosphate/sodium citrate buffer in the pH range of 2.8-6.5. Rate constants ( $k_{\text{obs}}$ ) are consistent with an increase in concentration of base in solution (Figure 10).

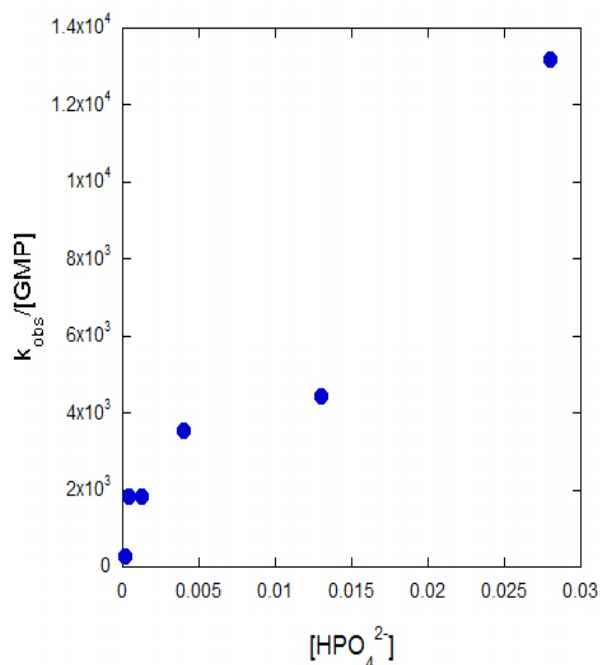


Figure 10: Plot of  $k_{\text{obs}}/[\text{GMP}]$  vs  $[\text{HPO}_4^{2-}]$  as measured by stopped flow in phosphate/citrate buffered solution at pH 2.2-6.8 a phosphate concentration of  $1.0 \times 10^{-4}$ -0.03M. The plot is consistent with ssDNA data obtained by electrochemical and spectrochemical techniques and exhibits a first order dependence on phosphate.

#### 5.4.4 Oxidation of ssDNA with a Base Complement

Guanine oxidation by  $\text{Ru}(\text{bpy})_3^{3+}$  in the ssDNA 5'AAA-TAT-AGT-ATA-AAA3' was studied electrochemically in the presence of either  $0.1 \times 10^{-3}$  M dCMP or  $0.1 \times 10^{-3}$  M of the complementary 7-mer ssDNA 5'-ATA-CTA-T-3'. In these experiments, the concentration of phosphate was 100 mM, pH=7.0, and 1.5 excess of the acidic form of the buffer with buffer base induced reactivity dominated by the MS-EPT pathway in Scheme 1.

Significant current enhancements were observed with both added dCMP and the 7-mer DNA complement over 0.1M phosphate background. Analysis of the enhanced current-time profiles with 0.1 to  $1.0 \times 10^{-3}$  M dCMP by digital simulation gave  $K_A K_A' k_{\text{red}} = 1.6 \pm 0.5 \times 10^6 \text{ M}^{-2} \text{ s}^{-1}$  Figure 11.

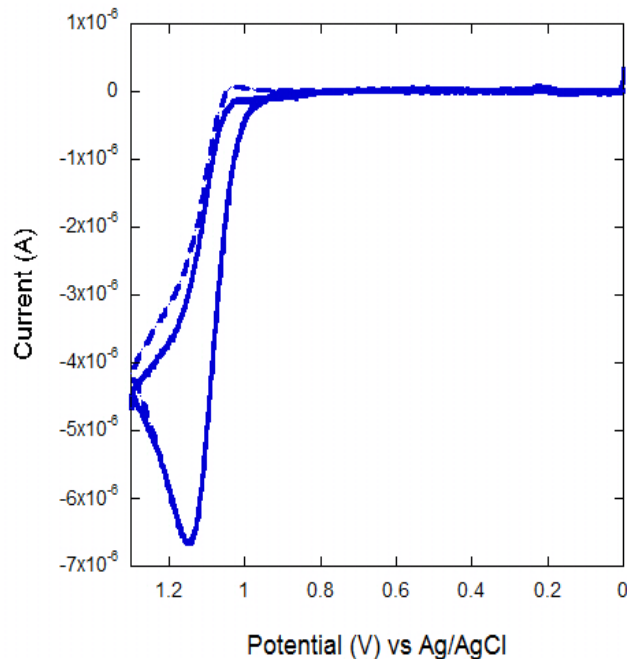


Figure 11: Experimental cyclic voltammogram (solid line) overlaid with digital simulation of  $1.0 \times 10^{-4} \text{ M}$  dGMP with  $1.0 \times 10^{-3} \text{ M}$  dCMP in  $0.1 \text{ M}$  pH 7.0 phosphate buffer at  $23 \pm 2^\circ \text{C}$ . Digital simulation parameters using eq SI 5-SI 8 resulted in a  $k_{\text{obs}} = 5.5 \times 10^6 \text{ M}^{-1} \text{ s}^{-1}$ .

In the oxidation of the ssDNA at  $0.1 \times 10^{-3} \text{ M}$  in the presence of  $1.0 \times 10^{-3} \text{ M}$  of the 7mer complement, the voltammetric profiles were insensitive to the concentration of added phosphate buffer from 0.01 to 0.05 M at pH = 7.0. Current enhancements compared to background were directly attributable to the 7mer complement. Digital simulation of the current-potential profiles gave  $k_{\text{obs}} = 1.1 \pm 0.3 \times 10^6 \text{ M}^{-1} \text{ s}^{-1}$ .

Rate enhancement with the added 7-mer complement provides evidence for the expected guanine-cytosine hybridization and formation of the 15-mer/7-mer complex.

#### 5.4.5 Oxidation of dsDNA

In a final set of experiments, oxidation of dsDNA by  $\text{Ru}(\text{bpy})_3^{3+}$  was also investigated by the electrocatalytic technique. The 15-mer ssDNA containing guanine was annealed to its

15-mer complementary strand (which was present in excess), and hybridization was verified by gel electrophoresis. Oxidation of the hybridized dsDNA was investigated electrochemically under the same conditions as in the ssDNA studies with 0.1-0.5M phosphate buffer at pH 7.0 with [ssDNA] = 0.1mM and [ssComplement] = 2mM.<sup>34</sup> Digital simulation of cyclic voltammograms gave  $2.5 \pm 0.6 \times 10^6 \text{ M}^{-1} \text{ s}^{-1}$ .

As for the ssDNA/7-mer complement, the current-time profiles of the voltammograms were independent of phosphate concentration over the range 10-50 mM in  $\text{H}_2\text{PO}_4^- / \text{HPO}_4^{2-}$  at pH = 7 (Figure 10 B). Digital simulation of voltammograms in  $\text{D}_2\text{O}$  at pD = 7.4, gave  $k_{\text{obs}} = 1.1 \pm 0.3 \times 10^6 \text{ M}^{-1} \text{ s}^{-1}$ . and the KIE,  $k_{\text{obs}}(\text{H}_2\text{O}) / k_{\text{obs}}(\text{D}_2\text{O}) = 1.5 \pm 0.4$ . This value is in good agreement with previously reported KIE values for guanine oxidation in DNA.<sup>33,34,42</sup>

In an independent study, oxidation of the dsDNA 5'TAG-TTG-AGTATGTTGAGTTGAGTAGTGT 3' with its complement 5'ACACTACTCAACTACATACTCAACTA3' by  $\text{Ru}(\text{bpy})_3^{3+}$  was investigated by the stopped flow technique.<sup>42</sup> In this study the influence of  $[\text{HPO}_4^{2-}]$  and pH over the pH range 2.6-6.8 was also investigated with no significant rate enhancement as a function of buffer concentration consistent with C acting as a proton acceptor in dsDNA, Figure 11.

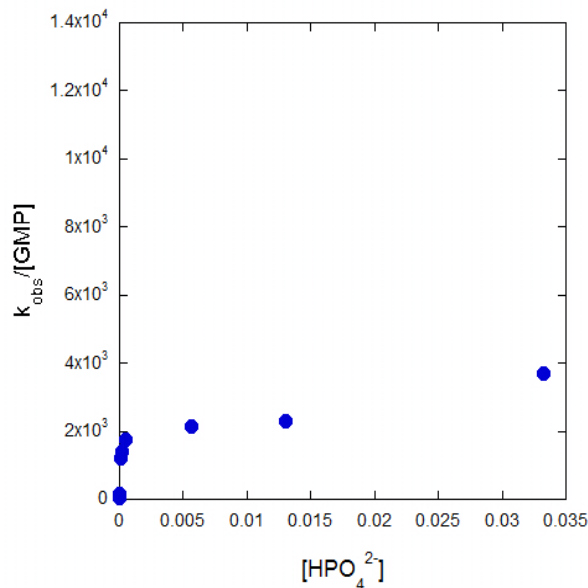


Figure 11: Plot of  $k_{\text{obs}}/[\text{GMP}]$  vs  $[\text{HPO}_4^{2-}]$  as measured by stopped flow in phosphate/citrate buffered solution at pH 2.2-6.8 a phosphate concentration of  $1.0 \times 10^{-4}$ -0.03M. The plot is consistent with dsDNA data obtained by electrochemical and spectrochemical techniques and a phosphate dependence is not observed.

We explored the H-bonding affinity between guanine and cytosine in solution is low; however, from comparison of voltometric experiments for annealed dsDNA compared to values obtained for guanine in ssDNA and mononucleotide environments, we obtained an association constant of  $K_A = 3.0 \pm 0.7 \text{ M}^{-1}$ , which is in good agreement with literature data obtained by NMR in DMF and DMSO at  $23 \pm 2^\circ\text{C}$ .<sup>46,47</sup>

## 5.5 Conclusions

### 5.5.1 Concerted Electron-Proton Transfer in Guanine Oxidation

The results on oxidation of dGMP by  $\text{Ru}(\text{bpy})_3^{3+}$  over extended pH and buffer base concentration ranges are consistent with Scheme 1. It explains the origin of rate enhancements with added buffer to initial formation of a H-bonded adduct between the

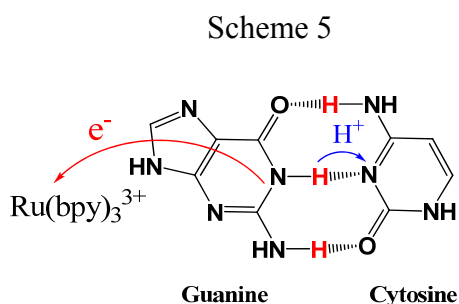
buffer base and dGMP which enables two pathways for oxidation; initial proton loss followed by rapid oxidation of dGMP(-H<sup>+</sup>) (PT-ET in Scheme 1) and concerted or coupled electron-proton transfer within an association complex with the oxidant (MS-EPT in Scheme1). The critical factor in both pathways is prior H-bonding and use of the buffer base as a proton acceptor. Comparison of kinetic parameters for oxidation of dGMP and tyrosine (TyrOH) in Table 1 suggests the generality of these coupled pathways and parallel mechanisms have been identified in the oxidation of cysteine and tryptophan.<sup>48</sup>

Results obtained here and for TyrOH oxidation reveal a complex mechanistic hierarchy in the oxidations of both amino acid and nucleobase. In aqueous solutions with added bases **four distinct mechanistic pathways have been identified**: 1) Outer-sphere oxidation of dGMP, eq 1(**ET**); 2) Proton loss followed outer-sphere oxidation of dGMP(-H<sup>+</sup>) (**PT-ET**); 3) Multiple Site-Electron Transfer (**MS-EPT**) with electron transfer to the oxidant and proton transfer to an acceptor base (MS-EPT); 4) MS-EPT but with **OH<sup>-</sup> as acceptor base**. As noted above, MS-EPT is more complex microscopically, given the demands arising from transfer of the proton<sup>13,40,41</sup> but has the advantage of avoiding the high energy intermediate dGMP<sup>+•</sup> with  $E^{\circ}(\text{dGMP}^{+/\bullet}) = 1.58 \text{ V vs NHE}$ .<sup>7</sup> The driving force for oxidation of the anion dGMP(-H<sup>+</sup>) by Ru(bpy)<sub>3</sub><sup>3+</sup> is favorable ( $\Delta G^{\circ} = -0.36 \text{ eV}$ ) and oxidation is rapid with  $k = 1.1 \pm 0.2 \times 10^7 \text{ M}^{-1} \text{ s}^{-1}$  in phosphate buffer at 23 ± 2 °C but, given pK<sub>a</sub>(dGMP) = 9.3, it is present in appreciable concentrations only at high pH. Oxidation of dGMP through variation of oxidant and base indicates that the reaction is insensitive to how driving force is varied as well as to the necessity to move the proton and electron simultaneously as found previously for tyrosine.<sup>38</sup> It also indicates the previously reported pH dependence in buffered solution is better attributed to the concentration and type of proton acceptor in solution.<sup>34</sup>

### 5.5.2 Cytosine as Electron-Proton Transfer Base in Guanine Oxidation

Given  $pK_a = 4.3$  for deoxycytidine and 3.9 for deoxyguanine radical cation,  $\text{guanine}^{\cdot+}$ , the driving force for proton transfer following oxidation,  $\text{guanine}^{\cdot+} + \text{cytosine} \rightarrow \text{guanine}^{\cdot}(-\text{H}^+) + \text{cytosine-H}^+$ , is small,  $\sim 0.02\text{eV}$ .<sup>17</sup> These are solution values and the driving force for proton transfer in dsDNA may be considerably different. However, as noted in the Introduction, there is transient IR evidence that oxidation of guanine in DNA is accompanied by proton transfer to cytosine.<sup>18</sup>

*There is clear evidence in our data for kinetic involvement of cytosine as an EPT acceptor base in guanine oxidation, in fact, as an exceptional base.* Even given comparable  $pK_a$ 's, and  $\Delta G^0$  values for EPT, cytosine has a  $\sim 10^3$  rate advantage over acetate as EPT acceptor base. In an earlier study it was shown that rate constants for EPT oxidation of tyrosine by a series of bases ranging from acetate to tris vary systematically with  $-\Delta G^0$ .<sup>38</sup> The same is true for  $\text{HPO}_4^{2-}$  as a competitive EPT acceptor base. Even in solutions with relatively high concentrations of  $\text{HPO}_4^{2-}$ , dCMP contributes to oxidation catalysis. MS-EPT with cytosine as acceptor base is illustrated in Scheme 5.



The origin of the kinetic enhancement is not in a highly favorable interaction in the guanine-cytosine association complex. From the spectrochemical study in 1:1 V:V MeCN- $\text{H}_2\text{O}$ ,  $K_A = 3.0 \pm 0.7$ .

The importance of cytosine as EPT acceptor base appears in the data for oxidation of guanine in dGMP, guanine in 1:1 V:V MeCN-H<sub>2</sub>O, the ssDNA, and in dsDNA. In oxidation of the ssDNA with its 7-mer partial complement HPO<sub>4</sub><sup>2-</sup> there is no evidence for HPO<sub>4</sub><sup>2-</sup> as a competitive EPT base. Similarly, in oxidation of the ssDNA with its full ssDNA complement there is no evidence for competition with cytosine in the double stranded helix by HPO<sub>4</sub><sup>2-</sup>.

Rate comparisons between pre-formed guanine-cytosine pairs in dsDNA and ssDNA with the 7-mer partial complement and the diffusional reactions are made in Table 2. A striking observation is that the EPT reactivity factor,  $K_A K_A' k_{red}$ , for Ru(bpy)<sub>3</sub><sup>3+</sup> oxidation of guanine with cytosine as the proton acceptor falls in a narrow range. This is true with guanine and cytosine as nucleosides or short oligonucleotides (Table 2).

<b>G-H-adduct</b>	<b><math>K_A K_A' k_{red}</math></b> <b>(<math>M^{-2}s^{-1}</math>)</b>
dGMP-OAc <sup>-a</sup>	$3.5 \pm 0.7 \times 10^3$
dGMP-HPO <sub>4</sub> <sup>2-b</sup>	$1.5 \pm 0.1 \times 10^6$
dGMP-dCMP <sup>c</sup>	$5.5 \pm 0.1 \times 10^6$
G-C <sup>a*</sup>	$7.5 \pm 0.9 \times 10^5$
ssDNA-HPO <sub>4</sub> <sup>2-c</sup>	$9.0 \pm 0.2 \times 10^5$
ssDNA-dCMP <sup>c</sup>	$1.6 \pm 0.5 \times 10^6$
ssDNA-7mer <sup>c</sup>	$K_A' k_{red} = 1.1 \pm 0.3 \times 10^6$
dsDNA <sup>c</sup>	$K_A' k_{red}$ $= 2.5 \pm 0.6 \times 10^6$

**Table 2.** Kinetic data for Ru(bpy)<sub>3</sub><sup>3+</sup> EPT oxidation of guanine, guanine monophosphate (dGMP), or guanine in single (ss-DNA)-or double-stranded DNA (dsDNA) with cytosine as acceptor base either as cytosine, cytosine monophosphate (dCMP), or in 7-mer or complete ssDNA complements. Values of  $K_A' k_{red}$ , Scheme 1, are cited in 0.05M phosphate at 23±2°C and were obtained by voltammetric or spectrophotometric methods, see text. Measurements are reported using spectrochemical (a) stopped flow (b) and electrochemical (c) techniques. \*A 1:1 v:v acetonitrile:water solution was used as a solvent in G-C studies.

Comparable reactivity toward EPT oxidation also exists between the diffusional reactions and ss and dsDNA complements with preformed guanine-cytosine adducts, Table 2. As noted above, from the results on Ru(bpy)<sub>3</sub><sup>3+</sup> oxidation of guanine with cytosine in 1:1 MeCN-H<sub>2</sub>O,  $K_A \sim 3$ . With  $K_A$  values of this magnitude, the quantities  $k_{red} K_A K_A'$  for the diffusional reactions and  $k_{red} K_A'$  for the DNA adducts  $K_A' k_{red}$  for EPT oxidation within the H-bonded hybrids are within a factor of ~8 throughout the entire series.

There is no evidence in these data for an appreciable role for  $\pi$ -stacking between adjacent nucleosides in ssDNA or dsDNA MS-EPT oxidation.

### **Electron-Proton Transfer Base in Guanine Oxidation and DNA Hole Transport**

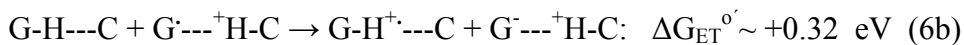
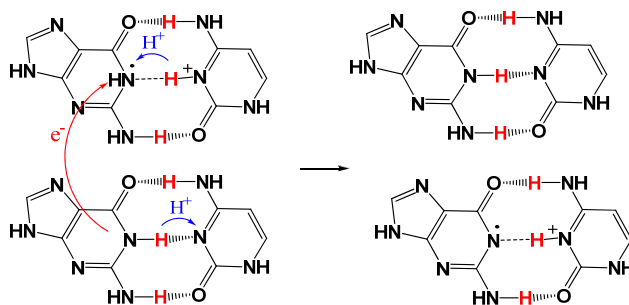
Our results reinforce the suggestion that PCET plays a role in guanine oxidation in DNA.<sup>6-8</sup> They point to an important kinetic role for coupled electron-proton transfer with transfer of the electron to an external oxidant and simultaneous proton transfer to cytosine, Scheme 3. MS-EPT provides a considerable rate advantage by avoiding guanine<sup>+</sup> as an intermediate. This is illustrated by comparing the rate constant for Ru(bpy)<sub>3</sub><sup>3+</sup> oxidation of the dGMP-HPO<sub>4</sub><sup>2-</sup> association complex by MS-EPT with  $k_{\text{red}}K_{\text{A}} = 3.3 \pm 0.4 \times 10^6 \text{ M}^{-1} \text{ s}^{-1}$  with  $k_{\text{ET}} = 3.6 \pm 0.5 \times 10^2 \text{ M}^{-1} \text{ s}^{-1}$  for outer sphere oxidation of dGMP to give dGMP<sup>+</sup>.

Loss of an electron from DNA generates a radical cation (“hole”) that migrates through the base stacks by electron transfer hopping. Hole transfer continues until the hole is trapped irreversibly, usually at a guanine or *Gn* sequence where a chemical reaction with H<sub>2</sub>O or O<sub>2</sub> occurs.<sup>28,49-55</sup> An important issue to consider is a possible role for EPT in these transfers.

Hole transport between adjacent guanine-cytosine (G-H---C) pairs by electron transfer and EPT are shown in Scheme 4 with the latter illustrated below. Site-to-site EPT “self-exchange” in eq 6a occurs with  $\Delta G_{\text{EPT}}^{\circ} = 0$ . It offers a pathway for long-distance hole (electron) transfer coupled with local proton transfer and no requirement for coupled long-range proton transfer.

Electron transfer without proton transfer, eq 6b, would give initially the high energy, guanine radical cation,  $G-H^{+\bullet}---C$ . Electron transfer occurs with  $\Delta G_{ET}^{o'} \sim +0.32$  eV followed by proton transfer with  $\Delta G^{o'} \sim -0.32$ .

Scheme 6



Even though EPT is favored energetically there is clear evidence that long-range hole transfer occurs by electron transfer. Results obtained by Giese and Wessely with abasic methylguanosine show that hole transport can continue by electron transfer even in the absence of its base complement.<sup>15,16</sup> Similarly, Ghosh and Schuster found that exchange of cytosine in DNA by 5-fluoro-2'-deoxycytidines, which is less basic than cytosine by  $\Delta pK_a = 1.7$ , did not inhibit hole transfer.<sup>20</sup> EPT may be favored energetically but is microscopically more complex. The two pathways are known to be competitive in the oxidation of tyrosine, for example.<sup>32,38</sup>

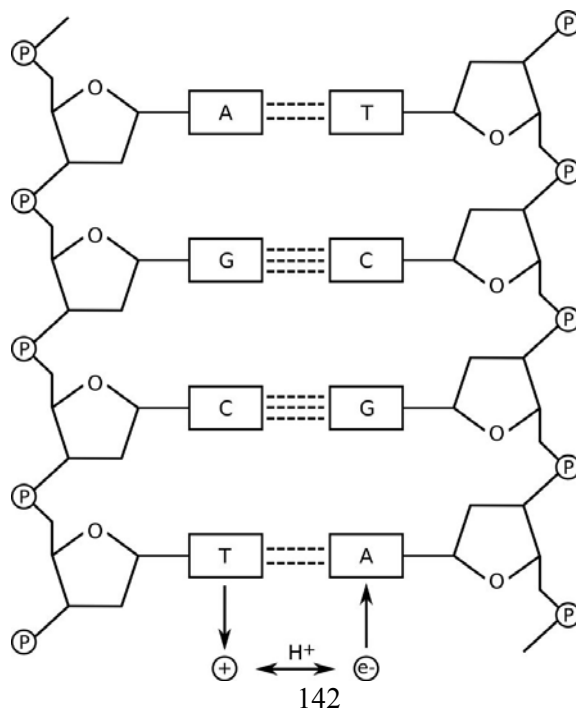
These observations point to another pathway for hole transfer, one that avoids the energetically unfavorable oxidation of G-H by  $G^{\bullet}$  exploiting the small driving force for

proton transfer from  $G-H^+$  to C. As shown in eq 7, it involves initial internal proton transfer and electron transfer “self exchange” between nucleobases on neighboring stacks.



Our results provide insight into a possible role for proton transfer and coupled electron-proton transfer in initial oxidation of DNA. In dsDNA the existence of complementary base cytosine enhances oxidative reactivity. Once oxidation has occurred, the close match in  $pK_a$  values between guanine radical cation ( $G-H^+$ ) and protonated cytosine ( $^+\text{H-C}$ ) provides a pathway for long range electron transfer without complications from coupled proton transfer (Scheme 7).

Scheme 7



## 5.6 References

- 1) Ceccatelli, S.; Tamm, C.; Zhang, Q.; Chen, M. **Mechanisms and modulation of neural cell damage induced by oxidative stress.** *Physiol and Behav.* **2007**, *92*, 87-92.
- 2) Baraj, G. **Free Radicals and Aging** *Trends, Neurosci.* **2004**, *27*, 595-600.
- 3) Chan, P. H. **Reactive Oxygen Radicals in Signaling and Damage in the Ischemic Brain.** *J. Cereb. Blood Flow Metals.* **2001**, *21*, 2-14.
- 4) Fancchinetti, F.; Dawson, V. L.; Dawson, T. M. **Free Radicals as mediators of neuronal injury.** *Cell, Mol. Neurobiol.* **1998**, *18*, 667-682.
- 5) Mattson, M. P.; Pederson, W. A.; Duan, W.; Culmsee, C.; Camanola, S. **Cellular and molecular mechanisms underlying perturbed energy metabolism and neuronal degeneration in Alzheimer's and Parkinson's diseases.** *Ann. NY Acad. Sci.* **1999**, *893*, 154-175.
- 6) Steenken, S.; Javanovic, S. V. **How Easily Oxidizable Is DNA? One-Electron Reduction Potentials of Adenosine and Guanosine Radicals in Aqueous Solution.** *J. Am. Chem. Soc.* **1997**, *119*, 617-618.
- 7) Steenken, S.; Jovanovic, S. V.; Candeias, L. P.; Reynisson, J. **DNA-Strand Breakage via the Guanine Radical Thermodynamically and Sterically Possible?** *Chem. Eur. J.* **2001**, *7*, 2829-2833.
- 8) a) Steenken, S. **Oxidative Damage to DNA: Formation Measurement and Biological Significance.** *Chem. Rev.* **1989**, *89*, 503-520. b) Steenken, S. **Electron Transfer in DNA? Competition by UltraFast Proton Transfer?** *Biol. Chem.* **1997**, *378*, 1293-1297.
- 9) Pratviel, G.; Meunier, B. **DNA Oxidation by Copper and Manganese Complexes.** *Chem. Eur. J.* **2006**, *12*, 6018-6030.
- 10) Sistare, M. F.; Codden, S. J.; Heimlich, G.; Thorp, H. H. **Effects of Base Stacking on Guanine Electron Transfer: Rate Constants for G and GG Sequences of Oligonucleotides from Catalytic Electrochemistry** *J. Am. Chem. Soc.* **2000**, *122*, 4742-4749.
- 11) Duarte, V.; Muller, J. G.; Burrows, C. J. **In Vitro DNA Synthesis Opposite Oxazolone and Repair of this DNA Damage using Modified Oligonucleotides** *Nucleic Acids Res.* **1999**, *27*, 496-502.
- 12) Burrows, C. J.; Muller, J. G. **Oxidative Nucleobase Modifications Leading to Strand Scission** *Chem. Rev.* **1998**, *98*, 1109-1152.
- 13) Gasper, S. M.; Schuster, G. B. **Intramolecular Photoinduced Electron Transfer to Anthraquinone Linked to Duplex DNA : The Effects of Gaps and Traps on Long Range Radical Cation Migration.** *J. Am. Chem. Soc.* **1997**, *119*, 12762-12771.

- 14) Shafirovich, V.; Dourandin, A.; Gaecintov, N. E. **Proton Coupled Electron Transfer Reactions at a Distance in DNA Duplex: Kinetic Deuterium Isotope Effects.** *J. Phys. Chem. B* **2001**, *105*, 8431-8435.
- 15) Giese, B.; Wessely, S. **The Significance of Proton Migration during Hole Hopping through DNA.** *Chem. Commun.* **2001**, 2108–2109.
- 16) Giese, B. and Wessely, S. *Angew. Chem., Int. Ed.*, 2000, **39**, 3490.
- 17) Abo-Riziq, A.; Grace, L.; Nir, E.; Kabelac, M.; Hobza, P.; deVries, M.S. **Vibrational spectroscopy of the G...C base pair: experiment, harmonic and anharmonic calculations, and the nature of the anharmonic couplings.** *Proc. Natl. Acad. Sci. U.S.A.* **2005**, *102*, 20-23.
- 18) Elias, B. Creely, C. Doorley, G. W. Feeney, M. Moucheron, W. Kirsch-DeMesmaeker, A. Dyer, J.; Grills, D. G.; George, M. W.; Matousek, P.; Parker, A. W.; Towrie, T.; Kelly J. M. **Photooxidation of Guanine by a Ruthenium Dipyridophenazine Complex Intercalated in a Double Stranded Polynucleotide Monitored Directly by Picosecond Visible and Infrared Transient Absorption Spectroscopy.** *Chem. Eur. J.* **2008**, *14*, 369 – 375
- 19) Sun, L.; Bu, Y. **Marked Variations of Dissociation Energy and H-Bond Character of the Guanine-Cytosine Base Pair Induced by One-Electron Oxidation and Li<sup>+</sup> Cation Coupling** *J. Phys. Chem. B* **2005**, *109*, 593-600.
- 20) Ghosh, A. K.; Schuster, G. B. **Role of the guanine N1 imino proton in the migration and reaction of radical cations in DNA oligomers.** *J. Am. Chem. Soc.* **2006**, *128*, 4172-4173.
- 21) Huynh, M-V. H.; Meyer, T. J. **Proton Coupled Electron Transfer.** *Chem. Rev.* **2007**, *107*, 5004-64.
- 22) Hammes-Schiffer, S.; Soudackov, A. V. **Proton-Coupled Electron Transfer in Solution, Proteins, and Electrochemistry.** *J. Phys. Chem. B.* **2008** *112*,14108-14123
- 23) Mayer, J. M. **Proton Coupled Electron Transfer: A Reaction Chemist's Point of View.** *Annu. Rev. Phys. Chem.*, **2004**, *55*, 363-90.
- 24) a) Chang, C. J.; Chang, M.; Cauer, N. H.; Nocera, D. G. *Biochim, Biophys. Acta, Bioenergetics*, **2004**, *1655*, 13-28 b) Meyer, T. J.; Huynh, M-V. H.; Thorp, H. H. **The Possible Role of Proton Coupled Electron Transfer (PCET) in Water Oxidation by Photosystem II** *Angew. Chem. Int. Ed.* **2007**, *46*, 5284-5304.
- 24) Kasai, H.; Yamaizumi, Z.; Berger, M.; Cadet, J. **Photosensitized Formation of 7,8-dihydro-8-oxo-2'-deoxyguanosine in DNA by Riboflavin: A Nonsinglet Oxygen Mediated Reaction.** *J. Am. Chem. Soc.* **1992**, *114*, 9692-9694.
- 25) Burrows, C. J.; Muller, J. G. **Oxidative Nucleobase Modifications Leading to Strand Scission** *Chem. Rev.* **1998**, *98*, 1109-1154.

- 26) Cadet, J.; Douki, T.; Gasparutto, D.; Ravanat, J.-L. **Oxidative Damage To DNA: Formation, Measurement, and Biochemical Features** *Mutat. Res.* **2003**, *531*, 5-23.
- 27) Misiaszek, M.; Crean, C.; Joffe, A.; Geacintov, N. E.; Shafirovich, V. **Oxidative DNA Damage Associated with Combination of Guanine and Superoxide Radicals and Repair Mechanisms via Radical Trapping** *J. Biol. Chem.* **2004**, *279*, 32106-32115.
- 28) Ly, D.; Kan, Y.; Armitage, B.; Schuster, G. B. *J. Am. Chem. Soc.* **1996**, *118*, 8747-8748.
- 29) Breslin, D. T.; Schuster, G. B. **Anthraquinone Photonucleases: Mechanism of GG-Selective and Nonselective Cleavage of Double Stranded DNA** *J. Am. Chem. Soc.* **1996**, *118*, 2311-2319.
- 30) Ndlebe, T.; Schuster, G. B. **One Electron Oxidation of DNA Oligomers that lack Guanine: Reaction and Strand Cleavage at Remote Thymines by Long Distance Radical Cation Hopping.** *Org. Biomol. Chem.* **2006**, *4*, 4015-4021.
- 31) Holmberg, R. C.; Thorp, H. H. **Electrochemical Determination of Triple Helices- Electrochemical Oxidation of Guanine in an Intramolecular Triplex** *Inorg. Chem.* **2004**, *43*, 5080-5085.
- 32) Fecenko, C. J.; Meyer, T. J.; Thorp, H. H. **The Oxidation of Tyrosine through Parallel Rate-Limiting Proton Transfer and MS-EPT** *J. Am. Chem. Soc.* **2006**, *128*, 11020-11021
- 33) Weatherly, S. C.; Yang, I. V.; Thorp, H. H. **Proton Coupled Electron Transfer in duplex DNA: Driving Force Dependence and Isotope Effects on the Electrochemical Oxidation of Guanine.** *J. Am. Chem. Soc.* **2001**, *123*, 1236-1237.
- 34) Weatherly, S. C.; Yang, I. V.; Armistead, P. A.; Thorp, H. H. **Proton Coupled Electron Transfer in Guanine Oxidation: The Effects of Isotope, Solvent, and Chemical Modification.** *J. Phys. Chem. B* **2003**, *107*, 372-378.
- 35) Willit, J. L.; Bowden, E. F. **Adsorption and Redox Thermodynamics of Strongly Adsorbed Cytochrome C on Indium Tin Oxide Electrodes** *J. Phys. Chem.* **1990**, *94*, 8241-8246.
- 36) Johnston, D. H.; Glasgow, K. C.; Thorp, H. H. **Electrochemical Measurement of the Solvent Accessibility of the Nucleobases using Electron Transfer between DNA and the Metal Complex.** *J. Am. Chem. Soc.* **1995**, *117*, 8933-8938.
- 37) Sistare, M. F.; Holmberg, R. C.; Thorp, H. H. **Electrochemical Studies of Polynucleotide Binding and Oxidation by Metal Complexes: Effects of Scan Rate, Concentration, and Sequence.** *J. Phys. Chem. B* **1999**, *103*, 10718-10728.
- 38) Fecenko, C. J.; Thorp, H. H.; Meyer, T. J. **The Role of Free Energy Change in Coupled Electron Proton Transfer Reactions.** *J. Am. Chem. Soc.* **2007**, *129*, 15098-15099
- 41) Schowen, K. B.; Limbach, H. H.; Denisov, G. S.; Schowen, R. L. **Hydrogen Bonds and Proton Transfer in General Catalytic Transition State Stabilization in Enzyme**

- Catalysis** *Biochim. Biophys. Acta* 2000, 1458, 43. Gold, V. *Adv. Phys. Org. Chem.* **1969**, 7, 259
- 40) Hammes-Schiffer, S; Iordanova, N. **Theoretical Studies on Proton Coupled Electron Transfer Reactions** *Biochim Biophys Acta*, **2004**, 1655, 29-36
- 41) Hammes-Schiffer, S. **Theoretical Perspectives on Proton Coupled Electron Transfer Reactions.** *Acc. Chem. Res.* **2001**, 34, 273-281.
- 42) Weatherly, S. C. **The Mechanisms of Metal-Mediated Guanine Oxidation in Native and Non-Native DNA Environments.** University of North Carolina, Chapel Hill, 2001
- 43) Murphy, C. F.; Brennaman, M. K.; Thorp, H. H.; Meyer, T. J. **Tyrosine Oxidation pH Dependence or Base-Assisted Oxidation** *J. Am. Chem. Soc.* **2008** *Manuscript in prep.*
- 44) Marcus, R. A. **Chemical and Electrochemical Electron Transfer** *Theory Annu. Rev. Phys. Chem.* **1964**, 15, 155-196.
- 45) Ram, M. S.; Hupp, J. T. **Linear free energy relations for multielectron transfer kinetics: a brief look at the Broensted/Tafel analogy** *J. Phys. Chem.* **1990** 94 2378-80
- 46) Metzger, S.; Lippert, B. **A Methylated Guanine, Cytosine Base Quartet with a Novel GC Pairing Pattern involving H(5) of C.** *J. Am. Chem. Soc.* **1996**, 118, 12467-68
- 47) Newmark, R.A.; Cantor, C.R. **Nuclear Magnetic Resonance Studies Study of the Interactions of Guanosine and Cytidine in Diethylsulfoxide** *J. Am. Chem. Soc.* **1968**, 90, 5010
- 48) Murphy, C. F.; Gagliardi, C. J.; Thorp, H. H.; Meyer, T. J. **Coupled Electron Proton Transfer in Amino Acid Oxidation.** *J. Am. Chem. Soc.* **2009**, *manuscript in prep.*
- 49) Schuster, G. B. **Long Range Charge Transport in DNA: Transient Structural Distortions Control Distance Dependence.** *Acc. Chem. Res.* **2000**, 33, 253–260.
- 50) Giese, B.; Spichty, M.; Wessely, S. *Pure Appl. Chem.* **2001**, 73, 449–453
- 51) O'Neill, M. A.; Barton, J. K. **DNA Charge Transport: Conformationally Gated Hopping through Stacked Domains** *J. Am. Chem. Soc.* **2004**, 126, 11471–11483
- 52) Lewis, F. D. **DNA Electron Transfer Mechanisms** *Photochem. Photobiol.* **2005**, 81, 65–72.
- 53) Kawai, K.; Majima, T. *Pure Appl. Chem.* **2005**, 77, 963–975.
- 55) Schuster, G. B. **Long-Range Charge Transfer in DNA I, II**; Springer-Verlag: Heidelberg, 2004; Vol. 236, p 237.

## Bibliography

- Abo-Riziq, A.; Grace, L.; Nir, E.; Kabelac, M.; Hobza, P.; deVries, M.S. **Vibrational spectroscopy of the G...C base pair: experiment, harmonic and anharmonic calculations, and the nature of the anharmonic couplings.** *Proc. Natl. Acad. Sci. U.S.A.* **2005**, *102*, 20-23
- Albery, W. J.; Davies, M. H. **Mechanistic Conclusions from the Curvature of solvent Isotope Effects.** *J. Chem. Soc., Faraday Trans. 1* **1972**, *68*, 167.
- Alstrum-Acevedo, J. H.; Brennaman, M. K.; Meyer, T. J. **Chemical Approaches to Artificial Photosynthesis 2.** *Inorg. Chem.* **2005**, *344* 6802-27.
- Ando, K.; Hynes, J. T. **Acid Ionization of HF in Water: An Electronic Structure and Monte Carlo Study** *J. Phys. Chem. A*, **1999**, *103*, 10398.
- Ando, K.; Hynes, J. T. **Acid Base Proton Transfer and Ion Pair Formation in Solution** *Adv. Chem. Phys.* **1999**, *119*, 381-430
- Andreiux, C. P.; Gamby, J.; Hapiot, P.; Saveant, J.-M. **Evidence for Inverted Region Behavior in Proton Transfer to Carbanions** *J. Am. Chem. Soc.* **2003**, *125*, 101119-101124
- Armistead, P. M.; Thorp, H. H. Oxidation Kinetics of Guanine in DNA Molecules Adsorbed onto Indium Tin Oxide Electrodes *Anal. Chem.* **2000**, *72*, 3764-3770.
- Babcock, G.T.; Rodriguez, I. D.; Hoganson, C.; Sandusky, P.O.; El-Deeb, M. **Redox Active Amino Acids in Photosystem II and in Other Enzyme Systems.** *Royal Society of chemistry*, **1991**, *94*, 55-58
- Baraj, G. **Free Radicals and Aging** *J. Neurosci.* **2004**, *27*, 595-600
- Bard, A. J.; Faulkner, L. R. **Electrochemical Methods: Fundamentals and Applications**; John Wiley and Sons, Inc., Hoboken, NJ **2004**
- Beisiadka, J.; Loll, B.; Kern, J.; Irrang, K.-D.; Zouni, A. **Toward Complete Crystal Structure of Cyanobacterial Photosystem II at 3.2Å Resolution: A Closer Look at the Mn cluster.** *Phys. Chem. Chem. Phys.* **2004**, *6*, 4733
- Breslin, D. T.; Schuster, G. B. **Anthraquinone Photonucleases: Mechanism of GG-Selective and Nonselective Cleavage of Double Stranded DNA.** *J. Am. Chem. Soc.* **1996**, *118*, 2311-2319.
- L. Biczok, L; Gupta, N; Linschitz, H. **Coupled Electron-Proton Transfer in Interactions of Triplet C<sub>60</sub> with Hydrogen-Bonded Phenols: Effects of Solvation, Deuteration, and Redox Potentials.** *J. Am. Chem. Soc.* **1997**, *119*, 12601-12609

Bock, C. R.; Connor, J. A.; Gutierrez, A. R.; Meyer, T. J.; Whitten, D. G.; Sullivan, B. P.; Nagle, J. K. **Estimation of excited-state redox potentials by electron-transfer quenching. Application of electron-transfer theory to excited-state redox processes.** *J. Am. Chem. Soc.* **1979**, *101*, 4815-4824.

Borgis, D.; Hynes, J. T. **A Curve Crossing Approach to Chemical Reactions in Solution.** *J. Phys. Chem.* **1996**, *100*, 1118.

Brudvig, G. W.; Thorp, H. H.; Crabtree, R. H. **Probing the Mechanism of Water Oxidation.** *Acc. Chem. Res.* **1991** *24*, 311-316

Burrows, C. J.; Muller, J. G. **Oxidative Nucleobase Modifications Leading to Strand Scission** *Chem. Rev.* **1998**, *98*, 1109-1154.

Cadet, J.; Douki, T.; Gasparutto, D.; Ravanat, J.-L. **Oxidative Damage To DNA: Formation, Measurement, and Biochemical Features** *Mutat. Res.* **2003**, *17 531*, 5-23.

Carra, C.; Iordanova, N.; Hammes-Schiffer, S. **Proton Coupled Electron Transfer in a Model of Tyrosine in Photosystem II.** *J. Am. Chem. Soc.* **2003**, *125*, 10429-10436  
Chan, P. H. **Reactive Oxygen Radicals in Signaling and Damage in the Ischemic Brain.** *J. Cereb. Blood Flow Metals.* **2001**, *21*, 2-14

Ceccatelli, S.; Tamm, C.; Zhang, Q.; Chen, M. **Mechanisms and modulation of neural cell damage induced by oxidative stress.** *Physiol and Behav.* **2007**, *92*, 87-92

Chen, P. Y.; Meyer, T. J. *Chem. Rev.* 1998, *98*, 1439. Bixon, M.; Jortner, J. **In Electron Transfer-From Isolated Molecules to Biomolecules**; Jortner, J., Bixon, M., Eds.; Wiley-Interscience: New York, 1999.

Costentin, C.; Robert, M.; Saveant, J. **Electrochemical and Homogeneous Proton-Coupled Electron Transfers: Concerted Pathways in the One-Electron Oxidation of a Phenol Coupled with an Intramolecular Amine-Driven Proton Transfer.** *J. Am. Chem. Soc.* **2006**, *128*, 4552-53.

Costentin, C.; Louault, C.; Robert, M.; Saveant, J.-M. **Evidence of Concerted Proton Electron Transfer in the Electrochemical Oxidation of Phenols with Water as a Proton Acceptor.** *J. Am. Chem. Soc.* **2008**, *130*, 15817-15819.

Costentin, C.; Robert, M.; Saveant, J. M. **Concerted Proton-Electron Transfer Reactions in Acts as Proton Donor or Acceptor?** *J. Am. Chem. Soc.* **2007**, *129*, 5870-5879.

Costentin, C.; Robert, M.; Saveant, J. M. **Concerted Proton Coupled Electron Transfer Reactions in Water. Are the Driving Force and the Rate Constant**

**Depending on pH when Water Acts as a Proton Donor or Acceptor.** *J. Am. Chem. Soc.* **2007**, *129*, 5870-5879.

Cukier, R. I.; Nocera, D. G. **Proton Coupled Electron Transfer**, *Annu. Rev. Phys. Chem.* **1998** *49* 337-69

Cukier, R. I.; Zhu, J. **Simulation of Proton Transfer Reaction Rates: The Role of Solvent Polarization.** *J. Phys. Chem. B* **1997**, *101*, 7180.

Das, T. N.; Huie, R. E.; Neta, P. Reduction Potentials of  $\text{SO}_3^{\cdot-}$ ,  $\text{SO}_5^{\cdot-}$ , and  $\text{S}_4\text{O}_6^{3\cdot-}$  Radicals in Aqueous Solution *J. Phys. Chem. A.* **1999** *103* 3581-88

Decornez, H.; Hammes-Schiffer, S. **Model proton-coupled electron transfer reactions in solution: Predictions of rates, mechanisms, and kinetic isotope effects** *J. Phys. Chem. A.* **2000**, *104*, 9370-9384

Demadis, D. D.; Dattelbaum; Kober, E. M.; Concepcion, J. J.; Paul, J. J.; Meyer, T. J.; White, P. S. **Vibrational and Structural Mapping of  $\text{Os}(\text{bpy})_3^{3+/2+}$  and  $\text{Os}(\text{phen})_3^{3+/2+}$** , *Inorg. Chim. Acta.* **2007**, *360*, 1143-1153.

Di Bilio, A. J.; Crane, B. R.; Wehbi, W. A.; Kiser, C. N.; Abu-Omar, M. M.; Carlos, R. M.; Richards, J. H.; Winkler, J. R.; Gray, H. B. **Properties of Photogenerated Tryptophan and Tyrosyl Radicals in Structurally Characterized Proteins Containing Rhenium(I) Tricarbonyl Diimines.** *J. Am. Chem. Soc.* **2001**, *123*, 3181-3182.

Dixon, W. T.; Murphy, D. **Determination of Acidity Constants of Some Phenol Radical Cations by Means of Electron Spin Resonance.** *J. Chem. Soc. Faraday Trans. 2.* **1976**. *72*, 1221-1230

Duarte, V.; Muller, J. G.; Burrows, C. J. **In Vitro DNA Synthesis Opposite Oxazolone and Repair of this DNA Damage using Modified Oligonucleotides** *Nucleic Acids Res.* **1999**, *27*, 496-502.

Elias, B. Creely, C. Doorley, G. W. Feeney, M. Moucheron, W. Kirsch-DeMesmaeker, A. Dyer, J.; Grills, D. G.; George, M. W.; Matousek, P.; Parker, A. W.; Towrie, T.; Kelly J. M. **Photooxidation of Guanine by a Ruthenium Dipyridophenazine Complex Intercalated in a Double Stranded Polynucleotide Monitored Directly by Picosecond Visible and Infrared Transient Absorption Spectroscopy.** *Chem. Eur. J.* **2008**, *14*, 369 – 375

Fancchinetti, F.; Dawson, V. L.; Dawson, T. M. **Free Radicals as mediators of neuronal injury.** *Cell, Mol. Neurobiol.* **1998**, *18*, 667-82

- Fecencko, C. F.; Meyer, T. J.; Thorp, H. H. **Electrocatalytic Oxidation of Tyrosine through Rate-Limiting Proton Transfer and MS-EPT** *J. Am. Chem. Soc.* **2006**, *128*, 11020-11021
- Fecencko, C. J.; Thorp, H. H.; Meyer, T. J. **The Role of Free Energy Change in Coupled Electron Proton Transfer** *J. Am. Chem. Soc.* **2007**, *129*, 15098-15099
- Fuöss, R. M. **Ionic Association. III. The Equilibrium between Ion Pairs and Free Ions** *J. Am. Chem. Soc.* **1958**, *80*, 5059-5061.
- Gagliardi, C. J.; Thorp, H. H.; Meyer, T. J. **Tryptophan Oxidation, 2008 unpublished results**
- Gaspar, S. M.; Schuster, G. B. **Intramolecular Photoinduced Electron Transfer to Anthraquinone Linked to Duplex DNA : The Effects of Gaps and Traps on Long Range Radical Cation Migration.** *J. Am. Chem. Soc.* **1997**, *119*, 12762-12771.
- Giese, B.; Wessely, S. **The Significance of Proton Migration during Hole Hopping through DNA.** *Chem. Commun.*, **2001**, 2108–2109
- Giese, B.; Spichty, M.; Wessely, S. *Pure Appl. Chem.* **2001**, *73*, 449–453
- Geissler, P. L. P. L.; Dellago, C.; Chandler, D.; Hutter, J.; Parrinello, M. **Autoionization in Liquid Water.** *Science* **2001**, *291*, 2121.
- Ghosh, A. K.; Schuster, G. B. **Role of the guanine N1 imino proton in the migration and reaction of radical cations in DNA oligomers.** *J. Am. Chem. Soc.* **2006**, *128*, 4172-73
- Grabowski, S. J. **Hydrogen Bond Strength-Measures based on Geometric and Topological Parameters.** *J. Phys. Org. Chem.* **2004**, *17*, 18-31
- Guilini, C.; Traaseth, N. J.; Davies, K. J. **Tyrosine oxidation products: analysis and biological relevance** *A. Amino Acids*, 2003 227-23
- Hall, D. L.; Holmlin, R. E.; Barton, J. K **Oxidative DNA damage through long-range electron transfer.***Nature*, **1996**, *382*, 731-35
- Hammes-Schiffer, S. **Theoretical Perspectives on Proton Coupled Electron Transfer Reactions** *Acc. Chem. Res.* **2001** *34* 273-81
- Hammes-Schiffer, S.; Iordanova, N. **Theoretical Studies of Proton Coupled Electron Transfer Reactions.** *Biochim. Biophys. Acta, Bioenergetics*, **2004**, *1655*, 29-336
- Hammes-Schiffer, S.; Soudackov, A. V. **Proton-Coupled Electron Transfer in Solution, Proteins, and Electrochemistry.** *J. Phys. Chem. B.* **2008** *112*, 14108-14123

Heeb, L.; Peters, K. S. **Further Evidence of an Inverted Region Proton Transfer within the Benzophenone/Substituted Aniline Contact Radical Ion Pairs; Importance of Vibrational Reorganizational Energy.** *J. Phys. Chem. A.* **2006**, *110*, 6408-6414

Holmberg, R. C.; Thorp, H. H. **Electrochemical Determination of Triple Helicies: Electrocatalytic Oxidation of Guanine in an Intramolecular Triplex** *Inorg. Chem.* **2004**, *43*, 5080-5085.

Huynh, M.-V. H.; Meyer, T. J. **Proton Coupled Electron Transfer.** *Chem. Rev.* **2007** *107* 5004-5064

Hynes, J. T. **The Protean Proton in Water** *Nature* **1999**, *397*, 565.

Ionescu, A.; Grand, D.; Sicard-Roselli, C.; Houee-Levin, C. **Micellular Effect on Tyrosine: One Electron by Azide Radicals.** *Radiation Physics and Chemistry* **2005**, *72*, 497-506

Irebo, T.; Reece, S. Y.; Sjödin, M.; Nocera, D. G.; Hammarström, L. Proton-Coupled Electron Transfer of Tyrosine Oxidation: Buffer Dependence and Parallel Mechanisms *J. Am. Chem. Soc.* **2007**, *129*, 15462-15464.

Ishikita, H.; Soudackov, A. V.; Hammes-Schiffer, S. Buffer-Assisted Proton-Coupled Electron Transfer in a Model Rhenium-Tyrosine Complex. *J. Am. Chem. Soc.* **2007**, *129*, 11146-11152.

Johnston, D. H.; Glasgow, K. C.; Thorp, H. H. **Electrochemical Measurement of the Solvent Accessibility of the Nucleobases Using Electron Transfer between DNA and Metal Complexes** *J. Am. Chem. Soc.* **1995**, *117*, 8933-38

Kasai, H.; Yamaizumi, Z.; Berger, M.; Cadet, J. **Photosensitized Formation of 7,8-dihydro-8-oxo-2'-deoxyguanosine in DNA by Riboflavin: A Nonsinglet Oxygen Mediated Reaction.** *J. Am. Chem. Soc.* **1992**, *114*, 9692-9694.

Kawai, K.; Majima, T. *Pure Appl. Chem.* **2005**, *77*, 963-975.

Krishtalik, L. I. **The Mechanism of Proton Transfer, An Outline** *Biochim. Biophys. Acta* **2000**, *1458*, 6.

Krishtalik, L. I. **Activation Energy of photosynthetic oxygen evolution: An Attempt at Theoretical Analysis.** *Bioelectrochem. Bioenerg.* **1990**, *23*, 249.

Land, E. J.; Porter, G.; Fang, J. Y.; Strachan, E. **Primary Photochemical Processes in Aromatic Molecules. Part 6.-The Absorption Spectra and Acidity Constants of Phenoxy Radicals** *Trans. Faraday Soc.* **1961** *57*, 1885

- Lewis, F. D. **DNA Electron Transfer Mechanisms** *Photochem. Photobiol.* **2005**, *81*, 65–72.
- Lind, J.; Shen, X.; Eriksen, T. E.; Merenyi, G. **The one-electron reduction potential of 4-substituted phenoxyl radicals in water** *J. Am. Chem. Soc.* **1990**, *112*, 479-482
- Lund, H.; Hammerich, O.; *Organic Electrochemistry* **2001** New York: Marcel Dekker
- Luz, Z.; Meiboom, S. **Rate and Mechanism of Proton Exchange in Phosphate Buffer** *J. Am. Chem. Soc.* **1964** *86*, 4766-4768.
- Ly, D.; Kan, Y.; Armitage, B.; Schuster, G. B. *J. Am. Chem. Soc.* **1996**, *118*, 8747-8748.
- Marcus, R. A. **Chemical and Electrochemical Electron Transfer Theory** *Annu. Rev. Phys. Chem.* **1964**, *15*, 155-196.
- Mattson, M. P.; Pederson, W. A.; Duan, W.; Culmsee, C.; Camanola, S. **Cellular and molecular mechanisms underlying perturbed energy metabolism and neuronal degeneration in Alzheimer's and Parkinson's diseases.** *Ann. NY Acad. Sci.* **1999**, *893*, 154-75
- Markle, T. F.; Rhile, I. J.; DiPasquale, A. G.; Mayer, J. M. **Probing Concerted Proton Coupled Electron Transfer in Phenol-imidazoles.** *Proc. Natl. Acad. Sci. U. S. A.* **2008**, *105*, 8185-8190
- Markle, T. F.; Mayer, J. M. **Concerted Proton-Electron Transfer in Pyridyl Phenols: The Importance of the Hydrogen Bond.** *Angew. Chem. Int. Ed.* **2008**, *47*, 738-740
- Mayer, J. M.; Rhile, I. J.; Larsen, F. B.; Mader, E. A.; Markle, T. F.; DiPasquale, A. G. **Models for Proton Coupled Electron Transfer in PSII.** *Photosynth. Res.* **2006**, *87*, 21-24
- Mayer, J. M. **Proton Coupled Electron Transfer: A Reaction Chemist's Point of View.** *Annu. Rev. Phys. Chem.* **2004** *55* 363-90
- Metzger, S.; Lippert, B. **A Metalated Guanine, Cytosine Base Quartet with a Novel GC Pairing Pattern Involving H(5) of C.** *J. Am. Chem. Soc.* **1996**, *118*, 12467-123468
- Meyer, T. J.; Huynh, M-H. V.; Thorp, H. H. **The Possible Role of Proton Coupled Electron Transfer (PCET) in Water Oxidation by Photosystem II** *Angew. Chem., Int. Ed.* **2007**, *46*, 5284-5304
- Misiaszek, M.; Crean, C.; Joffe, A.; Geacintov, N. E.; Shafirovich, V. **Oxidative DNA Damage Associated with Combination of Guanine and Superoxide Radicals and Repair Mechanisms via Radical Trapping** *J. Biol. Chem.* **2004**, *279*, 32106-32115.

Murphy, C. F.; Brenneman, M. K.; Thorp, H. H.; Meyer, T. J. **Tyrosine Oxidation Base-Assisted or pH Dependent?**, *J. Am. Chem. Soc.* **2009** manuscript in prep

Murphy, C. F.; Gagliardi, C. J.; Thorp, H. H.; Meyer, T. J. **Buffer-Assisted Amino Acid Oxidation at a Carbon Electrode** *J. Am. Chem. Soc.* **2009**, manuscript in prep.  
Nakano, M.; Nakano, N. I.; Higuchi, T. *J. Phys. Chem.* **1967** 71 3954-59

Napier, M. E.; Hull, D. O.; Thorp, H. H. Electrocatalytic Oxidation of DNA-Wrapped Carbon Nanotubes. *J. Am. Chem. Soc.* **2005**, 127, 11952-11953.

Ndlebe, T.; Schuster, G. B. **One Electron Oxidation of DNA Oligomers that Lack Guanine: Reaction and Strand Cleavage at Remote Thymines by Long Distance Radical Cation Hopping** *Org. Biomol. Chem.* **2006**, 4, 4015-4021.

Newmark, R.A.; Cantor, C.R. **Nuclear Magnetic Resonance Study of the Interactions of Guanosine and Cytodine in Dimethylsulfoxide.** *J. Am. Chem. Soc.* **1968**, 90, 5010

O'Kelley, S; Barton, J. K. **Electron transfer between bases in double helical DNA.** *Science*, **1999**, 15, 375-81

O'Neill, M. A.; Barton, J. K. **DNA Charge Transport: Conformationally Gated Hopping Through Stacked Domains** *J. Am. Chem. Soc.* **2004**, 126, 11471-11483

Peters, K. S. **A Theory-Experiment Conundrum for Proton Transfer** *Acc. Chem. Res.* **2008**

Pratviel, G; Meunier, B. **DNA Oxidation by Copper and Manganese Complexes.** *Chem. Eur. J.* **2006**, 12, 6018-30

Rhile, I. J.; Mayer, J. M. **One-Electron Oxidation of a Hydrogen-Bonded Phenol Occurs by Concerted Proton-Coupled Electron Transfer** *J. Am. Chem. Soc.* **2004**, 126, 12718-12719.

Rudolph, M., Reddy, D. P., Feldberg, S. W. **A Simulator for Cyclic Voltammetric Response** *Anal. Chem.* **1994** 66, 589A-600A

Schowen, K. B.; Limbach, H. H.; Denisov, G. S.; Schowen, R. L. **Hydrogen Bonds and Proton Transfer in General Catalytic Transition State Stabilization in Enzyme Catalysis** *Biochim. Biophys. Acta* **2000**, 43, 1458

Schuster, G. B. *Long-Range Charge Transfer in DNA I, II*; Springer-Verlag: Heidelberg, 2004; Vol. 236, p 237.

Schuster, G. B. **Long Range Charge Transfer in DNA : Transient Structural Distortions Control Distance Dependence.** *Acc. Chem. Res.* **2000**, 33, 253-260.

Shafirovich, V.; Dourandin, A.; Gaecintov, N. E. **Proton Coupled Electron Transfer Reactions at a Distance in DNA Duplex: Kinetic Deuterium Isotope Effects.** *J. Phys. Chem. B* **2001**, *105*, 8431-8435.

Sistare, M. F.; Codden, S. J.; Heimlich, G.; Thorp, H. H. **Effects of Base Stacking on Guanine Electron Transfer: Rate Constants for G and GG Sequences of Oligonucleotides from Catalytic Electrochemistry** *J. Am. Chem. Soc.* **2000**, *122*, 4742-4749.

Sistare, M. F.; Holmberg, R. C.; Thorp, H. H. **Electrochemical Studies of Polynucleotide Binding and Oxidation by Metal Complexes: Effects of Scan Rate, Concentration, and Sequence** *J. Phys. Chem. B.* **1999** *103* 10718-10728

Sjodin, M.; Styring, S.; Akermark, B.; Sun, L.; Hammerstrom, L. **Proton-Coupled Electron Transfer from Tyrosine in a Tyrosine-Ruthenium-tris-Bipyridine Complex Comparison with Tyrosine<sub>Z</sub> Oxidation in Photosystem II:** *J. Am. Chem. Soc.* **2000** *122*, 3932

Sjodin, M.; Styring, S.; Wolpher, H.; Xu, Y.; Sun, L.; Hammarström, L. **Switching the Redox Mechanism: Models for Proton-Coupled Electron Transfer from Tyrosine and Tryptophan** *J. Am. Chem. Soc.* **2005**, *127*, 3855-3863.

Steenken, S. *Chem. Rev.* **Oxidative Damage to DNA: Formation Measurement and Biological Significance.** 1989. *89*. 503-520

Steenken, S. **Electron Transfer in DNA? Competition by UltraFast Proton Transfer?** *Biol. Chem.* **1997**, *378*, 1293-1297.

Steenken, S.; Javanovic, S.V **How Easily Oxidizable Is DNA? One-Electron Reduction Potentials of Adenosine and Guanosine Radicals in Aqueous Solution** *J. Am. Chem. Soc.* **1997**, *119*, 617-618

Steenken, S.; Jovanovic, S.V.; Candeias, L.P.; Reynisson, **DNA-Strand Breakage via the Guanine Radical Thermodynamically and Sterically Possible?** *J. Chem. Eur. J.* **2001**, *7*, 2829-2833.

Steiner, T. **The Hydrogen Bond in the Solid State** *Angew Chem. Int. Ed.* 2002, *41*, 48-76

Stubbe, J.; Nocera, D. G.; Yee, C. S.; Chang, M. C. Y. **Radical initiation in the Class I ribonucleotide reductase: long-range proton-coupled electron transfer?** *Chem Rev* **2003**, *103* 2167-2202.

Sun, L.; Bu, Y. **Marked Variations of Dissociation Energy and H-Bond Character of the Guanine-Cytosine Base Pair Induced by One-Electron Oxidation and Li<sup>+</sup> Cation Coupling** *J. Phys. Chem. B* **2005**, *109*, 593-600.

Sutin, N. *Prog. Inorg. Chem.* 1983, 30, 441.

Tommos, C.; Babcock, G. T. **The protein environment appears to regulate the biological function of tyrosyl radicals** *Acc. Chem. Res.* **1998**, 31, 18-25.

Warshel, A. **Molecular Dynamics Simulations of Biological Reactions** *Acc. Chem. Res.* **2002**, 35, 385.

Tommos, C.; Babcock, G. T. **Proton and Hydrogen Currents in Photosynthetic Water Oxidation.** *Biochim. et Biophys. Acta.* **2000**, 1458, 199-219

Weatherly, S. C. **The Mechanisms of Metal-Mediated Guanine Oxidation in Native and Non-Native DNA Environments.** University of North Carolina, Chapel Hill, 2001

Weatherly, S. C.; Yang, I. V.; Thorp, H. H. **Proton-coupled electron transfer in duplex DNA: driving force dependence and isotope effects on electrocatalytic oxidation of guanine.** *J. Am. Chem. Soc.* **2001**, 123, 1236-37

Weatherly, S. C.; Yang, I. V.; Armistead, P. A.; Thorp, H. H. **Proton Coupled Electron Transfer in Guanine Oxidation: Effects of Isotope, Solvent, and Chemical Modification** *J. Phys. Chem. B* **2003**, 107, 372-378.

Willit, J. L., Bowden, E. F., Adsorption and redox thermodynamics of strongly adsorbed cytochrome c on tin oxide electrodes *J. Phys. Chem.* **1990** 94, 8241-8245

Yates, K. S. **Application of Marcus theory to photochemical proton transfer reactions. II. Modifications based on intersecting state models** *J. Phys. Org.* **2002**, 2 300-322